Reactive dicalcium silicate binders: Microstructure and transport properties

Adrian-Alexandru PÎRVAN

EPFL

École
polytechnique
fédérale
de Lausanne

2022

Scientia potentia est.

(from Latin "Knowledge is power.")

Acknowledgements

I would like to express my gratitude to certain people who contributed to achieving the work presented in this thesis and who supported me during these beautiful and sometimes challenging years.

First of all, I would like to acknowledge Prof. Karen Scrivener, my academic supervisor at EPFL-LMC, who was the first one to think I could be a good match for the ERICA Project. I am very grateful for the chance to work both in an amazing lab with dedicated people and in a company with extremely skilled researchers. I am also grateful for all your guidance, for sharing your vision with me and for all ideas and feedback on my work, these contributed immensely to the quality of this thesis.

Dr. Mohsen Ben Haha, my industrial supervisor at HeidelbergCement, deserves equal amount of credit and gratitude for all his supervision and for pushing me more than I was pushing myself. Thank you for always making time to discuss research problems and to share with me from your academic and industrial experience.

I would like to thank the Jury members: Prof. Robert Flatt, Prof. Thomas Matschei and Dr. Hong Wong for taking time to read the thesis, for the fruitful discussion during the oral exam and the excellent feedback than helped me improve the thesis. The Jury president, Dr. Yves Leterrier is warmly thanked for chairing the oral exam in a nice manner.

Many thanks to Dr. Maciej Zajac, from HeidelbergCement, who offered his kind support countless times. No matter if I needed an opinion about my results, ideas for my experiments or support with thermodynamic calculations, I always knew I would find answers when talking to you.

This project has helped me grow in more than one way, and the ERICA meetings, workshops and training schools have contributed to this to a large extent. I would like to thank Prof. Peter McDonald from University of Surrey, project manager, and also Lynn Boniface and Marie-Alix Dalang-Secretan, together with all the Steering Committee for making this experience so valuable.

This journey just wouldn't have been the same without my dearest colleague, Monisha Rastogi. I was very lucky to have you at HTC during these years and to share with you both the happy moments and the occasional struggle. We pushed each other and we learned a lot from each other's experience. I'm extending the gratitude as well to your husband, Aditya Chauhan, for all motivational discussions and for all the nice trips we took together.

I would like to thank all ERICA ESRs for all memorable moments. To Monisha, Maya, Magda, Nabor, Miryea, Khalil, Petr, Örs, Anastasiia, Rémi, Masood, Arifah. From the beginning of the project, I knew we would form a great team and I'm proud of how we managed all the group tasks, such as the dissemination videos. I especially enjoyed the occasional scientific sessions and the birthday celebrations during some of the ERICA events.

I am extremely grateful to everyone at HTC for all their support with the experimental work. Everyone from the R&D team and the ANC department has been extremely welcoming and helpful. Many thanks to Frank, Pawel and Arnaud, for their support with various characterization techniques. I would also like to acknowledge Dominik Nied for always being supportive and my offices colleagues, Steve and Tanja, for all the coffee breaks and pieces of German knowledge.

Although we got to spend only a few months together, the LMC team has made me feel a part of them each time I visited the lab. I am thankful to Yosra for taking me under her wing then I first settled into the lab, for all the fun activities and also the time spent in Heidelberg when she visited HTC. To Fabien and William for all helpful discussions about chloride transport and for their support when reproducing the mini-migration setup at HTC and to Emmanuelle for the support with the electron microscopes. To Anna, Maya, Khalil, Sarra, Andrea, Wioletta, François, Diana, Solène, Alexandre, Franco, Julien, Shiyu, Mink, Silas, Mahsa, Maude, Marcel, Mariana, Qiao, Mirabela, for all the help with characterization techniques, for the hikes we took to discover beautiful landscapes, the ski seminars and the fun activities.

It would have been hard to stay sane during these years away from home without all the fun holidays and visits to Bucharest, where my friends kept planning awesome activities and made sure to include me each time I visited.

Very special thanks to my cousin Mirela, in Saint-Sulpice and to her lovely family, they hosted me each time I was in Lausanne and made me feel a lot like home.

I definitely wouldn't have made it so far without the support of my family, who kept motivating me and believing that somehow, I would succeed, even when I didn't believe it myself. To my parents, Ioana and Constantin, my brother, Daniel, and my dear cousin, Roxana.

Heidelberg, October 13th 2021

Abstract

The calcium silicate hydrates (C-S-H) are without doubt one of the most important hydration products in a hardened cement paste. Giving the complexity of the microstructure that forms by hydration of ordinary Portland cement (OPC) and the more recently used cements with supplementary cementitious materials (SCMs), studying the main feature and properties of C-S-H is not an easy task. Various methods for precipitating synthetic C-S-H with controlled composition have been developed, but the resulting products lack a solid microstructure and the characteristic pore network found in cementitious materials.

The research plan of this thesis includes using a reactive dicalcium silicate binder which possess two advantages, compared to alite or OPC: it hydrates fully is less than 7 days and very low amounts of portlandite form, especially at lower water-to-binder ratios. The evolution of the C-S-H composition with time and w/b in the hydrated C_2S microstructure was investigated. A slight drop in the Ca/Si ratio of C-S-H with hydration age was observed. A more significant decrease occurs when the w/b was increased from 0.35 to 0.80, and a higher amount of CH was precipitated in the hydrated matrix. With increased content of alkali introduced in the mixing water, the Ca/Si ratio of the resulting C-S-H further decreased from almost 2.0 to 1.80 and more portlandite formed. This was correlated with the metastable character of the high Ca/Si ratio C-S-H with respect to the pore solution and supersaturation with respect to C-S-H and CH are expected to play an important role.

The effect of two frequently used SCMs, micro-silica and metakaolin, on the C-S-H microstructure was investigated by hydrating mixtures of the reactive C_2S with different amounts of the two SCMs. The Ca/Si ratio of C-S-H decreased with higher amount of silica/metakaolin used and at 20% replacement level, the Ca/Si ratio at 28 days was close to 1.60. With hydration age up to 9 months, more silica and metakaolin is consumed, the specific surface area of C-S-H is reduced and the porosity is refined. A pozzolanic reaction was thus identified in a system without portlandite available to be consumed in the reaction.

Transport properties through hydrated matrix are particularly interesting, as chloride penetration is related to degradation of steel reinforced concrete elements. The C-S-H microstructures were tested for both chloride binding and chloride migration. A comparison with hydrated white cement microstructures and synthetic C-S-H powders was presented. In terms of chloride binding, the hydrated C_2S adsorbed less than the synthetic C-S-H, but some systems retained slightly more than the white cement paste. The amount of adsorbed chloride was significantly reduced in samples containing silica and metakaolin. Concerning the chloride migration, effective diffusion coefficients for all C_2S and white cement systems were calculated. Migration of chloride through the plain C_2S

microstructure was found to be much faster than through a hydrated white cement at the same water-to-binder ratio, but the performance could be improved by reducing the water-to-binder ratio and through the use of micro-silica and metakaolin.

These results are showing the strong potential of the reactive C_2S to be used for the study of C-S-H phase with various compositions in isolation and for the investigation of various transport phenomena associated with concrete durability issues.

Keywords: reactive dicalcium silicate, calcium silicate hydrate, silica, metakaolin, chloride binding capacity, chloride migration

Résumé

La phase des hydrates de silicate de calcium (C-S-H) est sans aucun doute l'un des hydrates les plus importants dans une pâte de ciment durcie. Étant donné la complexité de la microstructure qui se forme par l'hydratation du ciment Portland ordinaire (OPC) et des ciments plus substitués utilisés avec des matériaux cimentaires supplémentaires (SCMs), l'étude des principales caractéristiques et propriétés du C-S-H n'est pas une tâche facile. Les méthodes de précipitation de C-S-H synthétiques à composition contrôlée ont beaucoup évolué, mais les produits qui en résultent n'ont pas une microstructure solide et pas le même le réseau de pores caractéristique des matériaux cimentaires.

Le plan de recherche de cette thèse comprend l'utilisation d'un liant réactif à base de silicate dicalcique qui présente deux avantages par rapport à l'alite ou à l'OPC : son hydratation complète est inférieure à 7 jours et de très faible quantité de portlandite se forme, en particulier à des ratios eau/liant plus faibles. L'évolution de la composition C-S-H avec le temps et le w/b dans la microstructure de C_2S hydratée a été étudiée. Une légère baisse du rapport Ca/Si de C-S-H avec l'âge d'hydratation a été observée. Une diminution plus significative se produit lorsque le w/b a été augmenté de 0.35 à 0.80, et une plus grande quantité de CH a été précipité dans la matrice hydratée. Avec l'augmentation de la teneur en alcalin introduite dans l'eau de mélange, le rapport Ca/Si du C-S-H résultant a continué à diminuer de presque 2.0 à 1.80 et davantage de portlandite s'est formée. Ceci a été corrélé avec le caractère métastable du rapport Ca/Si élevé de la C-S-H par rapport à la solution des pores et la sursaturation par rapport à la C-S-H et au CH devrait jouer un rôle important.

L'effet de deux SCMs fréquemment utilisés, la micro-silice et le métakaolin, sur la microstructure du C-S-H a été étudié en hydratant des mélanges de le C_2S réactif avec différentes quantités des deux SCMs. Le rapport Ca/Si de C-S-H diminue avec l'augmentation de la quantité de silice/métakaolin utilisée et à un niveau de remplacement de 20%, le rapport Ca/Si à 28 jours était proche de 1.60. Avec un âge d'hydratation allant jusqu'à 9 mois, plus de silice et de métakaolin sont consommés, la surface spécifique de C-S-H est réduite et la porosité est affinée. Une réaction pouzzolanique a donc été identifiée dans un système sans portlandite disponible pour être consommée dans la réaction.

Les propriétés de transport à travers la matrice hydratée sont particulièrement intéressantes, car la pénétration des chlorures est liée à la dégradation des éléments en béton armé. Les microstructures de C-S-H ont été testées à la fois pour la fixation et la migration des chlorures. Une comparaison avec des microstructures de ciment blanc hydraté et des poudres synthétiques de C-S-H a été présentée. En termes de fixation des chlorures, le C_2S hydraté a moins adsorbé que le C-S-H

synthétique, mais certains systèmes ont retenu un peu plus que la pâte de ciment blanc. La quantité de chlorure adsorbée était significativement réduite dans les échantillons contenant de la silice et du métakaolin. Concernant la migration du chlorure, les coefficients de diffusion effectifs pour tous les systèmes de C_2S et de ciment blanc ont été calculés. La migration du chlorure à travers la microstructure de C_2S ordinaire s'est avérée beaucoup plus rapide que celle d'un ciment hydraté pour le même rapport eau/liant, mais les performances pourraient être améliorées en réduisant le rapport eau/liant et en utilisant de la micro-silice et du métakaolin.

Ces résultats montrent le fort potentiel de le C_2S réactif à être utilisée pour l'étude de la phase C-S-H avec diverses compositions en isolation et pour l'investigation de divers phénomènes de transport associés aux problèmes de durabilité du béton.

Mots-clés: silicate dicalcique réactif, silicate de calcium hydraté, silice, métakaolin, capacité de liaison des chlorures, migration des chlorures.

Zusammenfassung

Calciumsilicathydrate (C-S-H) sind zweifellos eines der wichtigsten Hydratationsprodukte in einem ausgehärtetem Zementstein. Angesichts der Komplexität der Mikrostruktur, die sich bei der Hydratation von gewöhnlichem Portlandzement (OPC) und den in jüngerer Zeit verwendeten Kompositzementen mit so genannten „supplementary cementitious materials" (SCM) bildet, ist die Untersuchung der Hauptmerkmale und Eigenschaften von C-S-H keine einfache Aufgabe. Es wurden verschiedene Methoden zur Ausfällung von synthetischem C-S-H mit kontrollierter Zusammensetzung entwickelt, wobei den daraus resultierenden Produkten eine feste Mikrostruktur und das charakteristische Porennetzwerk, welche in zementartigen Materialien zu finden sind, fehlt.

Der Versuchsplan dieser Arbeit umfasst die Verwendung eines reaktiven Dicalciumsilicat-Bindemittels, das im Vergleich zu Alit oder OPC zwei Vorteile aufweist: Es hydratisiert in weniger als 7 Tagen vollständig und es bilden sich nur sehr geringe Mengen an Portlandit (CH), insbesondere bei niedrigeren Wasser-Bindemittel-Verhältnissen (w/b). Es wurde sowohl die Entwicklung der C-S-H-Zusammensetzung über die Zeit als auch der Einfluss des w/b im hydratisierten C_2S-Mikrogefüge untersucht. Ein leichter Rückgang des Ca/Si-Verhältnisses im C-S-H mit zunehmenden Hydratationsalter konnte beobachtet werden. Ein deutlicherer Rückgang trat bei der Anhebung des w/b-Wertes von 0.35 auf 0.80 auf. Weiterhin wurde eine größere Menge an CH in der hydratisierten Matrix ausgefällt. Mit zunehmender Alkalikonzentration im Anmachwasser sank das Ca/Si-Verhältnis des resultierenden C-S-H weiter von fast 2.0 auf 1.8 und es bildete sich mehr Portlandit. Dies wurde mit dem metastabilen Charakter von C-S-H mit hohem Ca/Si-Verhältnis in Bezug auf die Porenlösung in Verbindung gebracht. Es wird ebenfalls erwartet, dass die Übersättigung in Bezug auf C-S-H und CH eine wichtige Rolle spielt.

Der Einfluss von zwei häufig verwendeten SCMs, Kieselsäure und Metakaolin, auf die Mikrostruktur von C-S-H, wurde durch Hydratation von Mischungen des reaktiven C_2S mit unterschiedlichen Mengen der beiden SCMs untersucht. Das Ca/Si-Verhältnis von C-S-H verringerte sich mit zunehmender Menge an Kieselsäure/Metakaolin. Bei einer SCM Zugabe von 20% lag das Ca/Si-Verhältnis nach 28 Tagen bei rund 1,6. Mit zunehmendem Hydratationsalter bis zu 9 Monaten werden mehr Kieselsäure und Metakaolin verbraucht, die spezifische Oberfläche von C-S-H verringert sich und die Porosität wird verfeinert. Es wurde also eine puzzolanische Reaktion in einem System festgestellt, in dem kein Portlandit zur Verfügung steht, dass bei der Reaktion verbraucht werden könnte.

Die Transporteigenschaften durch die hydratisierte Matrix sind besonders interessant, da das Eindringen von Chlorid mit der Korrosion von stahlbewehrten Betonelementen zusammenhängt. Die

C-S-H-Mikrostrukturen wurden sowohl auf Chloridbindung als auch auf Chloridmigration geprüft. Es wurden Vergleiche mit Zementsteinen basierend auf hydratisierten Weißzement sowie synthetischen C-S-H-Pulvern angestellt. Was die Chloridbindung betrifft, so adsorbierte das hydratisierte C_2S weniger als synthetische C-S-H-Pulver, wohingegen einige Systeme mehr Chlorid binden konnten als hydratisierte Weißzemente. Die Menge des adsorbierten Chlorids war bei Proben, die Kieselsäure und Metakaolin enthielten, deutlich geringer. Die effektiven Diffusionskoeffizienten der Chloridmigration wurden für alle C_2S- und Weißzementsysteme berechnet. Es wurde festgestellt, dass die Migration von Chlorid durch das Zementsteingefüge von hydratisiertem C_2S viel schneller verläuft als bei einem Weißzement mit demselben Wasser-Bindemittel-Verhältnis. Jedoch konnte die Chloridmigration durch die Verringerung des Wasser-Bindemittel-Verhältnisses und durch die Verwendung von Mikrokieselsäure oder Metakaolin reduziert werden.

Diese Ergebnisse zeigen das große Potenzial von reaktiven C_2S für die Charakterisierung der C-S-H-Phase mit verschiedenen Zusammensetzungen und für die Untersuchung verschiedener Transportphänomene im Zusammenhang mit der Dauerhaftigkeit von Beton.

Stichworte: reaktives Dicalciumsilikat, Calciumsilicathydrat, Kieselsäure, Metakaolin, Chloridbindungsvermögen, Chloridmigration.

Rezumat

Hidrosilicații de calciu (C-S-H) sunt fără îndoială unii dintre cei mai importanți produși de hidratare într-o pastă de ciment întărit. Având în vedere complexitatea microstructurii formate prin hidratarea cimentului Portland obișnuit (OPC) și a cimenturilor ce conțin materiale cimentoide suplimentare (SCMs), studiul caracteristicilor și proprietăților C-S-H nu este o sarcină ușoară. Au fost dezvoltate metode variate pentru precipitarea C-S-H sintetice cu compoziție controlată, însă produsul rezultat nu are o microstructură solidă și o structură a porilor regăsită în pastele de ciment.

Planul experimental al acestei teze include folosirea unui liant reactiv silicat dicalcic, ce prezintă două avantaje comparativ cu alitul sau OPC: se hidratează complet în mai puțin de 7 zile și cantități reduse de portlandit se formează, în special la rapoarte apă-ciment reduse. Evoluția compoziției C-S-H cu timpul și cu raportul a/c în microstructura silicatului dicalcic hidratat a fost investigată. Odată cu timpul de hidratare, o scădere minoră a raportului Ca/Si in C-S-H a fost observată. O creștere semnificativă s-a înregistrat odată cu creșterea raportului a/c de la 0,35 la 0,80, iar o cantitate mai mare de CH a fost precipitată în matricea hidratată. Introducerea unei cantități însemnate de alcalii în apa de hidratare a dus la scăderea raportului Ca/Si a C-S-H rezultat de la aproape 2,0 la 1,80 iar cantitatea de CH a crescut. Acest efect a fost cauzat de caracterul metastabil a C-S-H cu raport Ca/Si mare in soluția din pori, și este de asemenea de așteptat ca suprasaturația în raport cu C-S-H și CH să joace un rol important.

Efectul a două dintre materialele cimentoide suplimentare utilizate frecvent, micro-silicea si metacaolinul, asupra microstructurii C-S-H a fost investigat prin hidratarea unor amestecuri de C_2S reactiv cu diferite proporții din cele două SCMs. Raportul Ca/Si al C-S-H a scăzut cu creșterea cantității de silice/metacaolin folosite, iar la un nivel de substituție de 20%, raportul Ca/Si la 28 zile de hidratare a fost aproape 1,60. Cu timpul de hidratare până la 9 luni, o cantitate mai însemnată de silice/metacaolin este consumată, suprafața specifică a C-S-H este redusă iar porozitatea este redusă semnificativ. O reacție pozzolanică a fost astfel evidențiată într-un sistem fără portlandit disponibil pentru a fi consumat în reacție.

Proprietățile de transport prin matricea hidratată sunt în particular de interes, deoarece penetrarea clorurilor este în strânsă legătură cu degradarea elementelor de beton ranforsat. Microstructurile de C-S-H au fost testate atât pentru capacitatea de legare a clorurilor cât și pentru migrarea ionilor de clor. O comparație cu microstructuri de ciment alb hidratat și pulberi de C-S-H sintetic a fost, de asemenea, prezentată. În ceea ce privește capacitatea de legare a clorurilor, probele de C_2S hidratat au adsorbit mai puțin Cl decât C-S-H sintetic, dar unele dintre sisteme au reținut puțin mai mult Cl decât pastele de ciment alb. Cantitatea de clor adsorbit a fost semnificativ redusă în

probele ce conțineau silice și metacaolin. Pentru caracterizarea procesului de migrare, s-au determinat coeficienții de difuziune efectivă ale tuturor sistemelor cu C_2S reactiv și ciment alb. Migrarea clorurilor prin microstructura probelor conținând doar C_2S a fost mai rapidă decât în cazul unui ciment hidratat la același raport a/c, dar performanța acestuia a fost îmbunătățită prin reducerea raportului a/c și prin utilizarea silicei si a metacaolinului la hidratare.

Aceste rezultate demonstrează potențialul ridicat al C_2S reactiv de a fi folosit pentru studiul fazei izolate C-S-H de compoziție variabilă și pentru investigarea diferitelor fenomene de transport asociate cu probleme de durabilitate ale betonului.

Cuvinte cheie: silicat dicalcic reactiv, hidrosilicat de calciu, silice, metacaolin, capacitatea de legare a clorurilor, migrarea clorurilor.

Contents

List of Figures

List of Tables

Chapter 1.   Introduction

1.1. ERICA Programme

This thesis is part of an European Programme called 'Engineered Calcium-Silicate-Hydrates for Applications' (ERICA), under the Marie Skłodowska-Curie Actions (MSCA), Innovative Training Networks (ITN) [1]. The program is based on a multi-disciplinary approach and consists of 13 individual projects conducted in 5 research institutes in Europe. At the center of all projects are the calcium silicate hydrates (C-S-H), the main binding phase in a hydrated cement paste. This phase represents the matrix that hold all elements of a concrete structure together and is, at the same time, responsible for all significant bulk properties, such as moisture transport, carbonation, chloride and other ions transport. Although their importance is widely recognized, not all questions regarding the structure, nucleation and growth of the C-S-H have been answered.
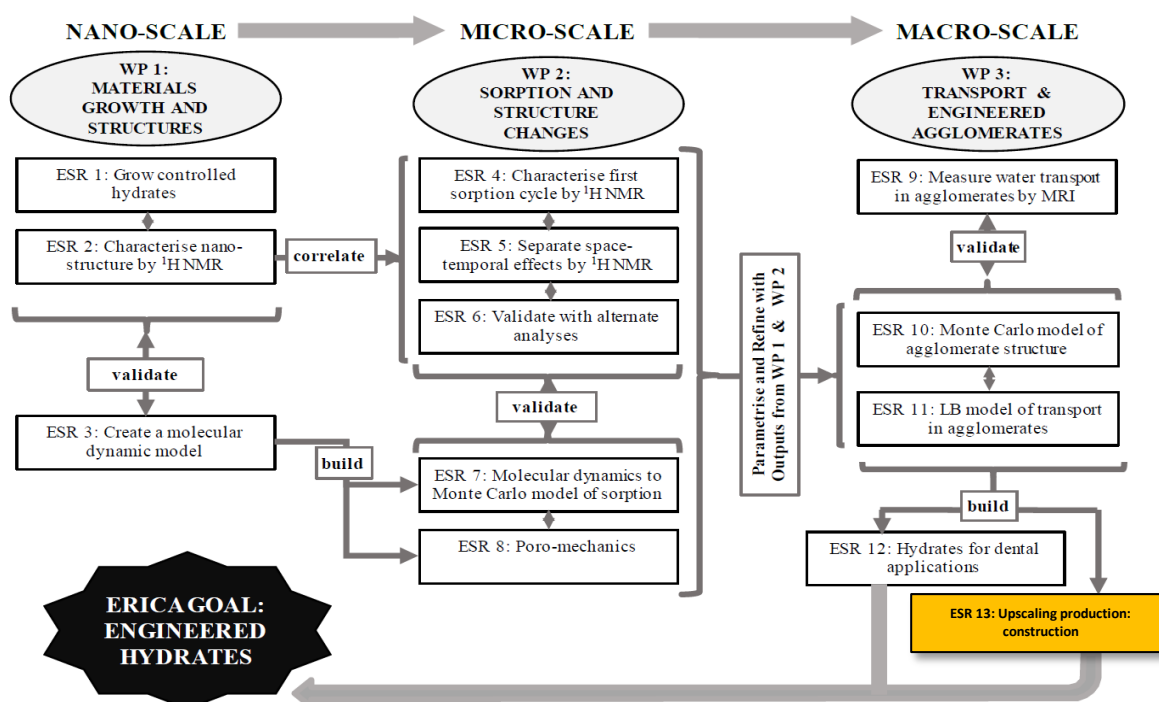
Figure 1-1. Interconnects between ERICA work packages and individual projects. The arrows show logical progression from understanding nano-scopic hydrate growth to macro-scopic engineering of agglomerates.

The ERICA programme aims to investigate some of the relevant processes concerning C-S-H based on an experimental approach combined with modelling insights. By contributing to the general understanding about the nucleation and growth of C-S-H, their behavior during the first and subsequent sorption cycles and their contribution to the overall water and ions transport, the performance of cementitious materials could be greatly improved.

1.2. Aim of the thesis

As it can be observed in the ERICA research chart in Figure 1-1, this project is listed as Project no.13. As a general scope, the project deals with important properties of C-S-H as an up-scaled product for construction applications. A final product with rapid hydration reaction and predictable, long term durability is required in order to investigate the transport of small ions into and out of agglomerates of hydrates with controlled composition.

The objectives can thus be defined as follows:

- to develop materials composed of C-S-H manufactured using industrial by-products;

- to engineer materials with optimized microstructure for transport properties;

- to develop means by which laboratory scale production of carefully controlled hydrates can be scaled-up to an industrial production environment & conditions.

The milestones expected to be achieved during the research program were as well defined:

- screening of suitable production methods for large scale production;

- up-scaled samples with variable composition produced using the production method selected;

- characterisation of transport properties of different samples;

- link made between chemical and mineralogical composition of engineered hydrates and desired properties for high volume production.

The experimental approach is based on producing C-S-H microstructure by hydrating a reactive C_2S binder, which achieves full hydration in less than 7 days. This material has several advantages compared to alite or OPC: it requires lower temperatures for the synthesis, it leads to a matrix of only C-S-H with low content of CH and it is free of other elements such as alkali, aluminium or iron, allowing the study of transport properties on a system much simpler and easier to characterize using conventional techniques such as X-Ray Diffraction (XRD), Thermal Differential Analysis (TGA,), Scanning and Transmittance Electron Microscopy (SEM/TEM), Mercury Intrusion Porosimetry (MIP).

Apart from understanding transport processes using the 'simpler' reference C_2S system, investigating microstructures with various compositions were as well of great interest. The Ca/Si ratio was the main parameter to be carefully varied, by using different amounts of silica and/or metakaolin, two important supplementary cementitious materials (SCMs) widely used in practice. Alumina is present in the metakaolin composition, thus uptake by the C-S-H could be as well investigated. Chloride interaction through binding and migration experiments was followed on one hand, by

immersing fully hydrated microstructures in NaCl solution for a long equilibration time and on the other hand, by subjecting microstructures to an accelerated test where chloride ions were rushed through pastes by applying an external electrical potential.

Connections between this project and other projects were achieved by including microstructures investigated by other early stage researchers (ESRs) in this experimental plan. Synthetic C-S-H with various Ca/Si ratios produced and studied by ESR 1 was considered for chloride uptake studies, while the hydrated white cement with micro silica cured at different temperatures investigated by ESR 6 was subjected to both uptake and migration testing. Some of the hydrated C_2S microstructures with different Ca/Si ratio were as well provided to ESR 6 for the recording of dynamic vapour sorption cycles and investigation of porosity thorough various techniques. This project and Project no. 10 both deal to some extent with ingress of chloride in solid microstructure, the main difference being that this project is based on an experimental approach, while Project no. 10 uses modelling tools to investigate this phenomena.

1.3. Structure of the work

Chapter 2 begins with a description of some key aspects regarding Portland cement hydration. Afterwards, a literature survey on the reactive C_2S binder used in this project is given. The chapter ends with a summary of main features of C-S-H and open questions regarding its nature and properties.

Chapter 3 is concerned with the study of the microstructure of the hydrated C_2S at different water to binder ratio, in paste as well as in suspension. The effect of alkali and gypsum on the C-S-H microstructure was investigated by mixing the C_2S with a fixed amount of gypsum and introducing NaOH in the mixing water.

In Chapter 4, the formation of a lower Ca/Si ratio C-S-H microstructure in C_2S systems containing silica and/or metakaolin was followed. Other differences in the microstructure, such as Al/Si substitution, morphology changes and porosity were also presented.

Chapter 5 contains experimental outcomes of the chloride adsorption and desorption study. C-S-H systems with various compositions were equilibrated for long time in NaCl solutions of different concentration and the retention of Cl on C-S-H surfaces was investigated.

The migration of chloride through microstructures with different composition is detailed in Chapter 6. Through the mini-migration approach, the effective chloride diffusion coefficient is determined and links with microstructure features such as porosity are explored.

Chapter 7 resumes the main findings of this thesis and discusses some interesting future perspectives.

Chapter 2. Context and background on reactive dicalcium silicate binder

2.1. Hydration of Portland cement and resulting microstructure

With almost 5 Billion Tons produced in 2020 [2], cement is one of the world's most widely used artificial material and the global demand is expected to increase to 5.8 Billion Tons by 2027. Cement is used in combination with water, sand and aggregate to form concrete. Upon hydration, the cement paste becomes the phase that binds all the elements together and is responsible for most properties of concrete structures. Production of cement starts with a mixture of raw materials, which normally contains limestone, clay, sand, iron ore and other components in definite proportions. When this mixture is heated to the sintering temperature range of about 1350–1450 °C, new compounds form, designated as clinker phases [3]. There are four clinker phases: alite (impure tricalcium silicate, Ca_3SiO_5 or $3CaO \cdot SiO_2$ or C_3S), belite (impure dicalcium silicate, Ca_2SiO_4 or $2CaO \cdot SiO_2$ or C_2S), tricalcium aluminate ($Ca_3Al_2O_6$ or $3CaO \cdot Al_2O_3$ or C_3A) and tetracalcium aluminoferrite ($Ca_4Al_2Fe_2O_{10}$ or $4CaO \cdot Al_2O_3 \cdot Fe_2O_3$ or C_4AF) [4]. As observed, all clinker phases are composed of oxides and that makes it possible to use the simplified writing in the cement field ($C=CaO$, $S=SiO_2$, $A=Al_2O_3$ and $F=Fe_2O_3$). By grinding together clinker with gypsum, cement powder is obtained. Gypsum is added to control the reaction of the aluminate phase and to prevent the flash setting of Portland cement [5]. Followed mixing with water, the clinker phases start dissolving and hydration phases are precipitating, which leads to setting within a few hours. The main hydration phase of a hydrated cement microstructure is the calcium-silicate-hydrate. It is abbreviated C-S-H, the hyphens signifying that there is no fixed stoichiometry. Other hydration products resulting from the reaction of cement with water are portlandite (calcium hydroxide or CH), ettringite (or alumina ferrite trisulfate or AFt) or aluminate ferrite phases (AFm). The amount of mixing water is related to the mass of dry cement and it is defined as water/cement ratio (w/c).

The rates of hydration of C_3S and even PC have been observed to vary significantly with time as it can be seen in Figure 2-1, where the calorimetry plot of hydration rate versus time is represented. The overall progress of hydration can be divided into four (or even five) stages, defined by somewhat arbitrary points of hydration time [6]:

i. initial reaction between C_3S and water, characterized by a large exothermic signal, the heat released by wetting of cement powder contributes as well to this early exothermic signal, but to a lower extent;

ii. period of slow reaction, where the dissolution rates transition from fast to slow;

iii. acceleration period, related to heterogeneous nucleation and growth of C-S-H on alite and perhaps on other mineral surfaces;

iv. deceleration period, where the rate of hydration decreases, there is no agreement on the exact cause of this, but possible explanation include consumption of small particles, lack of space or lack of water [7].
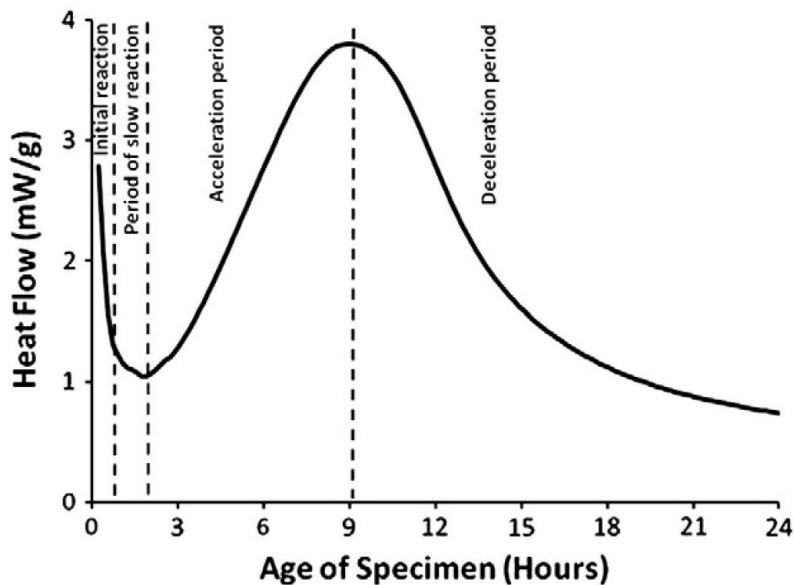
Figure 2-1. Rate of hydration as a function of time given by isothermal calorimetry measurements, reproduced from [7]

A typical microstructure of hydrated cement paste is given in Figure 2-2 [8]. The microstructure can be investigated by means of scanning electron microscopy (SEM), where a polished flat surface of a hydrated sample is analyzed in backscatter electron mode (BSE) [9]. This method provides compositional information about the investigate sample and the contrast shown in the image is given by the atomic weights of the elements in each phase. In Portland cement pastes, the hydration reaction is dominated by the reaction of C_3S which produces C-S-H and CH.

One can observe how C-S-H is the only percolating phase in the matrix, incorporating the unreacted clinker grains and CH clusters. This simple situation is complicated by the fact that Portland cement does not consist only of C_3S. In a mature cement mortar, due to the polymineralic nature of cement grains, several features of the microstructure can be observed: precipitation of ettringite and AFm, formation of 'separated hydration shells' and even interfacial transition zone at the cement paste-aggregate interface [9].
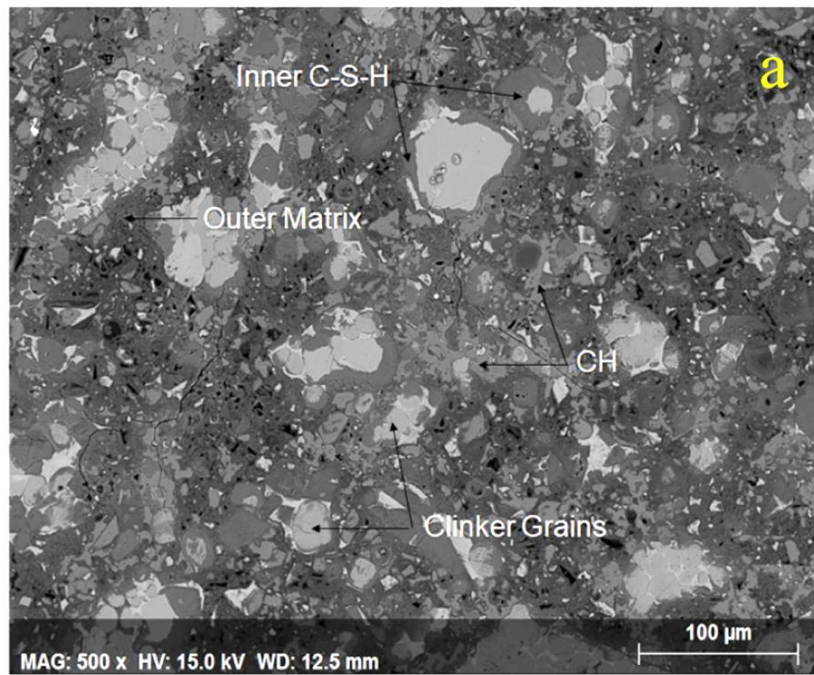
Figure 2-2. Microstructure of hardened cement paste, reproduced from [8]

Clinker phases do not always achieve a full degree of hydration. In a typical cement paste prepared with water-to-cement ratio 0.50, cured at 20°C, the evolution of the degree of hydration for all clinker phases is illustrated in Figure 2-3 [10]. C_3A is the most reactive phase, followed by C_3S which despite being reactive, will take significant amount of time to fully hydrate. Belite is less reactive and contributes to the development of microstructure as later ages, while the ferrite will react very slowly in the first 6 months.
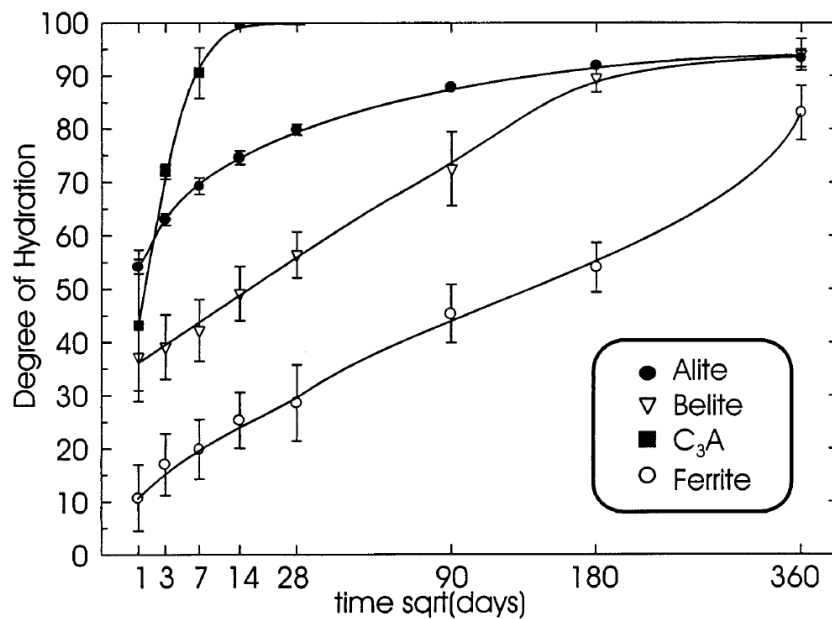
Figure 2-3. Degree of reaction of clinker phases with hydration age, reproduced from [10]

7

Today Portland cement is used more and more together with supplementary cementitious materials (SCMs), either as blended cement or added separately in the concrete mixer. The presence of SCMs influences the amount and kind of hydrates formed in the cementitious systems and thus the volume, the porosity and finally the durability of such systems. An extensive review about the main SCMs used nowadays is given in [11]. The microstructure is expected to change, as the phase assemblage in the composite systems is different. As previously mentioned, apart from C-S-H, significant amount of portlandite will precipitate in the hydration matrix, due to reaction of alite and belite. In most SCM containing systems, the CH is consumed and more C-S-H with lower Ca/Si ratio forms. Two important SCM types are silica fume and metakaolin and their influence on the hydrated cement microstructure is discussed in Chapter 4 of the thesis.

To overcome the two mentioned limitation of alite and OPC (long time to fully hydrate and formation of multiple hydration products), a reactive dicalcium silicate binder is used as an excellent candidate to produce a C-S-H rich microstructures. This phase is much more reactive than the β-belite found in clinker and its synthesis and properties are described in the next section.

2.2. Reactive dicalcium silicate binder

Belite cements have received increased attention from researchers due to their potential to reduce the CO_2 emissions associated with the production of cement [12]. This is achievable through reduction in the CaO/SiO_2 (C/S) ratio of the starting materials and burning at lower temperatures (about 1300°C [13] or even 800°C [14]). An interesting approach to synthesize dicalcium silicate phases with increased reactivity as compared to β-belite from OPC is to calcinate an intermediate crystalline calcium silicate hydrate phase. The general name of calcium silicate hydrate phase includes more than 40 different, predominantly crystalline compounds (see Figure 2-4). This term does not contain any information about the exact chemical composition, as the water content is very dependent on the drying conditions [15]. For this reason, the CaO/SiO_2 molar ratio is usually given. As opposed to the crystalline phases mentioned in the diagram in Figure 2-4, during the hydration of OPC, amorphous C-S-H phases (or C-S-H gels) are formed.

α-dicalcium silicate hydrate [$Ca_2(SiO_4H)(OH)$], hillebrandite [$Ca_2(SiO_3)(OH)_2$] and dellaite [$Ca_6(SiO_4)(Si_2O_7)(OH)_2$], and are three known calcium silicate hydrates having a Ca/Si ratio of 2 [16]. Among the three hydrates, the α-C_2SH presents the lowest thermal dissociation temperature. The α-C_2SH can be synthesized hydrothermally using a variation of raw materials, such as lime and silicic acid [16], [17], lime and quartz [18]–[21], lime and nano-SiO_2 [22] or coal fly ash of high Ca content [23], [24]. Recently, an industrial product based on previously unknown calcium hydrosilicates was developed under the name Celitement [25]. Celitement is a family of new hydraulic binders, the basic physical principle and the production process were developed at the Karlsruhe Institute of Technology. Production of Celitement is based on autoclave synthesis of a suitable calcium hydrosilicate (such as α-C_2SH), followed mechanochemical activation together with a silicate source (quartz, sand, glass, feldspar) by means of energy-intensive grinding.

8
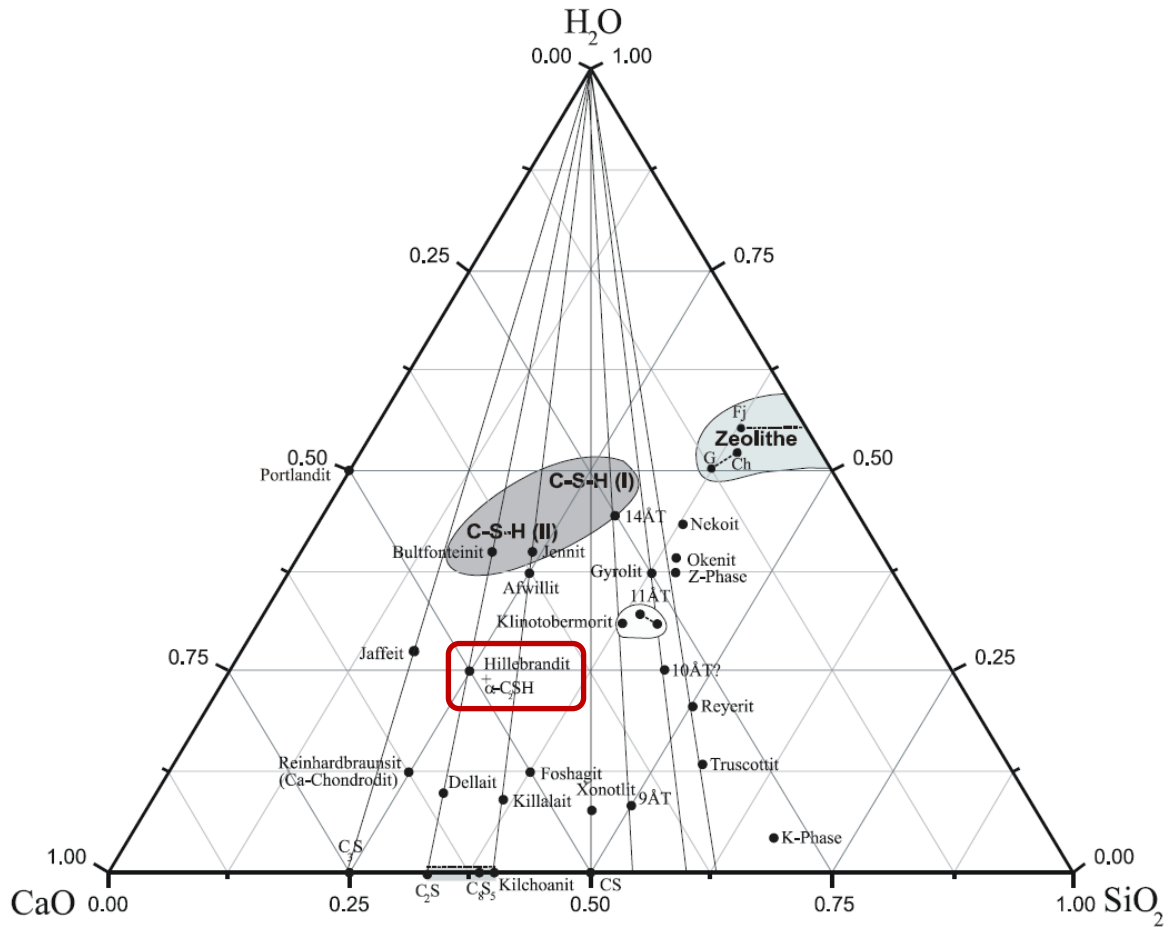
Figure 2-4. Selection of important phases in the ternary system CaO-SiO$_2$-H$_2$O. The grey area roughly indicates the composition range of different C-S-H gels. α-C$_2$SH, the raw material to synthesize the reactive dicalcium silicate binder is marked in red. Reproduced from [15]

The decomposition of α-C$_2$SH into dicalcium silicate is not a simple process [16], [26]. The results showed the formation of dellaite as an intermediate phase during dehydration of α-C$_2$SH, which is stable at room temperature. Further heating showed that dellaite transformed into a previously unknown phase, x-C$_2$S. With the aid of IR micro-spectroscopy, Garbev et al [18] proposed a mechanism of phase transformation of α-C$_2$SH at temperatures up to 400°C. First, partial formation of killalaite (Ca$_3$[HSi$_2$O$_7$](OH)) occurs, then further dehydration of this phase and remaining α-C$_2$SH happens and then formation of x-C$_2$S phase is expected. Regarding the treatment temperature of α-C$_2$SH, a substantial increase in the heat flow for samples treated in the range 360-420°C was reported in [13]. A particularity of the cementitious material produced in that study via mechanical and thermal treatment is that it was amorphous on the XRD scale.

The formation of x-C$_2$S phase was firstly reported by Ishida et al [16]. Previously, dicalcium silicates (C$_2$S) have been known as five polymorphs, designated by using the symbols α, α'_H, α'_L, β and γ in the order of decreasing temperature for thermal stability [27]. The phase transformations of the C$_2$S phase can be observed in Figure 2-5. The γ-form is stable at room temperature, but it is inert in water. The β-form is a constituent of Portland cement and it is unstable at room temperature without stabilization or controlling particle size but it has hydration activity.

Miyazaki et al [17] have used powder X-ray diffraction and selected-area electron diffraction techniques to determine the unit-cell parameters and the space group of the new x-C$_2$S phase. Based on the determined unit-cell parameters for the five studied compounds, the authors grouped α-C$_2$SH and x-C$_2$S together, while α'_L-C$_2$S, β-C$_2$S and γ-C$_2$S could be classified as another group, a structural gap existing between the two groups. Powder data and crystallographic data of the x-C$_2$S were then further revised by Yamakazi and Toraya [28] with one of the axis length being corrected. The crystal structure of x-C$_2$S phase was determined by Toraya and Yamazaki [27] by simulated annealing and refined by the Rietveld method using synchrotron radiation powder diffraction data. They reported that disposition of SiO$_4$ and CaO$_n$ polyhedra in x-C$_2$S are similar to those in α'_L-C$_2$S, except the SiO$_4$ tetrahedra in x-C$_2$S share only their edge with neighboring CaO$_n$ polyhedral, whereas the SiO$_4$ tetrahedra in α'_L-C$_2$S share also their corners and faces. The crystal structure of x-C$_2$S also differs from the olivine-type, to which the γ-C$_2$S belongs, and therefore it forms a new structural type in the C$_2$S family [27].
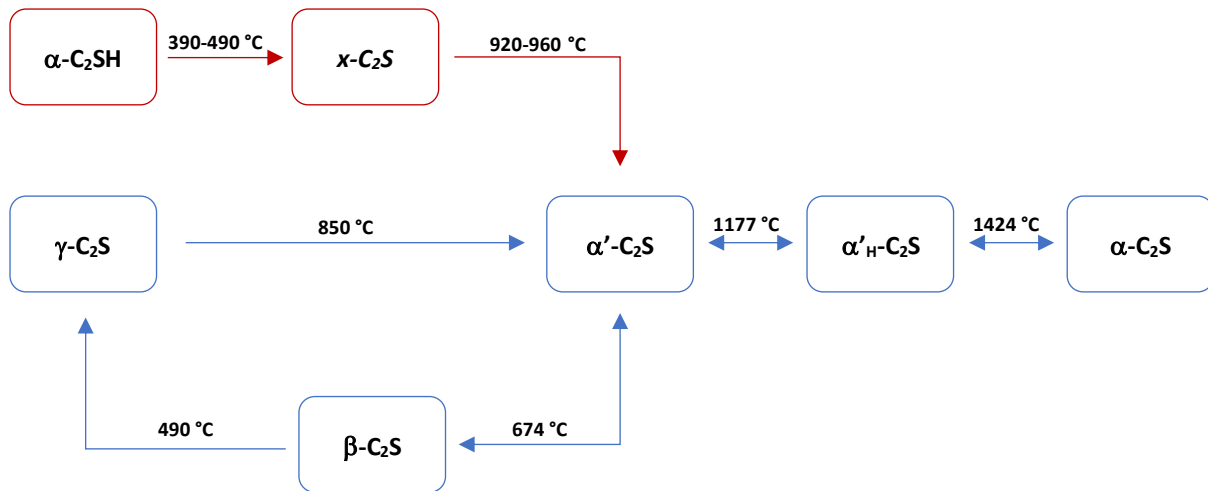
Figure 2-5. Temperature induced phase transformations of C$_2$S, reproduced from [27]

In order to illustrate the hydration mechanism of the reactive dicalcium silicate binder, which contains both amorphous and x-C$_2$S phases, a schematic model for phase-specific heat release was proposed in [22] and it is reproduced in Figure 2-6. The heat evolution during the first stage was substantially due to the reaction of the X-ray amorphous content. The second stage occurs due to the reaction of x-C$_2$S. Nevertheless, a superposition of both processes takes place. For the binders that contained an amount of β-C$_2$S, the reaction of this phase preferably took place after the reaction of x-C$_2$S. The γ-C$_2$S is not very reactive; no conversion of this phase into hydrates was recorded in the first 7 days.
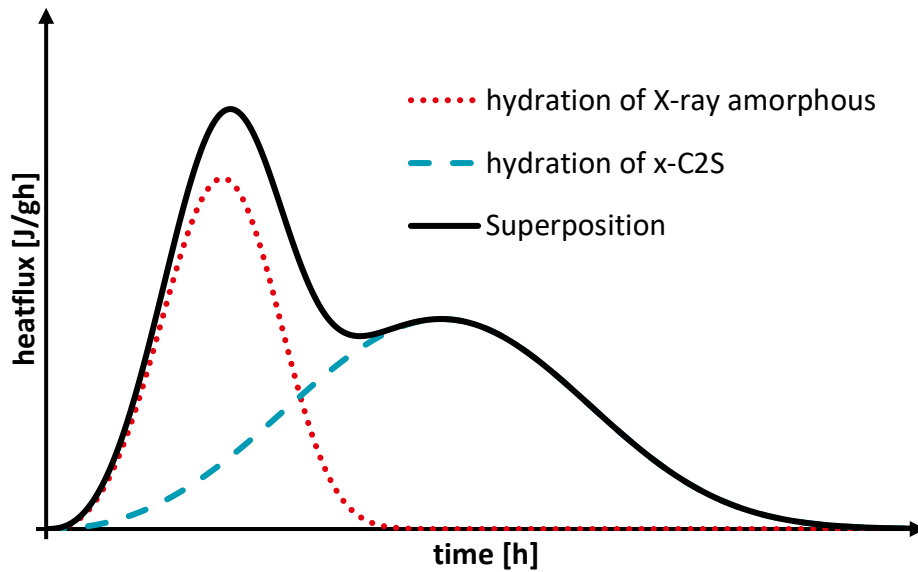
Figure 2-6. Hydration curve of reactive phases of the synthesized binder, reproduced from [29]

The morphology of the hydrates grown on the surface of C_2S particles was investigated in [29] and a related SEM micrograph is presented in Figure 2-7a. One can observe that the C-S-H phases were fibrous or needle-like. They were forming bundles of many individual fibers that were oriented almost in the same direction, with some of the individual bundles reaching up to 1.5 μm. The morphology is very similar with fibrous C-S-H grown on surface of alite, shown in Figure 2-7b.
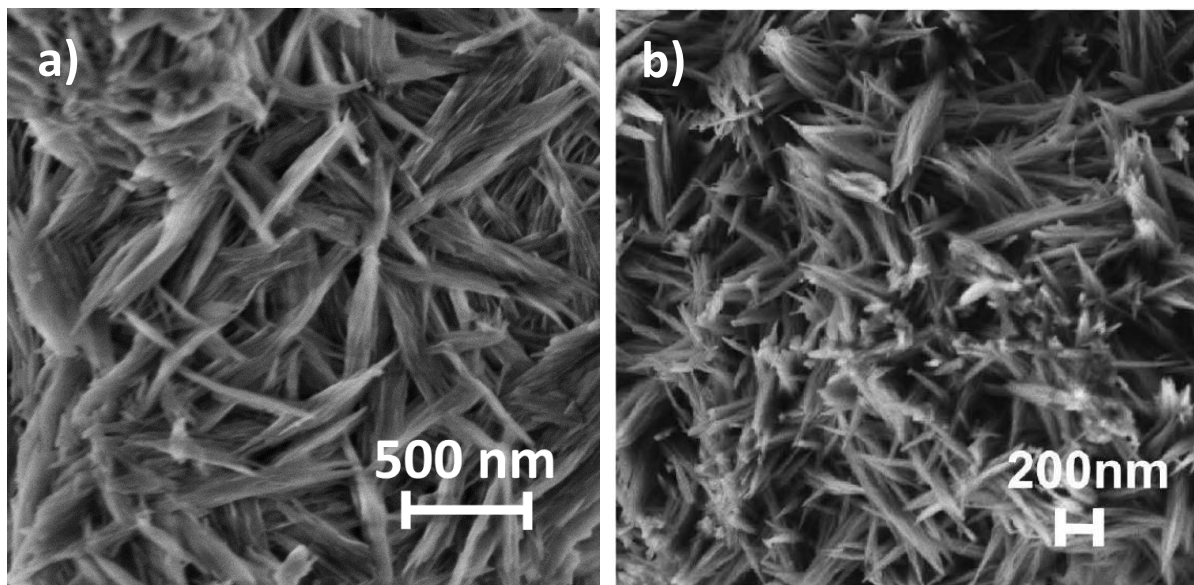
Figure 2-7. Morphology of (a) hydrated dicalcim silicate binder (reproduced from [29]) and of (b) hydrated tricalcium silicate (reproduced from [30])

Mechanical properties of the reactive dicalcium silicate binder were as well investigated in [29]. Mortar specimens of the binder containing either ground granulated blast furnace slag (ggbfs) or

limestone powder (lsp) with w/b ratio 0.3 were prepared and porosity measurements were carried out on fragments from the mechanical test, after they have been dried at 45°C to constant mass. As shown in Figure 2-8, powder with limestone reached 46 N/mm² after just 2 days and there was no significant increase in strength afterwards. The strength of the slag mixture was higher over the entire period of investigation, reaching 62 N/mm² after two days and 85 N/mm² after 28 days. The porosity of the tested mortars is as well shown in Figure 2-8. After two days, both mortars showed the same porosity values. With increasing hydration time, the porosity of the slag specimen decreases to 6%, while the mortars with limestone didn't show any further reduction in porosity. These results agreed well with the compressive strength and proved the potential of the reactive C_2S to achieve high compressive strength, which are vital if the binder is considered for construction applications.
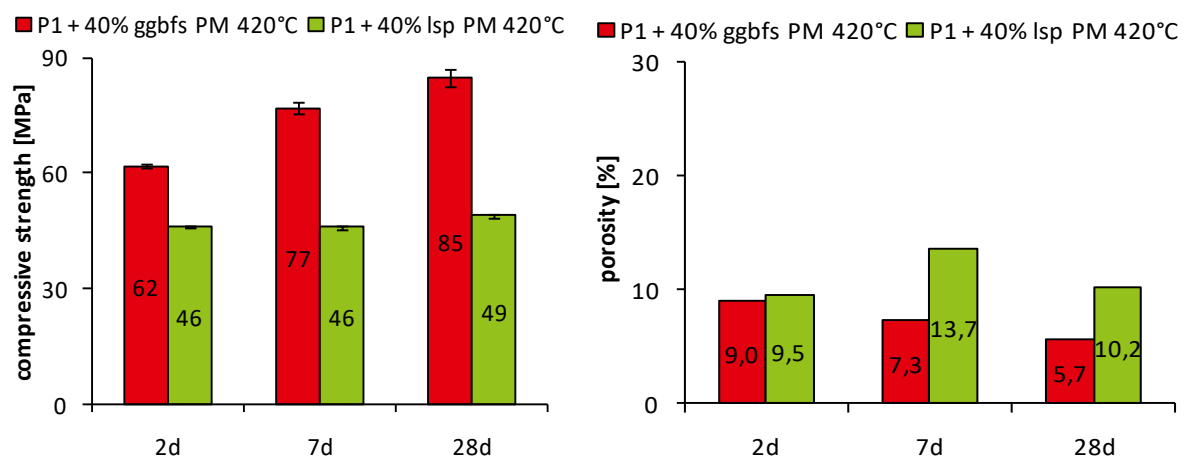
Figure 2-8. Compressive strength and total porosity of mortar specimens prepared using reactive binder, reproduced from [29]

Interaction of the reactive C_2S with some of the most important SCMs and even OPC was investigated in [29] in terms of hydration kinetics and morphology of the resulting C-S-H. A better understanding of the interaction with silica (in various proportions) and uptake of Al by C-S-H and the impact on the atomic ratios and microstructure porosity is considered necessary.

In the next section of this Chapter, some of the main features of the C-S-H phase are presented.

2.3. Structure and properties of calcium silicate hydrates

As already mentioned, the calcium-silicate-hydrate is the main binding phase in cement paste, developed from the hydration of clinker phases. As opposed to the crystalline phases shown in Figure 2-4, it is a poorly ordered phase, as a result characterization techniques such as XRD cannot reveal much about the crystal structure.

Several models for C-S-H have considered similarities with the natural mineral tobermorite ($Ca_4(Si_6O_{18}H_2) \cdot Ca \cdot 4H_2O$), having layers of calcium and oxygen with silicate tetrahedra attached and

interrupted by water and further calcium ions [31]. The structure of tobermorite was investigated for decades and it is composed of linear silicate chains in which the silicate tetrahedra are coordinated by Ca^{2+} in such a way that a patterns repeats after every three tetrahedra (called "dreierkette" form) [32]. Two of the three tetrahedra share O-O edges with the central Ca-O part of the layer and are often referred to as 'paired' tetrahedra, while the third tetrahedron connects the two paired tetrahedra and so is termed 'bridging' [32]. By the removal of some of the bridging tetrahedra and replacement by interlayer Ca^{2+} ions, the Ca/Si ratio can be increased above the value for tobermorite [33]. A higher Ca/Si ratio is also present in jennite ($Ca_9Si_6O_{18}(OH)_6 \cdot 8H_2O$), another crystalline calcium silicate hydrate that has dreierkette silicate chains. Two important C-S-H gel models based on tobermorite and jennite structure were proposed by Taylor [34] and Richardson [35]. Taylor's model [34] proposed that in C-S-H, most of the layers are structurally imperfect ones of jennite and to a smaller proportion are similarly related to the 1.4-nm form of tobermorite. Richardson and Groves [36] proposed a model which was then refined in [35] which included formulations for tobermorite/jennite and tobermorite/calcium hydroxide structural viewpoints, with maximum flexibility in the possible degree of protonation of the silicate chains. A more recent model for C-S-H structure was proposed by Kunhi Mohamed et al [37] which uses a building block approach. The building block description encodes all important features of a full atomistic C-S-H model and enables the most relevant properties such as Ca/Si ratio, silica chain length distribution, number of interlayer hydroxyl groups and degree of protonation of silanol groups to be directly calculated. One such bulk C-S-H structure determined for the Ca/Si ratio 1.50 is shown in Figure 2-9 [38]. The mentioned model could significantly facilitate the choice, construction and improvement of C-S-H models for a range of Ca/Si ratios in the near future [37]. The main substituent in the C-S-H phase is aluminium and Al-substituted C-S-H is referred to as C-A-S-H [39]. It is assumed that Al only substitutes for Si at bridging sites of the dreierketten chain and that Al cannot occur at adjacent bridging sites and that paired sites cannot be vacant. Experiments performed on synthetic C-S-H with various Ca/Si ratios showed that aluminium uptake in C-S-H depends on the total aluminium content present in the sample [40], [41]. Additionally, a close relation between aqueous aluminium concentrations and the molar Al/Si ratio in C-A-S-H is observed up to an Al/Si of approximately 0.1 [40].
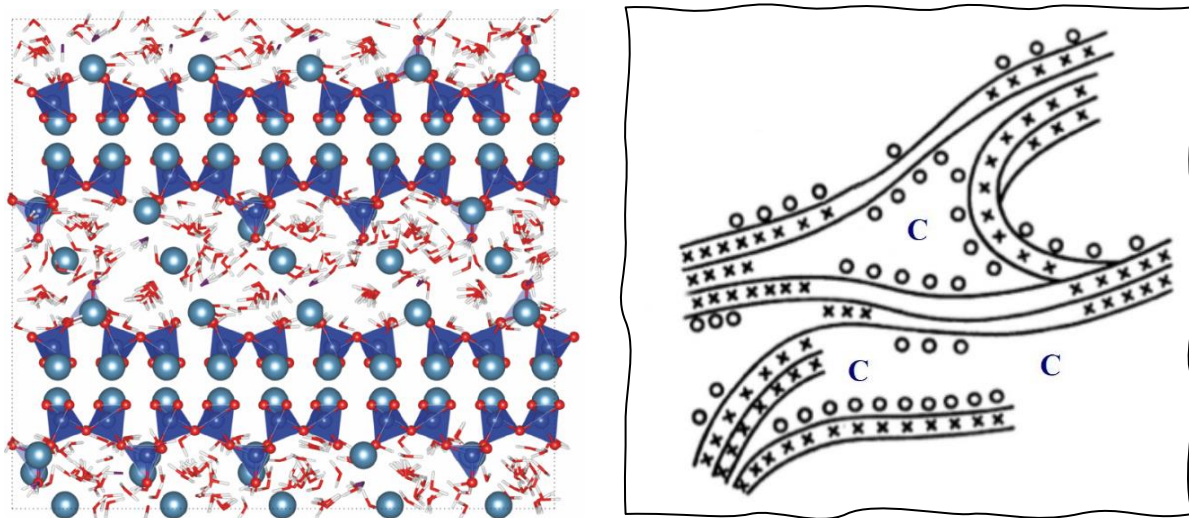
Figure 2-9. Atomistic model of a C-S-H unit with Ca/Si ratio 1.5 represented using the brick model (light blue spheres are Ca ions, dark blue spheres are Si, red spheres are O and the grey ones are H) [38] and Feldman-Sereda model of C-S-H (representing the tobermorite sheets, '+' the interlayer water, 'o' the absorbed water and 'C' the capillary pores) [42]

Besides the C-S-H atomistic arrangement, its nano-scale structure, referred to as C-S-H gel, has been of great interest. Several models have intended to describe the C-S-H gel structure. Power and Brownyard [43] have mentioned about the colloidal state of the hydration products of Portland cement. Within the boundaries of a body of pastes, there are two classes of pores: (1) gel pores, which are a characteristic feature of the structure of the gel, and (2) capillary pores or cavities, representing space not filled by gel or other solid components of the system. Later, Feldman and Sereda [42] proposed a model where the C-S-H gel was organized as tobermorite sheets, which forced into proximity, may produce a connection composed of both short and long-range bonds (van der Walls), the relative amount depending on the degree of matching of the lattice. A simplified diagram is illustrated in Figure 2-9. They suggested as well that the fibers and sheets are flexible, with water between the layers (called interlayer water), but they are probably badly aligned, as suggested by the impossibility to record any X-ray pattern for the c-axis. Faults in the tobermorite sheets lead to formation of larger pores, which were not attributed any name in the study, but they resembled the previously mentioned capillary pores. A refined model proposed by Jennings [44] had as basic unit, globules of C-S-H, or tightly packed spheres, with a cross section of 5 nm. The globules are particles of nanometer dimension that assemble into statistically well-defined patterns. Water-filled spaces include the interlayer spaces, the intraglobule spaces (IGP), the small gel pores (SGP), and the large gel pores (LGP), in each of which the water has a specific thermodynamic character. The common ground of all these models is the existence of C-S-H interlayer and gel pores, as an intrinsic property of the gels. Characterization techniques such as ^{1}H NMR could be used to follow the growth and evolution of C-S-H by distinguishing different pore families with hydration time [45]. In [46] it was shown that in a white cement paste mixed at w/b=0.40 and cured under water for 28 days, the big pores will represent only cca. 2 % of total porosity, the capillary porosity can reach 20 %, while the gel pores can take up to 78 % of the total porosity.

Development and validation of C-S-H models has relied to some extent on experimental results, such as morphology investigation by SEM or TEM. Richardson [35] identified different C-S-H morphologies in hydrated C_3S or alite at 20°C. Inner product (or Ip C-S-H) appears to consist of small globular particles, which are ≈ 4–8 nm in size. Fibrils of outer product (Op C-S-H) in C_3S or β-C_2S pastes appear to consist of aggregations of long thin particles that are of variable length, ranging from a few nanometers to many tens of nanometers. Op C-S-H in PC pastes is typically of finer morphology, with fewer coarse fibrils. The two types can be observed in Figure 2-10. Concerning the stoichiometry of C-S-H, the Ca/Si ratio of C-S-H in neat Portland cement pastes was shown to vary from ~1.2 to ~2.3 with a mean of ~1.75 [47]. This topic is more extensively approached in Chapter 3 of the thesis.

Besides the C-S-H resulting from hydration of Portland cement, synthetic C-S-H phases have been investigated intensely, with the purpose of explaining some of the unusual features of this nano-structured gel. Production of synthetic C-S-H is possible through precipitation from appropriate reagents (such as calcium oxide and silica fume [48]). Kumar et al [49] introduced a synthetic method for C-S-H that controls the pH throughout the process and leads to a uniform C-S-H with controlled Ca/Si ratio up to 2.0. By using the same method, Siramanont et al [50] showed how addition of Fe^{3+} ions affects the pH and Ca/Si ratio of C-S-H and leads to formation of ferrihydrite and iron-containing siliceous hydrogarnet. Two particularly interesting studied processes are the uptake of alumina in C-S-H, with formation of C-A-S-H phase [41], [48], [51] and the uptake of alkali in the C-A-S-H [52], [53].

These have the purpose of better understanding the hydration products formed in systems containing supplementary cementitious materials (SCMs).
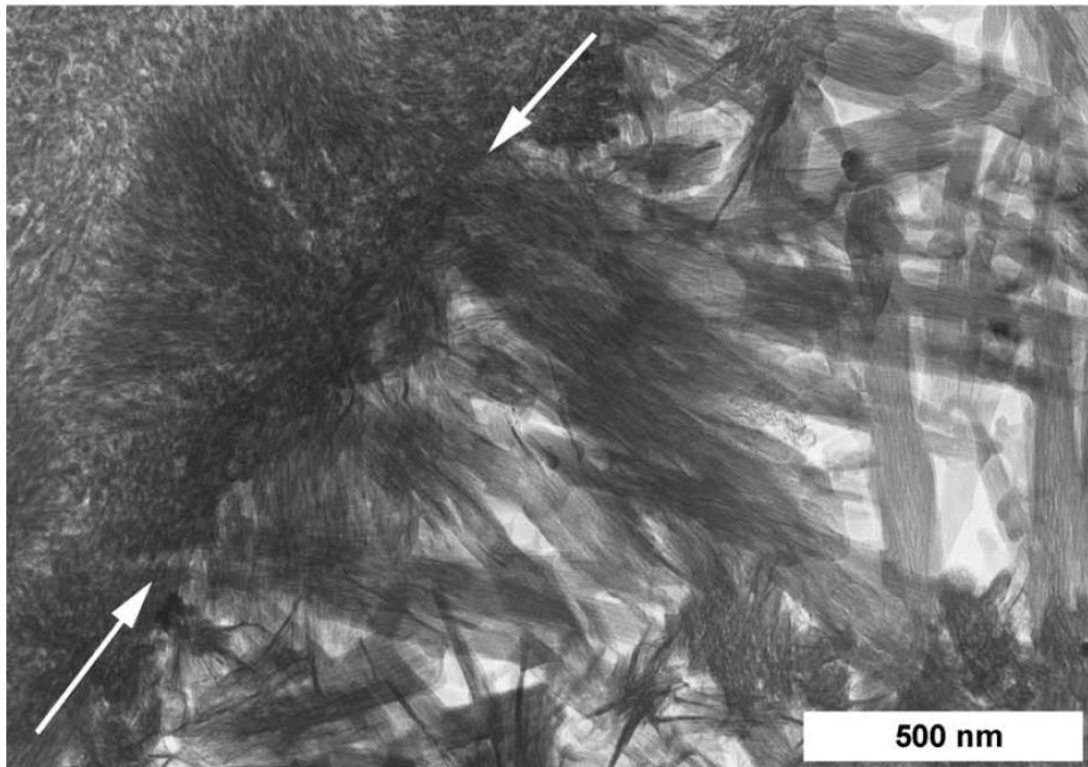
Figure 2-10. A TEM micrograph showing Ip and Op C-S-H present in a hardened C_3S paste with w/c=0.4 hydrated at 20°C for 8 years. White arrows indicate the Ip-Op boundary. Reproduced from [35]

Not many studies have tried to establish a connection between intrinsic properties of C-S-H and macroproperties such as mechanical performance or transport of ions. Kunther et al [54] evaluated the mechanical behavior of C-S-H on specimens formed directly by reaction between portlandite and amorphous silica in prismatic molds and then sealed cured. Even though samples had compositional variability, it was found that there is a relationship between Ca/Si values, and lower values lead to better mechanical behavior than systems with high Ca/Si values, especially at later ages. Nevertheless, the equilibration of the microstructure requires a long time period during which the mechanical properties change as well. A relationship between mechanical properties of synthetic C-S-H and its Ca/Si ratio has been reported also by Alizadeh et al [55]. They reported a decrease in the storage modulus as well as an increase in the internal friction as the Ca/Ca ratio of the C-S-H increased. They also suggested that the dynamical mechanical properties of C-S-H are influenced significantly by the absorbed and interlayer water.

Concerning processes related to durability issues, there are very few studies investigating the interaction of synthetic C-S-H with chloride ions, which are the main cause of steel reinforcement corrosion. Plusquellec and Nonat [56] have reported that chlorides, bromides and nitrates do not adsorb on synthetic C-S-H particles with various Ca/Si ratios, although they tend to accumulate in the diffuse layer. Studying interaction of chlorides with C-S-H, as well as transport through microstructure,

provides more insight when hydrated pastes are investigated. These topics are the central elements of Chapters 5 and 6, respectively.

Chapter 3.   Calcium-silicate-hydrates in hardened microstructure from reactive C₂S binder

Adrian-Alexandru Pîrvan[a,b], Maciej Zajac[a], Mohsen Ben Haha[a], Karen L. Scrivener[b]

[a] HeidelbergCement Technology Center GmbH, Oberklamweg 2-4, 69181 Leimen, Germany

[b] Laboratory of Construction Materials, LMC, EPFL-STI-IMX, Station 12, CH-1015 Lausanne, Switzerland

Abstract

In this study, a calcium silicate hydrate (C-S-H) microstructure formed by hydrating a reactive C₂S binder was investigated. The hydration was followed in pastes at various water-to-binder ratios and in the suspensions. When hydrated at low water-to-binder ratio, a Ca rich C-S-H forms with Ca/Si ratio close to 2, while portlandite precipitation does not occur. With hydration age and with increasing water-to-binder ratio, the Ca/Si decreases and this is associated with portlandite precipitation. It was shown that also alkali ions present in the pore solution can favor this process. Supersaturation indexes of C-S-H and portlandite calculated for the diluted systems showed that while C-S-H becomes close to be saturated after the first day, portlandite becomes slightly oversaturated. We believe the process responsible for this involves Ca being removed from the interlayer of C-S-H and released in the pore solution, where the increase in concentration leads to precipitation of portlandite.

3.1. Introduction

With almost 5 Gt produced in 2020 [2], cement is one of the world's most widely used artificial material. Following mixing with water, the developed microstructure of the hydrated cement systems can be complex in terms of hydration products. The main hydration product of alite and belite and the binding phase of the microstructure is the calcium-silicate-hydrate (C-S-H) [57]. Apart from C-S-H, another hydration product of the reaction of alite and belite is portlandite. Studies about the nature and properties of C-S-H go back many decades ago. The Ca/Si ratio of C-S-H has received significant attention, since it can vary between cement samples and even within the same specimen [35]. In a hydrated OPC, a C-S-H with Ca/Si ratio no higher than 1.80 is formed [58], but the value can get lower with increasing content of portlandite or increasing addition of silica fume [59].

In an early study, Lachowski and coworkers have reported a decrease of Ca/Si ratio for cement pastes at water-to-cement ratio 0.70 from 1 day to 28 days [60]. Later, Richardson and coworkers have determined the composition of C-S-H in a hydrated ordinary Portland Cement at water-to-cement ratio 0.40 by TEM and it was found that there was no systematic variation in C-S-H composition with age, and similarities between the Ca:Si ratio of Ip C-S-H and adiacent Op C-S-H were found [58]. In a different study done on cement pastes hydrated for 20 years at water-to-cement ratio 0.40, Taylor and coworkers have shown that when compared to 14 months, the Ca/Si ratio changes for both inner and outer product, the inner product C-S-H having a lower Ca/Si ratio after 20 years and the outer product having a higher ratio [61].

Apart from age, there was also early evidence of changes in C-S-H composition with water-to-cement ratio. In their work, Rayment and coworkers have investigated cement pastes hydrated at water-to-cement ratio 0.3 and 0.6 for 5 years. No variation of the Ca/Si ratio between the samples was found, although the Ca/(Si+Al+S+Fe) ratios were significantly different. The proportions of calcium in C-S-H show an increasing trend with decrease in the water-to-cement ratio used in preparing the paste. No conclusion could be drawn based on these results, as the paste prepared with 0.3 had substantially more unhydrated grains and presumably more regions of microcrystalline CH, although a change in the C-S-H/microcrystalline CH ratio within the analyzed volume could not be directly confirmed. There was as well six times more CH in the paste prepared at higher water-to-cement ratio [62], [63]. Zajac and coworkers [64] showed how in hydrated cement paste containing various amounts of limestone and hydrated at different water-to-binder ratios, the composition of the C-S-H phase measured by SEM-EDS changes both with water-to-binder ratio and with age. The Ca/Si ratio decreased with increasing w/b ratio and lower values were recorded at 90 days compared to 28 days. Higher w/c of the paste (in the range of 1.0) enabled reaching the thermodynamic equilibrium indicated by the GEMS model (a Ca/Si ratio close to 1.60). A different water-to-cement ratio was also found to affect the nucleation and growth of CH. With decreasing w/c ratio, the nucleation times decreased, probably as a result of a smaller available pore solution volume and a different rate at which supersaturation is achieved. There was no clearly identifiable effect on growth rate [65]. Work done by Bazzoni revealed there is a higher portlandite content at all times in a hydrated alite paste with w/c ratio 0.8, compared with w/c ratio 0.4. The study also showed there is a continuous increase in the Portlandite content with time for the higher w/c ratio paste, while for the lower w/c ratio paste the increase is low after 24 hours [30]. Portlandite was also observed to have different nucleation and growth patterns in pure C_3S and in OPC systems. By hydration of C_3S, fewer, larger and randomly

distributed clusters are generated, while in PC systems containing C$_3$A and gypsum, there are numerous small particles, evenly and closely distributed in the matrix [66].

When the water used to prepare the specimens contains alkali and sulfate ions present, this can cause an early acceleration of the hydration rate. Experiments done by Kumar and coworkers [67] on hydrated alite with increasing concentration of alkali hydroxide showed that the C-S-H had similar morphology in all samples. Although at higher alkali concentration, the amount of portlandite was as well higher, the Ca/Si ratio for all samples remained withing the range of 1.70 at 30 h hydration age. Mota and coworkers have investigated the influence of NaOH on the microstructure of hydrated white cement and it was found that the precipitation of portlandite is slightly higher in the presence of NaOH, while the (Ca-S)/(Si+Al) ratio in C-S-H was lower in presence of NaOH compared to the alkali free system. [68]. Macphee and coworkers have reported as well increased Ca(OH)$_2$ contents from hydrated alite in presence of NaOH solution, relative to hydration in water [69]. In their work, Berodier and coworkers studied the effect of adding 2% and 4% gypsum to the microstructure of hydrated white cement. A reduction of the C-S-H gel water and change in C-S-H morphology were reported. Addition of gypsum also slowed down the reaction of alite and the content of portlandite at a given age is lower for samples containing gypsum [70].

The present study aims to investigate how the C-S-H composition can change with time in pastes prepared with different water-to-cement ratio and containing different amounts of alkali or sulfate. A reactive dicalcium silicate binder was selected to produce the C-S-H rich microstructure in confined space. From fundamental aspects, hydration of this C$_2$S binder is similar to hydration of alite or OPC and leads to formation of C-S-H as fibrous crystals [71]. The main advantage of this type of binder is that the microstructure will contain mostly C-S-H as hydration product, enabling the study of this phase isolated from other phases. In recent years, there has been a revival of interest in high-belite cements, due to lab-scale successes of synthesizing reactive belites at low temperatures [72]. Recent studies have described a hydrothermal process followed by calcination to obtain a reactive C$_2$S binder, which consists of two hydrating phases: an X-ray amorphous calcium silicate phase with Ca/Si ratio 2 and x-C$_2$S [22], [73]. Important findings about this material are related to changes in Ca/Si ratio of C-S-H and resulting morphology when calcium sulfate hemihydrate or nano-SiO$_2$ were hydrated with the C$_2$S.

3.2. Materials and methods

3.2.1. Anhydrous binder

The starting material used in this study was an industrially synthesized α-C$_2$SH provided by HeidelbergCement. The α-C$_2$SH was synthesized via the hydrothermal route. For that, a mixture of calcium hydroxide, reactive silica and very fine α-C$_2$SH seeds was used to prepare a paste with CaO/SiO$_2$ molar ratio of 2.0. The mixture was autoclaved at 200°C for 20 hours and the resulting material was dried at 105 °C for 24 hours. After drying, the α-C$_2$SH was ground using a Siebtechnik disk-mill for 3 mins. SikaGrind®-870 grinding aid was used as 0.2% of the weight of the powder, to prevent big agglomerates from forming. For the particle size distribution of the powders, a Malvern Mastersizer 3000 was used. The d_{50} value of the obtained powder was lower than 3 μm. The material was then thermally processed in a Thermo Scientific™ M110 oven. The temperature was 460 °C and

the duration 2 hours. The resulting binder was rapidly cooled down in air and ground in the disk mill for 1 minute (Siebtechnik). The oxide composition of the synthesized C$_2$S binder was determined by X-ray fluorescence spectrometry using a PANalytical AxiosMax and is given in Table 3-1. The XRD patterns of the powders were obtained at room temperature using a Bruker D-8 Advance diffractometer in a θ-θ configuration with CuKα radiation (λ = 1.54059 Å) and for the Rietveld analysis the external standard method was used, using quartzite. The phase composition was determined by XRD coupled with Rietveld refinement and is shown in Table 3-2.

Table 3-1. Chemical composition of the reactive C$_2$S binder determined by XRF analysis

Oxide	CaO	SiO$_2$	MgO	K$_2$O	Al$_2$O$_3$	SO$_3$	LOI (1050°C)
Amount, %	61.36	33.29	0.57	0.13	0.00	0.17	4.07

Table 3-2. Mineralogical composition of the binder determined by XRD-Rietveld refinement

Phase	amorphous-C$_2$S	x-C$_2$S	γ-C$_2$S	CaCO$_3$ (as calcite and aragonite)	Other impurities (portlandite, afwillite, dellaite, scawtite, killalaite)
Amount, %	50	17	13	6	14

3.2.2. Hydration

Pastes were prepared at different water-to-binder ratios (from 0.25 to 0.80), mixed for 2 mins at high speed and at a high shearing rate using ULTRA-TURRAX® - IKA blender. For the pastes with water-to-binder ratio lower than 0.40, a superplasticizer admixture BASF ACE30 was added as 1% (weight of the solution) of the weight of the binder. The second set of pastes was prepared with the reactive C$_2$S binder and using instead of mixing water, a 0.1N and a 0.5N solution NaOH, keeping the curing conditions identical with the other systems. The third set of pastes was prepared by adding 5 % REA gypsum in the binder powder and dry mixing it for 1 hour prior to casting. Last set of samples contained 5 % gypsum and were prepared using 0.1 and 0.5N NaOH solution. All samples were kept sealed for 24 hours, then were demolded and cured in lime water, in plastic recipients having the diameter slightly bigger than the samples.

To follow the formation of C-S-H and portlandite in a diluted environment, suspensions were prepared. First, 25 grams of paste prepared at w/b=0.35 from the plain binder were kept sealed for 1 hour. After that, the paste, being still fluid, was transferred in a bigger container with 125 mL liquid. One set of suspensions was prepared in water and another one in 0.1N NaOH solution. The suspensions were kept sealed at room temperature and they were not stirred. After 1 hour, 1 day and 7 days of curing, the suspensions were shaken for 1 minute and then the solid part and liquid part were separated by gravitational filtration and characterized. A summary of all prepared samples in this study is presented in Table 3-3.

The total concentrations of the elements were determined using inductively coupled plasma optical emission spectroscopy/mass spectroscopy (ICP-MS Agilent 7800 and ICP-OES Agilent 5110 depending on the concentration of the elements). The measurements were performed not later than 2 h after pore solution extraction. Saturation indexes were calculated using the Gibbs free energy

minimization program GEMS v3.3 [74], [75]. The thermodynamic data for aqueous species, solids and gas phases include the PSI-GEMS thermodynamic database [76], [77] and the cement specific database [78] including some zeolites [79], [80].

Hydrate characteristics were observed at different hydration ages by stopping the hydration reaction using the solvent exchange technique, using isopropanol followed by a quick washing with petroleum ether [81].

An isothermal conduction calorimeter (Thermometric TAM Air) was used to determine the rate of hydration and heat release during the first 7 days at 20°C. A paste with water-to-binder ratio 0.8 was prepared and filled in the calorimeter directly after mixing. Thermogravimetric analysis was carried out on ground hydrated binder using a NETZSCH STA F449 device. The weight loss was monitored while heating up a 30±1 mg sample until 1050 °C at 20°C/min in N$_2$ atmosphere. X-Ray diffraction patterns were collected on powder samples as described in section 2.1. A scanning electron microscope Zeiss EVO LS10 with a Quantax400 Detector from Bruker was used to investigate the microstructure of the hydrated specimens. For chemical analysis of the C-S-H, EDS point analysis and mapping were carried out on selected areas. All samples for SEM investigations were impregnated under vacuum with a spectrally transparent epoxy resin (EpoTek® 301). Thin slices from hydrated specimens were used, except for the samples hydrated in suspension, where impregnated hydrated powders were preferred. The impregnated samples were gradually polished down to 1 μm with a diamond spray and petrol as a lubricant and coated with a thin conductive layer of carbon (15 nm). For morphology investigations of hydrates, dried powder specimens were dispersed on an adhesive carbon tab and coated with a 5 nm iridium layer. The samples were analyzed using Zeiss Merlin ultra-high-resolution FE-SEM (Field Emission SEM). For MIP measurements, bulk hydrated samples were crushed and the fraction 1-2 μm was selected. The analysis was performed using a Pascal 140/440 Porosimeter from Thermo Scientific up to a maximal pressure of 400 MPa.

For the assessment of the degree of hydration, the content of x-C$_2$S was determined by XRD-Rietveld refinement. It has been shown in [22] that the amorphous-C$_2$S is the first phase to hydrate so this phase is considered completely reacted when the DoH is calculated for samples hydrated for at least 12 hours. The following relation is used:

$$DoH = \frac{w_{amorph}+w_{x-C_2S,0}-w_{x-C_2S,t}}{w_{amorph}+w_{x-C_2S,0}} \cdot 100 \qquad (1)$$

where w_{amorph} is the X-Ray amorphous phase content, $w_{x-C_2S,0}$ is the initial content of x-C$_2$S and the $w_{x-C_2S,t}$ is the content of x-C$_2$S at a given hydration age.

Table 3-3. Summary of prepared samples. For the preparation of pastes with w/b 0.25 and 0.35, superplasticizer was used as described in the text. Paste prepared at w/b 0.80 didn't experience any bleeding.

Pastes				Suspensions	
Reactive C$_2$S	+ 5% gypsum	+ NaOH	+ 5% gypsum + NaOH	Reactive C$_2$S + water (w/b=0.35)	Reactive C$_2$S + 0.1M NaOH sol. (w/b=0.35)
		0.1M and 0.5M solutions			
w/b = 0.25, 0.35, 0.50, 0.80	w/b = 0.35			water/paste = 5.0	

3.3. Results and discussion

3.3.1. Hydration of reactive C₂S binder

The hydration reaction of C₂S leading to formation of C-S-H and portlandite is represented as follows:

$$C_2S + yH_2O \rightarrow C_x SH_y + (2\text{-}x)CH$$
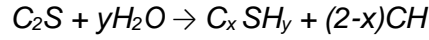
where, in a typical OPC paste, x value averages at 1.70, while y can be 4 or lower, depending on the saturation state of the C-S-H.

The calorimetry curve for the C₂S sample hydrated at w/b=0.80 is shown in Figure 3-1a. The main peak of hydration associated with the hydration of the amorphous phase occurs in the first 12 hours and there is a small shoulder present between 18 and 40 hours of hydration, corresponding to the hydration of the x-C₂S, which is less reactive than the amorphous phase. After 48 hours, no significant amount of heat was released from the hydration of the binder (only 8% of the heat was released between day 2 and day 7).
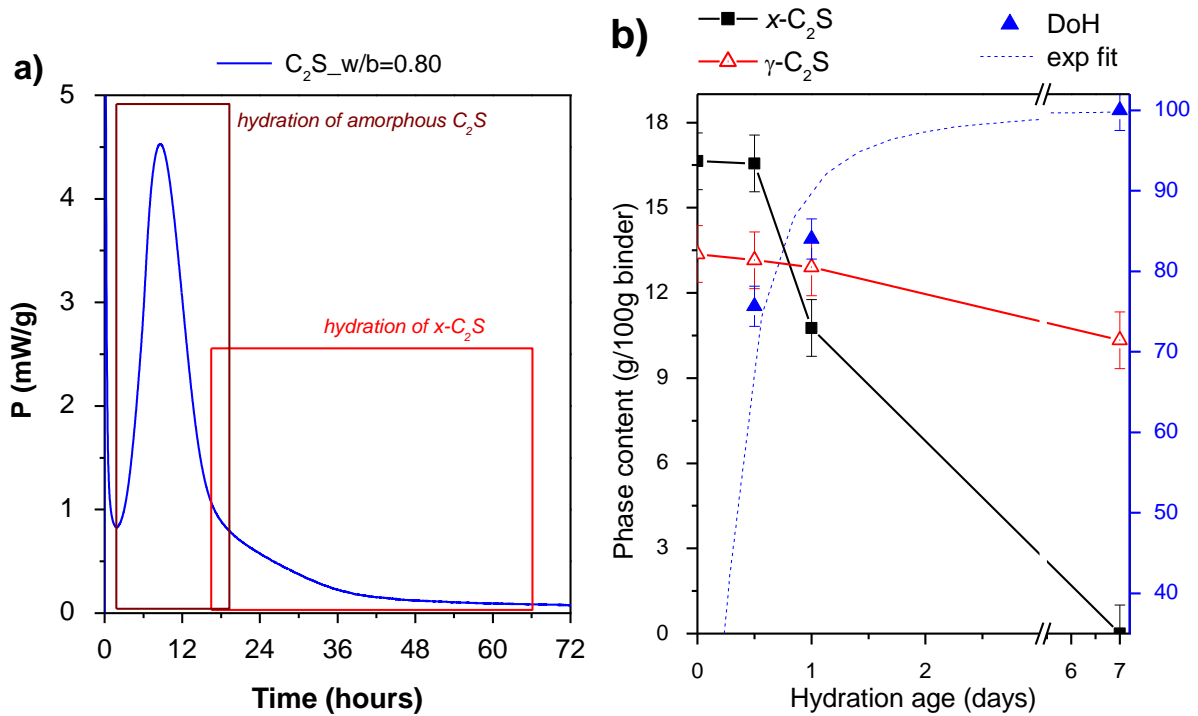
Figure 3-1. (a) Heat flow curve corresponding to paste prepared with w/b=0.80 and (b) x-C₂S & γ-C₂S content and DoH evolution for a paste prepared with w/b=0.35

In Figure 3-1b, the x-C₂S content, γ-C₂S content and degree of hydration calculated using Eq. (1) at different hydration ages for the paste prepared with w/b=0.35 are represented. DoH at 12h with respect to the x-C₂S phase is high, and it reaches more than 90% after 1 day. For samples analyzed after 7 days of hydration, no content of unreacted x-C₂S was observed by XRD. It was observed that a small amount of γ-C₂S phase has reacted within the first 7 days of hydration. The impurities described in Table 3-2 do not contribute to the hydration of the binder, due to being crystalline phases, they are inert in water and their content remains constant in time.

3.3.2. Evolution of C-S-H microstructure at different water-to-binder ratio

The microstructures of hydrated samples at w/b 0.25 and 0.80 are illustrated in Figure 3-2. In both SEM micrographs, one can observe that the hydrated matrix is formed of only one homogenous type of C-S-H, while the bright particles represent the inert phases (see Table 3-2). For the higher w/b ratio samples, some occasional large clumps of CH in close proximity of agglomerates of particles were also observed. From the SEM micrographs of the two samples, we can observe how the amount of pores of few μm in size is significantly reduced in the low water-to-binder ratio sample. A comparison of the porosities of the samples by MIP is given in Figure 3-15 in the Appendix of this chapter. A massive decrease in the total intruded volume and critical entry diameter was observed for sample prepared with w/b 0.35 compared to the higher w/b samples.

w/b = 0.25   w/b = 0.80
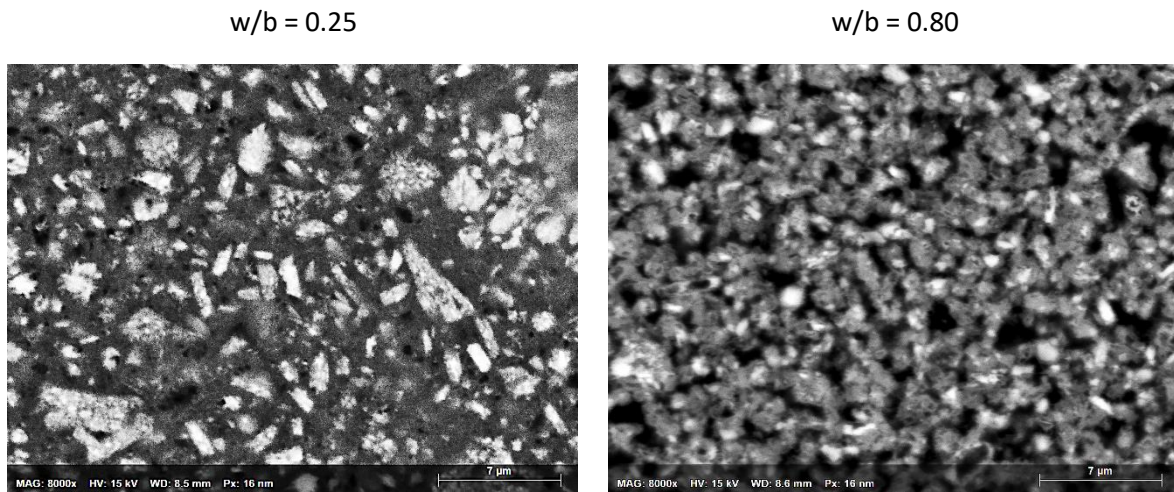
Figure 3-2. SEM micrographs of polished sections for samples with both high and low water-to-binder ratio, at same magnification (28 days of hydration)

The distribution of Ca/Si ratios from SEM-EDS analysis for a hydrated C$_2$S at w/b=0.35 at 7 days is given in Figure 3-3. The values reported in this study are average values determined from such histogram plots. The distribution is not wide, with a scatter of ±0.04. The Ca/Si ratio of C-S-H for the paste represented here is close to 2.0. In Figure 3-4, the DTG curves for three different water-to-binder ratios (0.35, 0.50 and 0.80) at same hydration age are given. With increasing water-to-binder ratio, an increase in the CH content is observed and the C-S-H dehydration peak is reduced in intensity. Furthermore, for the paste prepared with the lower water-to-binder ratio, portlandite presence could not be identified neither by TGA nor by SEM.
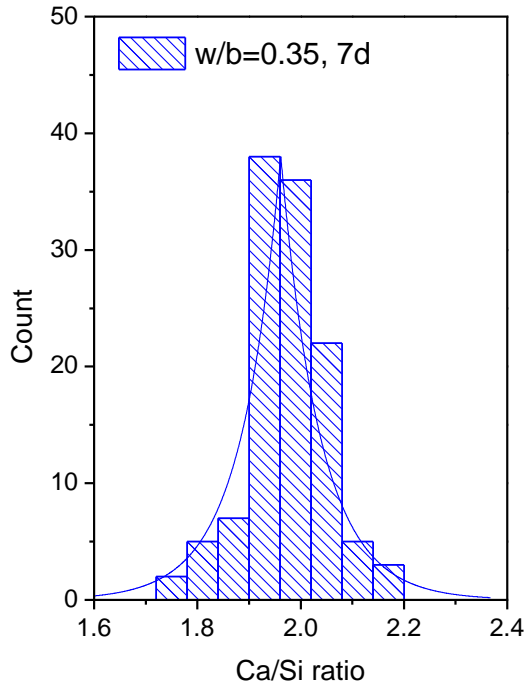
Figure 3-3. Distribution of Ca/Si ratio values from SEM-EDS
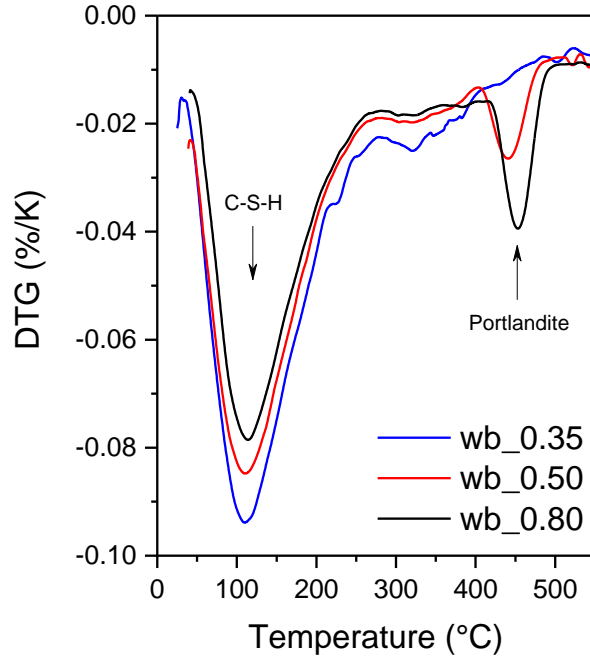
Figure 3-4. DTG curves for pastes prepared with various water-to-binder ratios at 7 days

The portlandite amount determined by TGA and the Ca/Si ratio determined by SEM-EDS for different samples is plotted in Figure 3-5. Quantification of CH content was done exclusively by TGA, as XRD did not provide results accurate enough in case of samples with very low content. For samples having water-to-binder ratios 0.35 and 0.80, the Ca/Si slightly decreased between 12 hours and 28 days of hydration age, this is associated with an increase in portlandite content. As the water-to-binder ratio is increased from 0.35 to 0.80, the Ca/Si ratio of the developed C-S-H at the same hydration age again decreased and portlandite content determined by TGA increased. For sample with w/b=0.5, the 7 days age was used for the comparison instead of 28 days age, which was compromised. Given the fast hydration of the reactive phases, significant changes are not expected between 7 days and 28 days, thus the Ca/Si ratio and the portlandite content of the paste prepared with w/b 0.5 agree well with the observed trend for pastes hydrated at w/b ratio 0.35 and 0.80 for 28 days. The values are in good agreement with the expected content of portlandite calculated using mass balance (plotted black line). A difference between the value calculated from mass balance and the experimental value is observed for sample prepared at w/b ratio 0.8 at 12 hours, due to incomplete hydration.
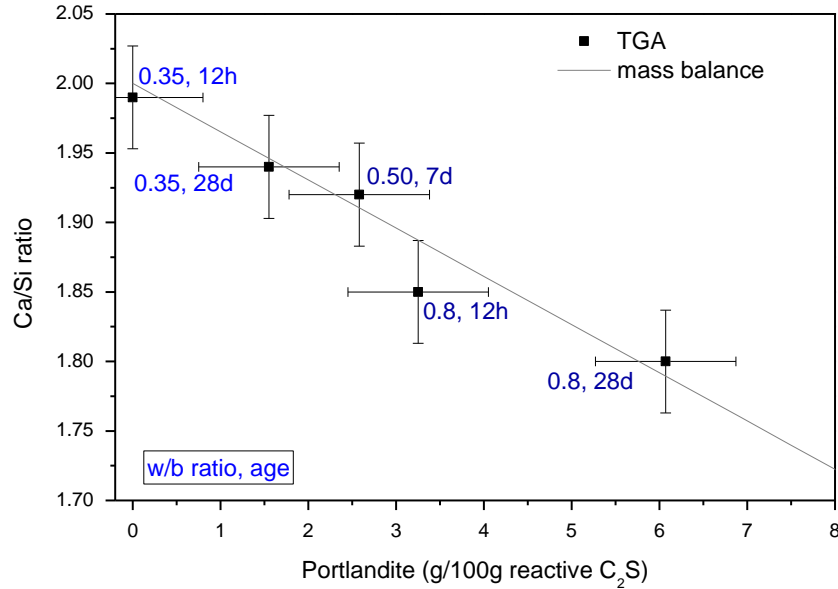
Figure 3-5. Portlandite content by TGA as a function of the hydration age for samples with different water-to-binder ratios

The evolution of the bound water content in C-S-H with hydration age for two pastes having different water-to-binder ratios (0.35 vs. 0.80) is illustrated in Figure 3-6. The bound water content of the C-S-H per Si (molar ratios) was determined by normalizing the bound water content from TGA to the Si content in the C-S-H, using the amorphous content from XRD-Rietveld refinement. It was observed that the H_2O/Si ratio goes down with hydration age in both samples and the samples prepared at w/b=0.35 have at all ages higher values than pastes with w/b=0.80.
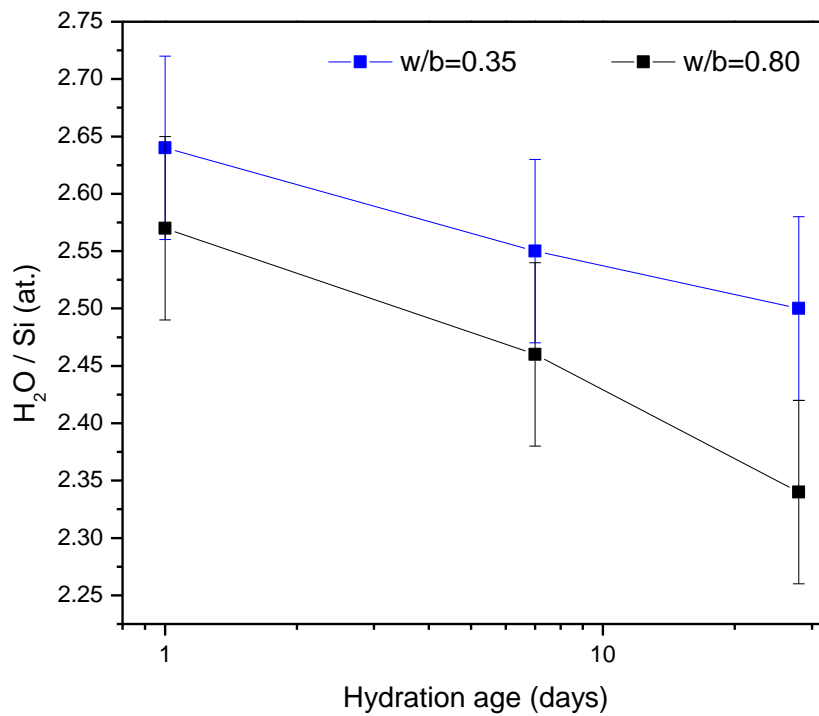
Figure 3-6. Evolution of the bound water per Si function of hydration age for two different water-to-binder ratios

3.3.3. Evolution of C-S-H composition in presence of alkali and sulfate

The Ca/Si ratios determined for 28 days pastes prepared with and without gypsum and with different concentrations of NaOH are given in Figure 3-7. In the case of the specimens containing gypsum, the (Ca-S)/Si is represented instead of the Ca/Si, to take into account the additional Ca from gypsum. With increasing concentration of alkali, there is a progressive decrease of the Ca/Si ratio of the C-S-H, this reduction being more pronounced for the systems without gypsum. The lowest value of the Ca/Si ratio was for the sample hydrated with 0.5N NaOH and without gypsum. Concerning the S/Ca ratio, the averaged value measured in all systems containing gypsum was 0.04 and it agrees well with the value calculated from mass balance. Uptake of alkali was as well quantified by SEM-EDS and it was observed that for the samples prepared with lower concentration of NaOH, the Na/Ca ratio was comparable to the background signal of the BSE detector. For the sample with higher NaOH concentration, there was no gaussian distribution of the Na/Ca ratios, but rather two peaks were identified, one around the value 0.02 and another one close to 0.070 (Figure 3-16 in the Appendix of this chapter).
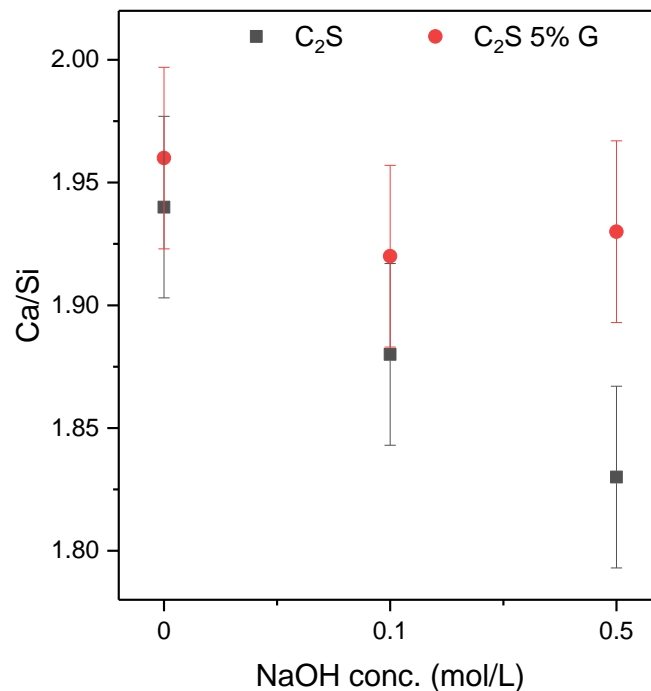
Figure 3-7. Average Ca/Si ratios of C-S-H after 28 days determined from SEM-EDS for sample with and without gypsum and prepared using 0.1 N or 0.5 N NaOH solution

Portlandite content of the six systems at 28 days of hydration is represented in Figure 3-8. In the alkali free pastes (both with and without gypsum), the portlandite content was relatively low (< 2g CH/100g binder). Hydration of C$_2$S in presence of NaOH but without gypsum resulted in more CH precipitated (black squares), the content being higher when the NaOH concentration was higher. In the pastes containing gypsum hydrated with NaOH (red circles), there was less CH formed at all ages as compared with the gypsum free pastes (black squares), but slightly more than in the case of alkali free system (left red circle). The microstructure of the sample with the highest content of CH is given in Figure 3-9. Instead of big clusters, portlandite was found precipitated in fine lines scattered throughout the matrix, possibly due to filling of micro-cracks from self-desiccation during hydration.
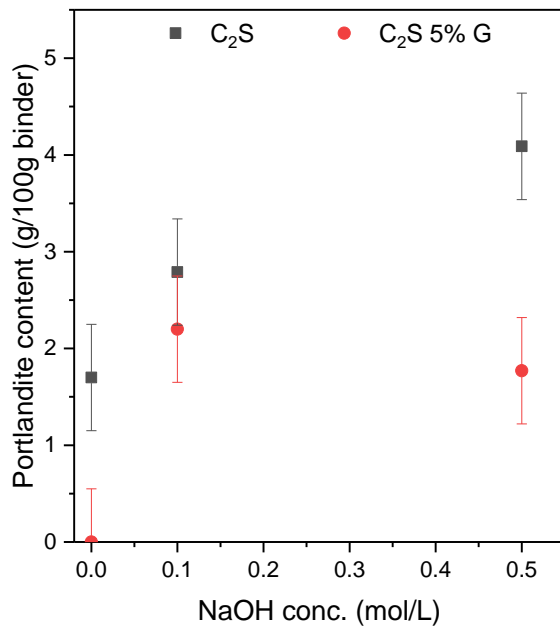
Figure 3-8. Portlandite content after 28 days determined from TGA for sample with and without gypsum and prepared using 0.1 N or 0.5 N NaOH solution
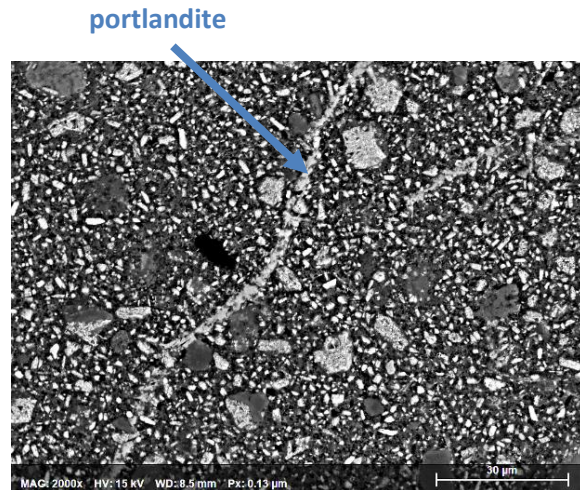
Figure 3-9. SEM microstructure of a paste prepared with 0.5 N NaOH solution after 28 days of hydration, illustrating a trail of precipitated CH, which filled a micro-crack

TGA and SEM results for the solid parts of C_2S suspensions in water and NaOH are given in Figures 3-10 – 3-12. In Figure 3-10, the DTA curves for the powders hydrated for 1 hour, 1 day and 7 days are illustrated. The carbonate content for all hydrated samples is comparable with the carbonate content of the anhydrous C_2S. After 1 hour of hydration, very low amounts of C-S-H were formed, while CH was not yet precipitated. After 1 day of hydration, a significant amount of both C-S-H and CH was present in both systems, the one with NaOH having formed more portlandite than the alkali free one. After 7 days of hydration, there were significant differences between the two systems: the sample hydrated in water had a higher content of C-S-H than the one prepared in NaOH solution, while in the latter system there was more CH precipitated than in the former.
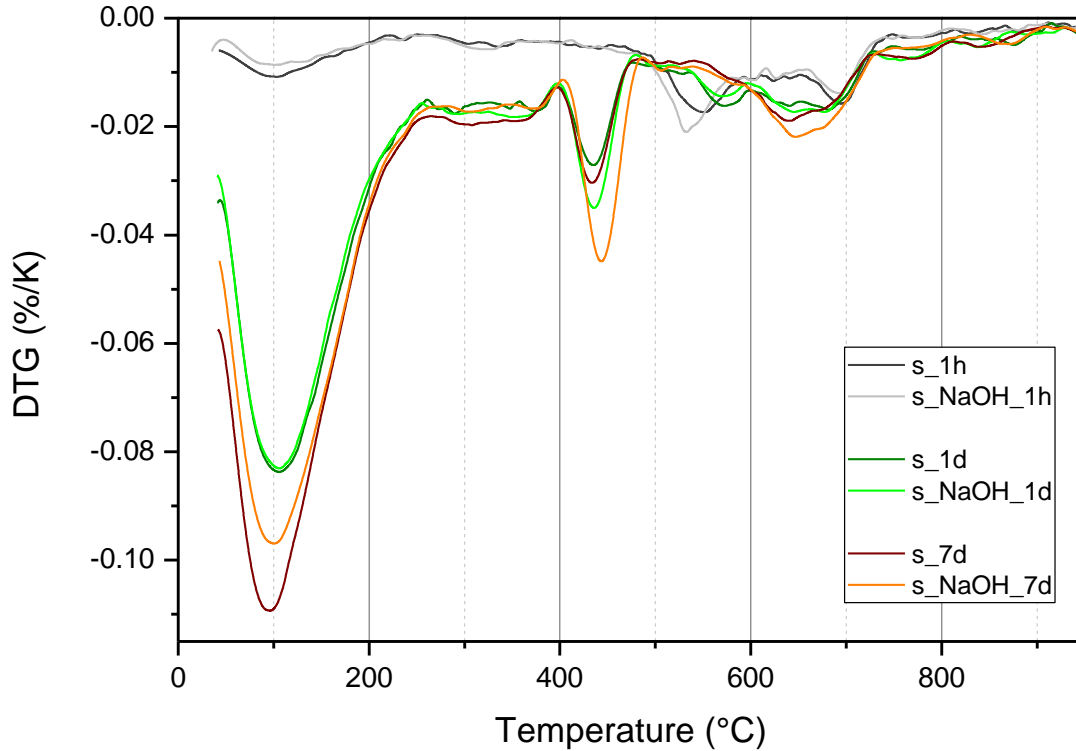
Figure 3-10. DTG curves for the two sets of samples hydrated in suspension at 1 hour, 1 day and 7 days

The evolution of the CH content with hydration age in each system is shown in Figure 3-11. For both represented systems there is more CH formed with hydration age, although the increase is higher in the case of the sample hydrated in NaOH solution. Additionally, in the alkali containing system more CH formed than the alkali free system at the same hydration age (20% more at 1 day and 40% more at 7 days). In Figure 3-12, the Ca/Si ratios of C-S-H for the two hydrated samples at 1 day to 7 days are given. Experimental values determined by SEM-EDS are compared with mass balance estimations, considering the CH content determined by TGA shown in Figure 3-10. Mass balance estimations predicted a slight decrease in Ca/Si ratio of C-S-H with age for both water and NaOH suspension samples. Additionally, at the same hydration age, the C-S-H formed in water should have a higher Ca/Si ratio than the C-S-H formed in NaOH. Values from SEM-EDS also had a decreasing trend with hydration age, but the differences between the water and NaOH sample were not significant. This could have been caused by the fact that in the absence of a solid microstructure, powder samples were impregnated in resin and analyzed. After 7 days of hydration, the Ca/Si ratio of C-S-H formed in both suspensions was 1.70 ± 0.04. This value is similar with the one that has been reported for C-S-H in the hydrated OPC systems [58]. When comparing the Na/Si ratios of the C-S-H for the alkali containing pastes, we observed very low values for both 1 day and 7 days samples (0.041 and 0.046, respectively), suggesting a rather low Na uptake by the C-S-H at this NaOH concentration.
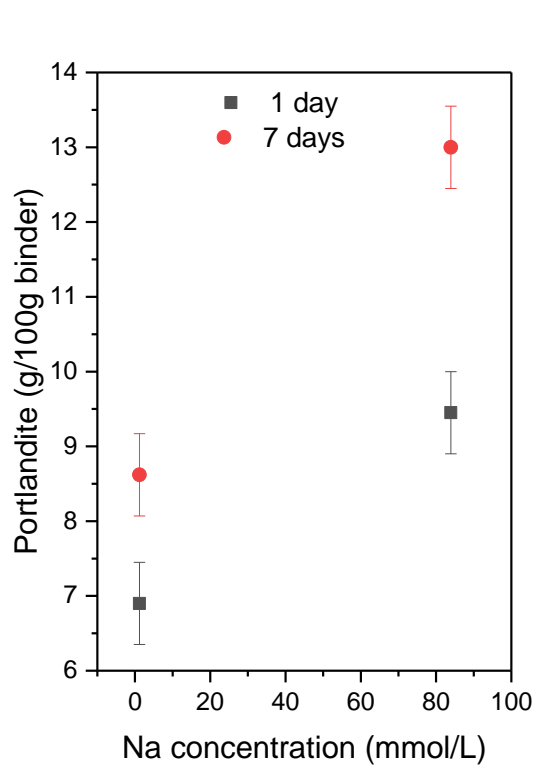
Figure 3-11. Portlandite content determined from TGA for samples hydrated in suspension after 1 day and 7 days of hydration
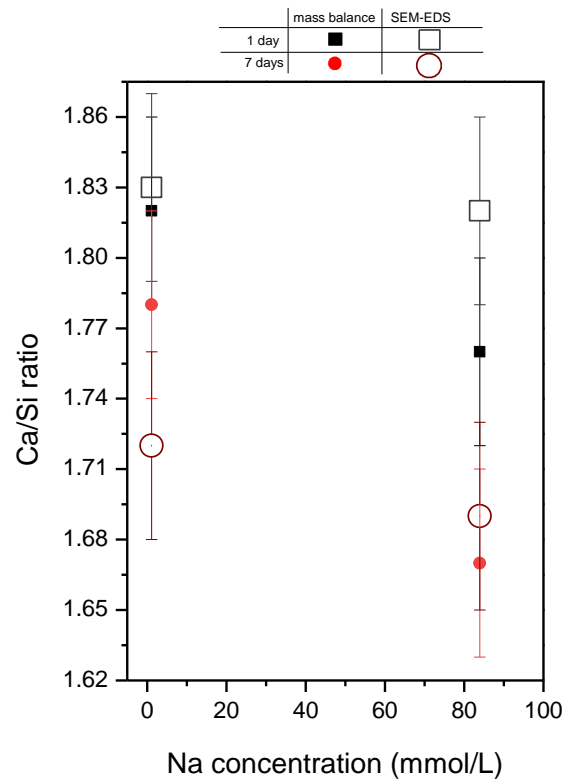
Figure 3-12. Average Ca/Si ratio for samples hydrated in suspension after 1 day and 7 days of hydration (full symbols-determined from mass balance, empty symbols-measured by SEM-EDS)

The saturation indexes of C-S-H and CH are given in Figure 3-13. Within the thermodynamic model applied, the calculation was conducted against a CSHQ solid solution. For more information about the model and the end member, the reader is referred to [82]. The elemental concentrations of the filtered solutions used for the calculation of the S.I. are given in Table 3-4 in the Appendix of this chapter. The S.I. of CH had values ≥ 0 at all ages and for both water and NaOH suspension, showing that the solution is slightly oversaturated with respect to this solid phase. Concerning the S.I. of the C-S-H, positive values for different C-S-H species were determined only for the samples kept for 1 hour in suspension. After 1 day the pore solution becomes slightly undersaturated with respect to the considered C-S-H phases, indicating that this should not precipitate, but rather dissolve during the experiment.
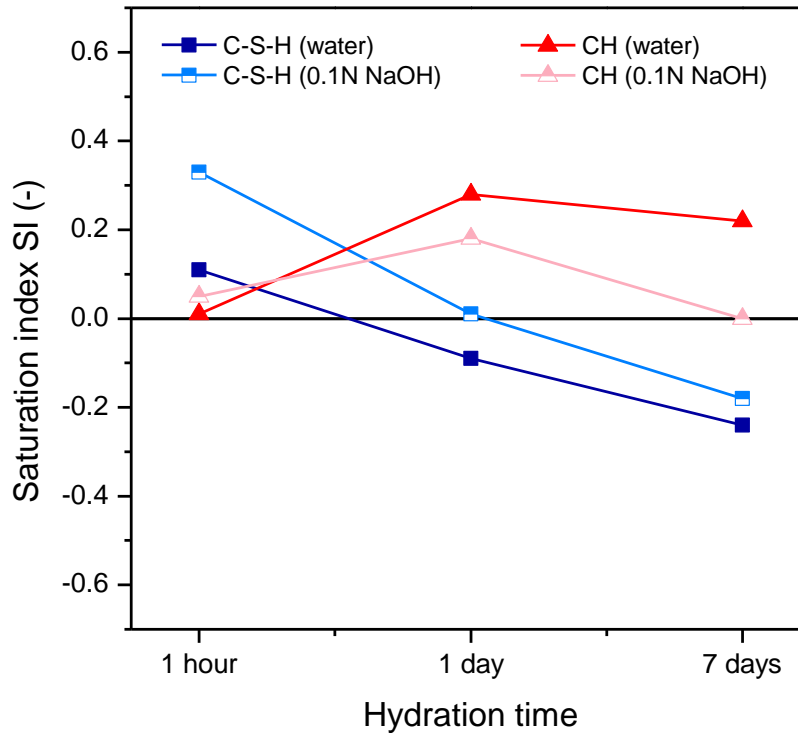
Figure 3-13. Evolution of the saturation indexes over the hydration time for C-S-H and CH from the water and NaOH suspensions

In Figure 3-14, SEM images collected on powder samples at 7 days for hydrated C$_2$S and C$_2$S with alkali are illustrated. The matrix is formed of elongated particles with needle-like aspect of different lengths and mostly intergrown (Figure 3-14 left). When comparing it with the C-S-H formed in presence of 0.5 N NaOH solution, we didn't observe the same homogenous morphology, but rather fibrils with very heterogenous lengths and shapes.
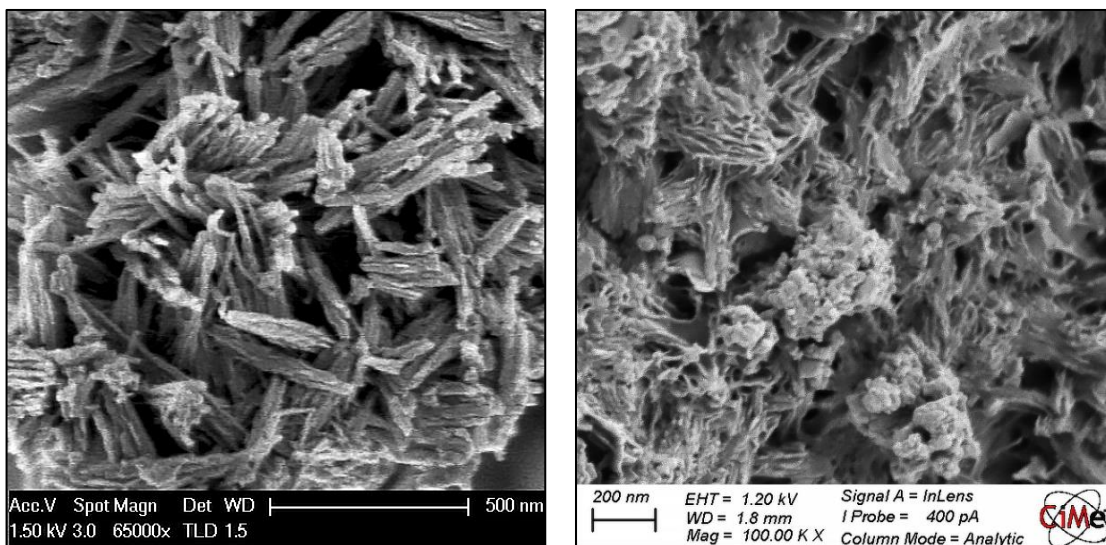
Figure 3-14. SEM morphology images of hydrated binder prepared at w/b ratio of 0.50 (left) and at 0.35 with 0.5 N NaOH solution (right), both after 7 days of hydration

3.3.4. Discussion – changes in the C-S-H chemistry

The Ca/Si ratio of C-S-H formed in the first 12 hours of hydration is higher than the one measured after 28 days, irrespective of the water-to-binder used. As the Ca/Si ratio decreases with hydration age, more CH precipitates in the matrix. In some C-S-H models, it was suggested that with increasing Ca/Si ratio, all protons in Si-OH groups are replaced with interlayer Ca before additional Ca (in excess of what is required to balance silicate anions) is introduced as Ca-OH [83]. This additional Ca-OH is mobile and could be removed from the interlayer and go into the pore solution, being responsible for the decrease of the Ca/Si ratio with age. As the Ca concentration increases in the pore solution and with Si concentration being low, it could increase the supersaturation with respect to CH, thus leading to precipitation of this phase. The removal of Ca-OH groups with hydration age could be as well responsible for the decrease of the H_2O/Si ratio illustrated in Figure 3-5. A possible trigger for the changes in Ca/Si ratio could be the changes in Ca and Si concentrations in the pore solution. Due to the fast reaction of the amorphous phase, the pore solution has a higher Ca and Si concentration in the first hours of hydration. This ensures that the pore solution is supersaturated with respect to C-S-H and hydrates are continuously precipitating. After the amorphous phase is depleted, Ca concentration decreases and the stability of the high Ca/Si ratio C-S-H is reduced. The initial absence of portlandite was observed in both low and high w/b paste and in the suspensions prepared with water and NaOH solution. An interesting observation about the S.I. of C-S-H and CH in the suspensions is that while at 1 hour, the values of S.I. for C-S-H are higher than the ones of CH, at 1 day and 7 days of hydration the situation is reversed. It is not very clear at this point what is responsible for this phenomena, although an interesting aspect regarding the hydration of the binder is that at 1 day, the amorphous phase is completely reacted, while approx. 38 % of the x-C_2S is still unreacted (in a suspension with w/b > 5). As mentioned by Zajac and coworkers [84], for the hydration of Portland cement and composite cements, the mechanism of the C-S-H phase growth does not change with time, even if the available space for the growth decreases and refines considerably. The same applies for the portlandite in the neat Portland cements, where the S.I. do not change with time, so the space available does not limit the hydration. While this could be valid for the hydrated C_2S at w/b ratios ≥ 0.50, for lower w/b ratio, given the extremely small amount of alkali, the supersaturation required for the precipitation of CH in confined microstructure might not be reached. The required supersaturation could be decreased if more alkali is introduced, which is why we observe CH in the matrix of the paste prepared with w/b 0.35 and using 0.5 NaOH (Figure 3-9). Presence of alkali in the pore solution will increase the pH and increase the concentration of silica and decrease the concentration of calcium [69], together with the solubility of portlandite [85]. One must also be careful when comparing the processes happening in suspension and in low w/c paste, as the trends observed for the S.I. of C-S-H and CH in suspension might be different for the other scenario. Additionally, the thermodynamically available data for C-S-H might not be fully representative for the high Ca/Si ratio C-S-H initially formed from the reactive C_2S. At the same time, a negative value of the S.I. of C-S-H could as well be an indication of its metastable character with respect to the pore solution, which tends to reach equilibrium through the lowering of the Ca/Si ratio.

Concerning the alkali uptake by the C-S-H, a low and heterogenous presence of alkali on the surface of C-S-H is not surprising, there are two factors that can account for this: first, the Ca/Si ratio of the C-S-H is very high, it was reported that above 1.6, alkali ions are not efficiently absorbed in the C-S-H; second, the concentration of NaOH was not sufficiently high. Studies on uptake of alkali in

synthetic C-S-H have reported very low Na/Si ratios when the Ca/Si ratios is higher than 1.50 [52]. When gypsum is present in the alkali hydrated systems, CH precipitation occurs, but in a lower amount than in the alkali system. The sulfate is absorbed by the C-S-H and it seems to slow down the release of Ca from interlayer, but more evidence is needed before any conclusions can be drawn.

Studies such as [68], [69] have reported that addition of alkali lead to significant changes in C-S-H morphology, such as more "divergent" needle structure. The high concentrations of alkali used lead to significant changes in the C-S-H composition as well, both of which are consequence of the changes in the pH of the pore solution. In this study, due to relatively low NaOH concentration, all the investigated C-S-H systems had a relatively high Ca/Si ratio and the only difference in morphology between samples prepared with and without alkali is the loss to some extent of morphological aspects.

3.4. Conclusions and perspectives

Evidence presented in this study indicates that the reactive C$_2$S binder leads to formation of a homogenous C-S-H matrix with limited amount of inert inclusions. The C-S-H that precipitates in low water-to-binder ratio conditions has a high Ca/Si ratio (almost 2.0), in the absence of portlandite. The main factor which we believe is responsible for this is the high supersaturation with respect to CH required for the precipitation in confined space, in the absence of alkali. The Ca/Si decreases with increasing w/b ratio and formation of portlandite is observed. Presence of alkali ions lead to formation of C-S-H with lower Ca/Si ratio and increased CH content. Presence of sulfate will counterbalance to some extent the alkali influence on the C-S-H, maintaining the Ca/Si higher and the CH amount lower. It was shown that precipitation of portlandite occurs much later than precipitation of C-S-H, even when the binder was hydrated in a suspension. CH was not observed after 1 hour of hydration, just limited amounts of C-S-H were formed, but significant amounts of CH were present in samples hydrated for 1 day. After 7 days of hydrating the binder in suspension, the Ca/Si ratio of C-S-H was close to 1.70, which is considered the thermodynamically stable form that is found in hydrated alite or OPC systems. The advantage of having a matrix formed only of one type of homogenous C-S-H include studying influences of added ions in the structure (such as alkali and aluminum) and also properties that can be related the durability issues, such as transport properties.

Acknowledgments

Appendix
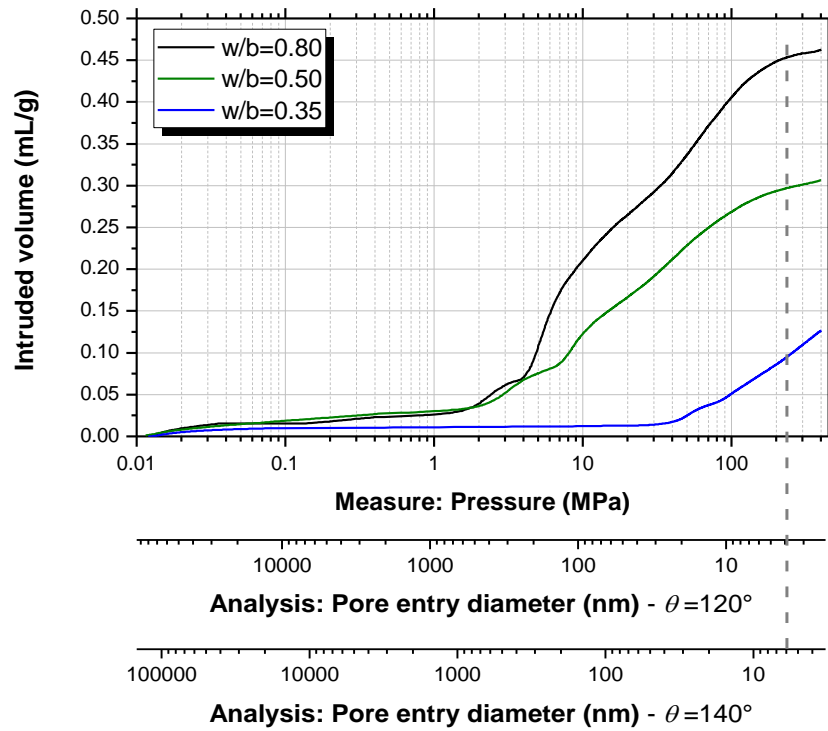
Figure 3-15. MIP curves for pastes prepared with water-to-binder ratio 0.80, 0.50 and 0.35 at 28 days of hydration. Clear differences can be observed between the total intruded volume and the critical entry diameter of paste with w/b 0.35 and the other two ones (vertical line was arbitrary placed at 6 nm pore diameter for visual guidance).
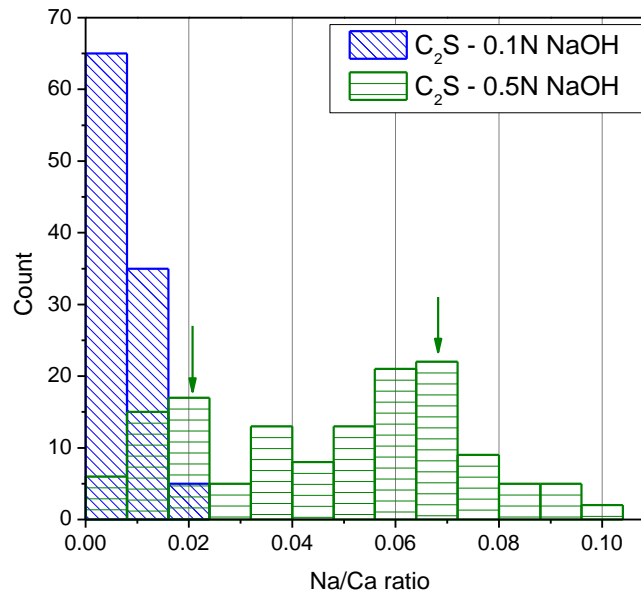
Figure 3-16. Distribution of Na/Ca values of C-S-H for pastes prepared with 0.1N NaOH and 0.5N NaOH at w/b=0.38, age 28 days. For the lower NaOH concentration paste, the alkali content in C-S-H is close to 0. For the higher NaOH concentration paste, there is no gaussian distribution of the values, rather a very broad distribution.

Table 3-4. Concentrations of elements in filtered solutions, determined by ICP-OES. For both water and NaOH system, the Ca concentration peaks at 1 day of hydration age and slightly decreases afterwards. In the suspension containing alkali, Ca concentration is four times lower at all ages, while Si concentration is almost two times higher. While the Na concentration is very low in the suspension prepared with water, in the NaOH suspension Na slightly decreases with age. All the other elements had very low concentrations for all hydration ages.

Suspension	Ca-ICP-OES Solution	Si-ICP-OES Solution	Al	Na	K	S	Mg	pH
	mmol/L	mmol/L	mmol/L	mmol/L	mmol/L	mmol/L	mmol/L	
water_1 hour	19.399	0.051	0.002	0.489	1.942	0.230	0.001	**12.59**
water_1 day	26.447	0.016	0.003	0.876	3.287	0.050	0.001	**12.81**
water_7 days	24.214	0.011	0.002	1.181	4.630	0.048	0.000	**12.81**
NaOH_1 hour	5.240	0.088	0.004	100.913	2.033	0.305	0.001	**13.13**
NaOH_1 day	7.298	0.026	0.002	91.670	3.159	0.136	0.001	**13.16**
NaOH_7 days	5.489	0.019	0.001	83.950	4.400	0.165	0.000	**13.11**

Chapter 4.   Reaction of silica and metakaolin with high Ca/Si ratio C-S-H microstructure

Abstract

The influence of silica and metakaolin on the microstructure of the hydrated C_2S binder was studied by means of SEM, TEM, MIP and FTIR. A reduction in the Ca/Si ratio of C-S-H was observed for all samples, although results from SEM are strongly influenced by the intermixing or C-S-H with silica in the interaction volume of the sample with the electron beam. Due to characteristic vibration of silicon-oxygen bond in micro-silica, progressive reaction could be followed by FTIR. The critical pore entry diameter measured by MIP on pastes at 28 days of hydration is significantly reduced in mixtures containing silica, but less in mixtures with metakaolin. Changes in microstructure observed by TEM include formation of finer hydrates and denser areas in sample with silica and metakaolin.

4.1. Introduction

The use of supplementary cementitious materials in blended cements represents a viable solution to partially substitute the Portland cement (PC). Silica fume is one of the SCMs that has received significant attention from researchers due to its high pozzolanic activity. Both the impact on the hydration and the resulting microstructure have been studied [86], [87]. When silica is used for the preparation of PC mortars or concrete, the microstructure is refined and the mechanical properties at later ages are improved [88], [89]. Micro- and nano-scaled silica particles have a filler effect by filling up voids between the cement grains. Besides the physical effect, the pozzolanic reaction of silica with portlandite formed during hydration of OPC, produces additional calcium silicate hydrates (C-S-H), which is the main constituent for strength and density in hardened cement paste [90]. Land and coworkers have suggested that the acceleration is caused by C-S-H seeds that are formed on the silica surface and this acceleration is dependent on the surface area of silica. Singh and coworkers have reported that addition of 10 % nano-silica had an influence from the first hours of hydration, leading to earlier precipitation of CH and additional C-S-H [91]. A frequently used technique that enables the reaction of OPC or C_3S and silica to be followed is ^{29}Si MAS NMR. Dobson and coworkers have showed as well that fine divided silica can greatly accelerate the hydration of C_3S without affecting the length of the induction period [87]. Hydration of OPC in presence of silica leads

to changes in Ca/Si ratios for both inner and outer product. Rossen and coworkers reported Ca/Si ratio in the inner product decreasing from 2.0 to 1.0 when 45% silica fume was used, the microstructure being depleted of CH [59]. Groves and coworkers showed that at significant levels of substitution of cement (>50% silica), the Ca/Si ratio of inner and outer product measured by TEM can decrease even below 1.0 [86].

Another frequently used SCM is metakaolin. MK is processed from high-purity kaolin clay by calcination at moderate temperatures (650-800°C) and it contains silica and alumina in an active form [92]. In pastes containing MK, portlandite is consumed, especially at higher replacement levels, and additional C-S-H and even other hydration phases such as strätlingite can form [93]. Additionally, with more metakaolin added, the pH of the pore solution will decrease [94]. Use of metakaolin accelerated the initial set time of concrete and compressive strength increased by as much as 20% with 15% metakaolin replacement [95]. This consequence is usually tightly connected to the refinement of porosity. It was found that the proportion of pores of radii < 0.02 μm within the pastes increased with increase in both MK content and curing time. The rate of pore refinement was very rapid up to 14 days curing after which pore size changed very little [92]. Metakaolin does not react completely even at later ages, as shown in this study by Avet and coworkers, where a lime calcined clay cement was hydrated at water-to-cement ratio 0.40 [96]. One way of improving the degree of reaction of MK is to ensure complete saturation of capillary pores with solution, as shown by Briki and coworkers [97]. Coupled substitutions of metakaolin and limestone for Portland cement can give excellent performance at relatively early ages. Up to 45% of substitution with a 2:1 blend of metakaolin and limestone yields better mechanical properties at 7 and 28 days than the 100% Portland cement reference. Calcium carbonate reacts with the aluminates in the metakaolin, forming significant amounts of hemicarboaluminate and to a lesser extent monocarboaluminate from as early as 1 day. TGA shows that the reactions of metakaolin and limestone consume calcium hydroxide, which may be completely absent at late ages [98]. Presence of alkali can improve the degree of reaction of metakaolin as well. In a study done by Love and coworkers [99], where ^{29}Si and ^{27}Al MAS NMR spectroscopy were used to follow the hydration of a white PC-20% metakaolin blends, the improvement was already noticed at 1 day of hydration. Additionally, the Al/Si ratio of C-S-H measured by TEM was higher and the microstructure at 28 days was formed of a long-chain highly aluminous C-S-H with most of the bridging sites occupied by Al^{3+} rather than Si^{4+}. The same two techniques were used by Dai and coworkers to show that there is a linear increase in Al/Si ratio with MK replacement levels [100].

The influence of micro-silica and other SCMs on the hydration and properties of a reactive C_2S similar with the one used in this research study was described here [29]. Isothermal calorimetry done on pastes with water-to-binder ratio 1.3 showed a significant acceleration of hydration when 10% nano-silica was used. The increased heat rates in the first few hours signaled that a larger amount of C-S-H was formed and the heat released continued for at least 3 days, as opposed to 40 hours for the plain hydrated C_2S. Significant changes in the microstructure of the mixture with 10% nano-silica include total consumption of portlandite and of the γ-C_2S phase after 7 days, increased loss on ignition (due to a higher amount of C-S-H formed) and hydrate morphology evolution from elongated particle to denser sheets.

This study aims to investigate the main transformations occurring in the chemical composition of C-S-H and the microstructure of hydrated reactive C_2S with various contents of silica and metakaolin.

4.2. Materials and methods

The binder used for this study is the reactive C_2S described in Chapter 3. Mixtures were then prepared with silica (ELKEM micro-white) and/or metakaolin (Metastar™501). The oxide composition of the three materials was determined by X-ray fluorescence spectrometry using a PANalytical AxiosMax and is given in Table 4-1. For the particle size distribution of the powders, a Malvern Mastersizer 3000 was used. The d_{50} values are also reported in Table 4-1, except for the micro-silica, where the mean particle size from the manufacturer product sheet is given instead.

Table 4-1. Oxide composition of reactive C_2S, micro-silica and metakaolin determined by XRF analysis

Oxide	Amount (%)		
	C_2S	Silica micro-white	Metakaolin Metastar 501
CaO	61.36	0.23	0.12
SiO_2	33.29	96.19	52.18
MgO	0.57	0.45	0.04
K_2O	0.13	0.8	0.18
Al_2O_3	0.00	0.19	44.92
Na_2O	0.00	0.16	0.17
Fe_2O_3	0.00	0	0.62
MnO	0.01	0.01	0
TiO_2	0.00	0	1.14
SO_3	0.17	0	0.14
P_2O_5	0.04	0.07	0.07
LOI (1050°C)	4.07	1	0.29
TOTAL	99.64	99.10	99.87
d_{50} (μm)	2.53	0.15*	2.11
BET s.s.a. (m^2/g)	10.9	min. 15.0#	13.4

* mean particle size (from product sheet)
# value from the Product Sheet provided by the supplier

The investigated mixtures are illustrated in Figure 4-1: two mixtures containing different amounts of silica (10% and 15%), one mixture containing 10% metakaolin and one mixture containing both (10% silica and 10% metakaolin) were prepared. The powders were dry mixed for 1 hour in a Turbula Mixer and then pastes were prepared at water-to-binder ratio 0.35 (excepting one mixture which had 0.36) by mixing for 2 mins at high speed and at a high shearing rate using ULTRA-TURRAX® - IKA. A superplasticizer admixture BASF ACE30 was added as 1% of the mass of the binder to improve workability. All samples were kept sealed for 24 hours, then were demolded and cured in lime water, in plastic recipients having the diameter slightly bigger than the samples.

Hydrate characteristics were observed at different hydration ages by stopping the hydration reaction using the solvent exchange technique, using isopropanol followed by a quick washing with petroleum ether [81].

Thermogravimetric analysis was carried out on ground hydrated binder using a NETZSCH STA F449 device. The weight loss was monitored while heating up a 30±1 mg sample until 1050 °C at 20°C/min in N_2 atmosphere. X-Ray diffraction patterns were collected on powder samples as described in section 2.1. A scanning electron microscope Zeiss EVO LS10 with a Quantax400 Detector from Bruker was used to investigate the microstructure of the hydrated specimens. For chemical analysis of the C-S-H, EDS point analysis and mapping were carried out on selected areas. All samples for SEM investigations were impregnated under vacuum with a spectrally transparent epoxy resin (EpoTek® 301), gradually polished down to 1 μm with a diamond spray and petrol as a lubricant and coated with a thin conductive layer of carbon (15 nm).

Figure 4-1. Investigated mixtures composition

For micrograph investigations, dried powder specimens were dispersed on an adhesive carbon tab and coated with a 5 nm iridium layer. The samples were analyzed using Zeiss Merlin ultra-high-resolution FE-SEM (Field Emission SEM). A transmission electron microscope (Tecnai Osiris TEM, FEI) equipped with an EDS detector (Nano XFlash, Bruker) was used for TEM and EDS analyses, operating with an accelerating voltage as low as 80 kV and a low current density (corresponding to a very small spot size) in order to limit the extent of potential beam damage.

The FTIR-ATR data were obtained using the device Perkin Elmer Spectrum 100, the transmittance measurements being carried out on powders samples in the wavelength range was 500–4000 cm^{-1}. The SSA$_{BET}$ was determined by five-point N_2 absorption / desorption isotherm measurements using a NOVA Touch NT4LX-1 from Fa. Quantachrome using the BET-equation (BET = Brunauer, Emmett and Teller). The s.s.a. values of the anhydrous materials are given in Table 4-1. Concerning hydrated samples, dried powders specimens were ground to < 63 μm and a gentler degassing protocol was used, 24 hours at 30 °C under constant N_2 flow and medium vacuum. For MIP measurements, bulk hydrated samples were crushed and the fraction 1-2 μm was selected. The

analysis was performed using a Pascal 140/440 Porosimeter from Thermo Scientific up to a maximal pressure of 400 MPa.

4.3. Results and discussion

4.3.1. C-S-H analysis by SEM & TEM

In Figure 4-2, the distribution of Ca/Si ratios of C-S-H from SEM-EDS is given for: the reference C_2S sample at 1 day (a), the mixture containing 15% silica at 1 day (c) at 28 days (c) and at 9 months (d). For all measurements, around 100 points corresponding to C-S-H areas were analyzed. Compared to the hydrated C_2S, the silica containing sample presents a shift of the Ca/Si ratio of C-S-H to lower values (from 1.99 to 1.32). When compared to the 28 days and 9 months samples, peak position does not change significantly (1.32 vs 1.28), just the distribution of the values gets narrower at later ages.
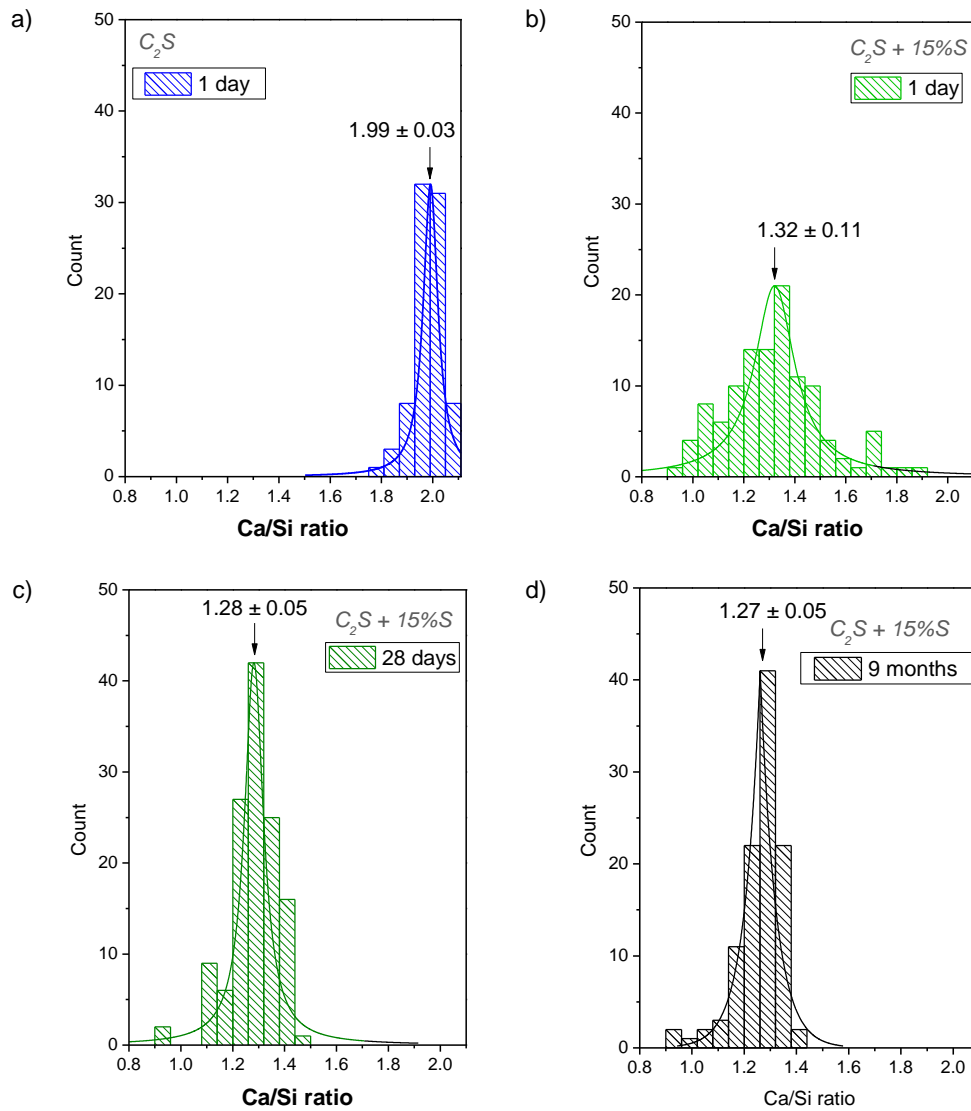
Figure 4-2. Distribution of Ca/Si ratios from SEM-EDS for hydrated C_2S at 1 day (a) and mixture with 15%S at 1 day (b), 28 days (c) and 9 months (d)

For a better understanding of the lower average value for Ca/Si ratio already at 1 day for sample containing 15% silica, TEM image of sample containing 10%S 10%MK at 28 days is illustrated in Figure 4-3. Particles of silica of 200 – 300 nm can be observed, they can easily get intermixed with the C-S-H composition during the SEM analysis, given that the interaction volume of the sample with the electron beam is approximately 1 μm [9].
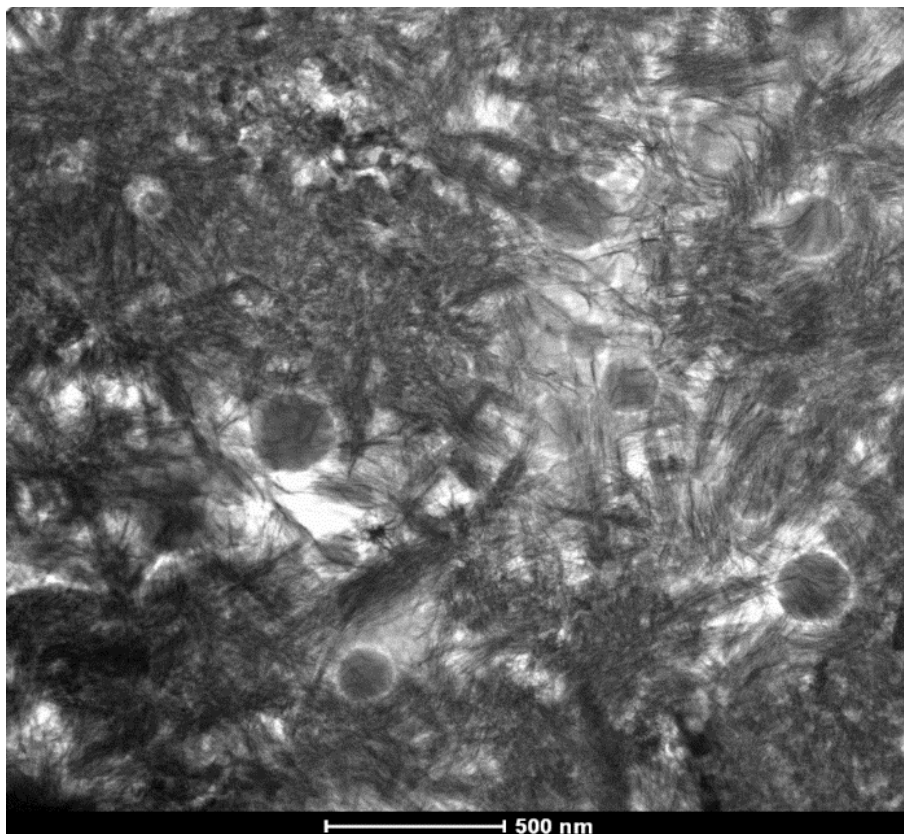
Figure 4-3. Microstructure of sample containing 10%S 10%MK at 28 days observed by TEM

The Ca/Si ratios determined by SEM-EDS for all samples at 28 days are shown in Figure 4-4 (values in black). For the two sample with the highest level of substitution of C_2S, 9 months cured samples were as well analyzed and it was observed that the average Ca/Si ratio did not decrease with hydration age. Chemical analysis by TEM for sample containing both silica and metakaolin lead to an average Ca/Si ratio in C-S-H of 1.59 (value in blue). When compared to the value from SEM, there is a significant difference between the two. This difference can be due to high level of intermixing of C-S-H phase with silica particles. The Al/Ca ratio of C-S-H for sample with 10%S 10% MK was 0.050 ± 0.020 from SEM, while TEM gave the value 0.046 ± 0.012. The TEM value was used to determine the amount of metakaolin reacted, considering that Ca comes exclusively from C_2S and Al from MK. This resulted in a degree of reaction of metakaolin of 31%, which further implied that 30% of the micro-silica had to react, to give the final value of the Ca/Si ratio of 1.59. Considering that the same amount of silica has reacted in all samples (which is approximately ~31%), the calculated values for the Ca/Si ratio of C-S-H are represented in red. The decrease in the obtained Ca/Si ratio is directly proportional to the amount of SiO_2 present in each mixture: 10% MK > 10% S > 15% S ~ 10%S10%MK.
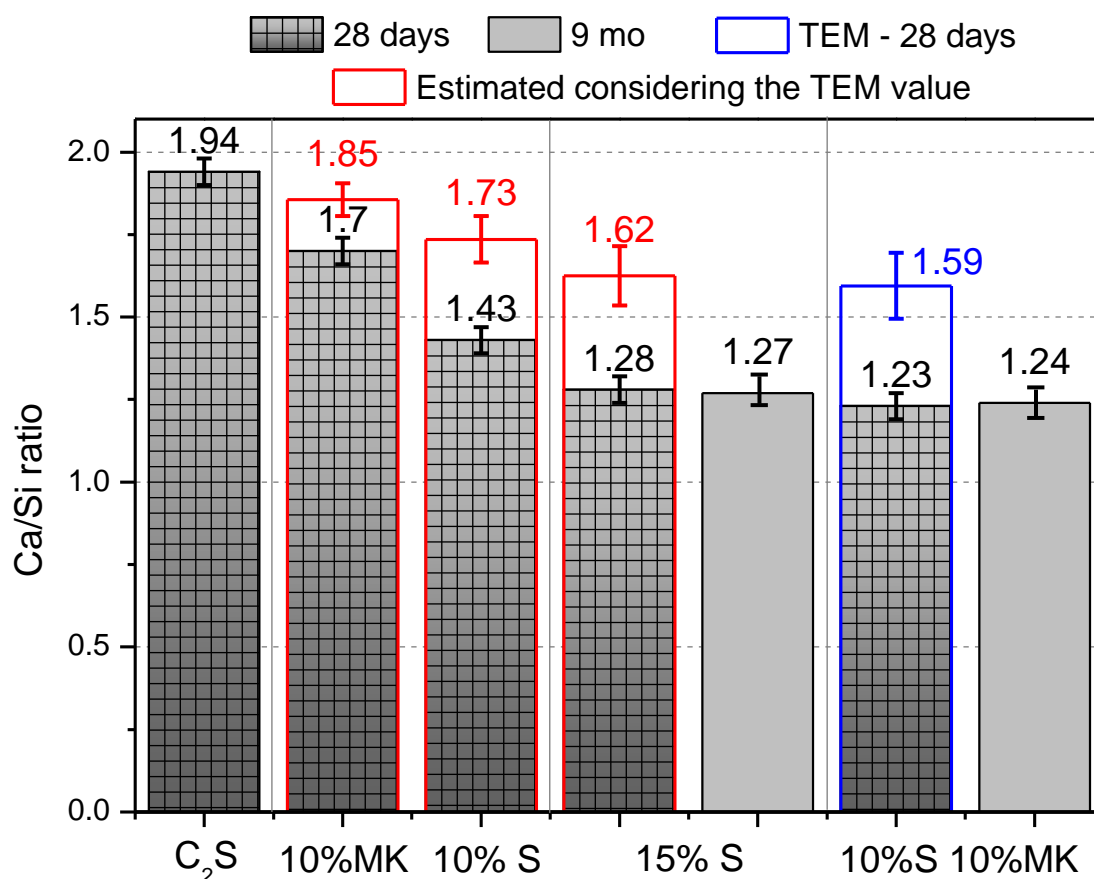
Figure 4-4. Ca/Si ratio of investigated samples at 28 days and 9 months by SEM and TEM (for one sample)

Besides the Ca/Si ratios, the Al/Si ratios were as well determined and they are plotted in Figure 4-5 as function of Ca/Si ratios for sample with 10% MK at 28 days. There is a broad variation of values, due to some degree of intermixing with unreacted metakaolin particles, as suggested by the position of the Al/Si ratio corresponding to metakaolin with respect to the position of C-S-H composition. It is also noticeable that with increasing Ca/Si ratio, the Al/Si ratio gets lower. The average values determined from the plots for both samples containing metakaolin at 28 days and 9 months are represented in Figure 4-6. There is a slight increase in the amount of Al going into the C-S-H at 9 months for both samples. For the sample analyzed by TEM (10%S 10%MK – 28 days, red triangle), the Al/Si ratio agrees very well with the value from SEM. More evidence of Al uptake is given in Figure 4-7, where the Al elemental map from sample with 10%S 10%MK at 28 days by TEM is shown. Areas rich in Al correspond to undissolved MK particles, but intermixing with MK is less of a problem than in the case of silica, as the particle size is bigger. Additionally, Al seems to be homogenously distributed in the C-S-H matrix.
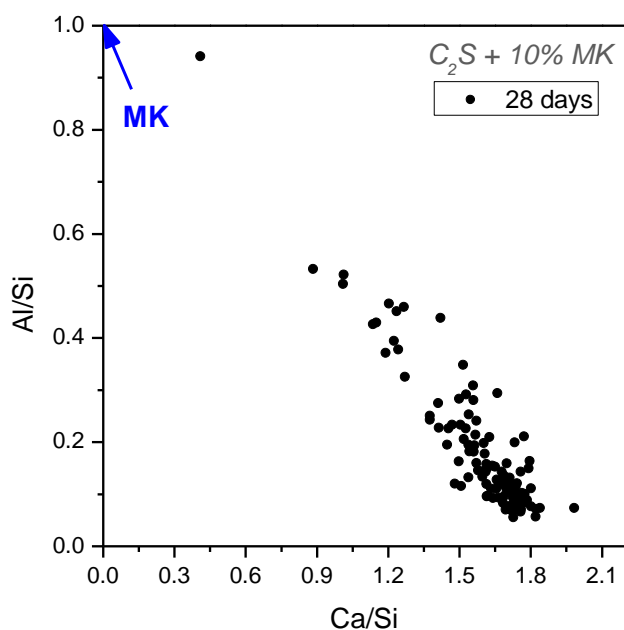
Figure 4-5. Distribution of Al/Si ratio as function of Ca/Si ratio for sample 10% MK at 28 days hydration, composition of MK is marked
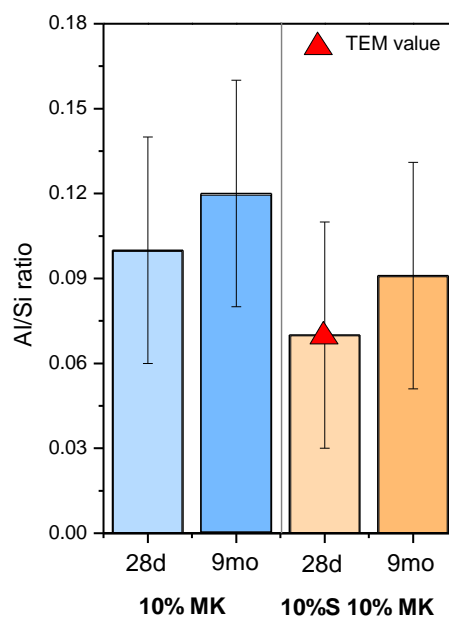
Figure 4-6. Al/Si ratio of samples containing MK at 28 days and 9 months by SEM and TEM (for one sample)
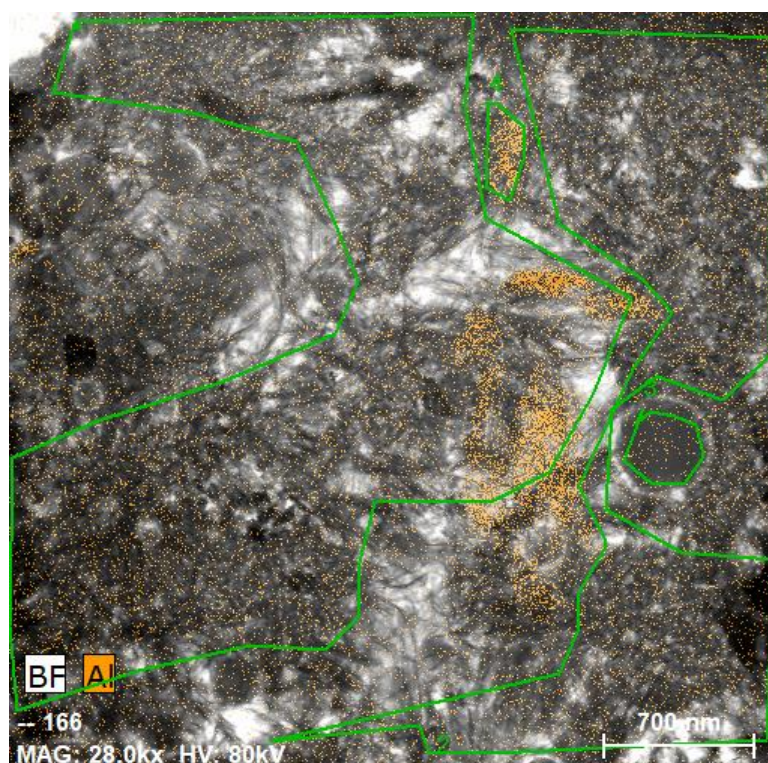
Figure 4-7. Microstructure of sample containing 10%S 10%MK at 28 days observed by TEM

In Figure 4-8, TEM images of reference hydrated C_2S samples and mixture with 10%S 10% MK at 28 days hydration are shown. The C-S-H in both samples has a similar morphology, with elongated fibers with lengths of few hundreds of nanometers. The difference between them is that in the case

of sample with silica and metakaolin, the C-S-H appears finer and forms a dense web which fills all available space, while in the hydrated C_2S microstructure there were more pores of few μm observed. Overall, by filling the larger pores with more hydration products from the reaction of silica, the system seems to become more homogenous in terms of porosity distribution.
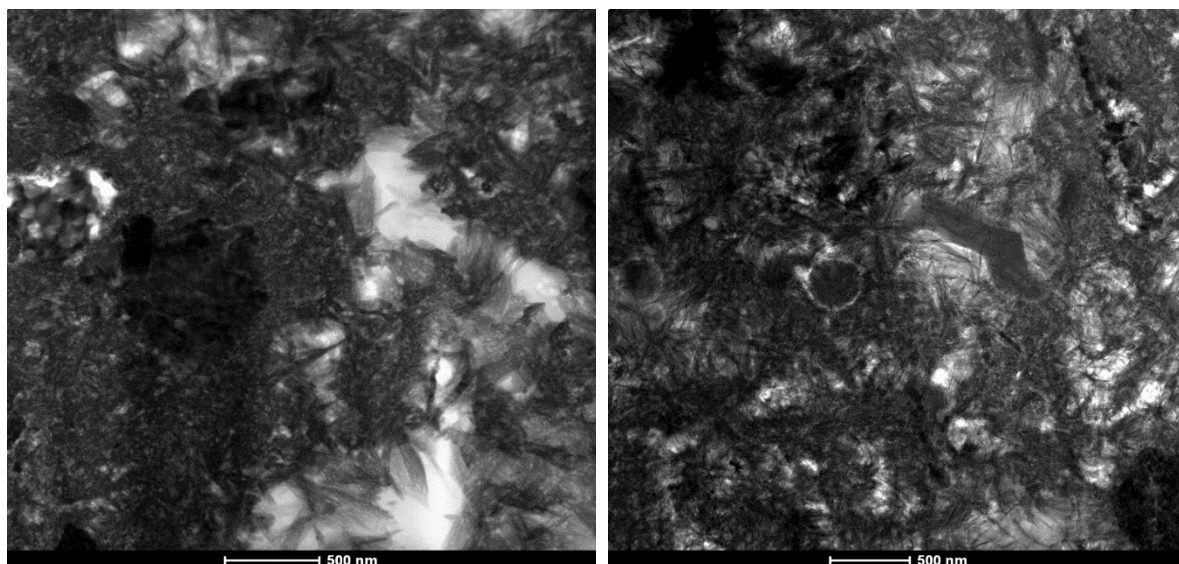
Figure 4-8. Microstructure of hydrated C_2S and mixture containing 10%S 10%MK at 28 days observed by TEM

4.3.2. Investigation of consumption of silica and metakaolin by FTIR

The FTIR analysis of samples containing 15% S and 10%S 10% MK at hydration ages 1d, 7d, 28d and 9 months are shown in Figure 4-9. For all hydrated samples, the characteristic C-S-H gel band occurred between 948 and 950 cm^{-1}, as a marker of the Si-O stretching in Q^2 tetrahedra [13], [101], [102]. The weak absorption bands at 848 and 872 cm^{-1} were attributed to the characteristic band for Si-O in unreacted γ-C_2S [13]. The band present 640 cm^{-1} is due to Si–O–Si bending vibrations from the silicate chains and the weak band at 815 cm^{-1} could be assigned to Si-O stretching of Q^1 tetrahedra [102]. H-O-H bending vibrations typical for molecular water were identified at 1640 cm^{-1} [13], [102]. Between 1340 and 1540 cm^{-1} there is a broad band corresponding to the asymmetric stretching of CO_3^{2-} [102], [103]. Other characteristic bands for the carbonate group in cement pastes reported at 750 and 875 cm^{-1} were not identified. The marked area in both graphs corresponds to characteristic band for Si-O in free SiO_4 (1120 cm^{-1}). The band is decreasing in intensity with hydration age, until it becomes a very weak shoulder for samples cured for 9 months.
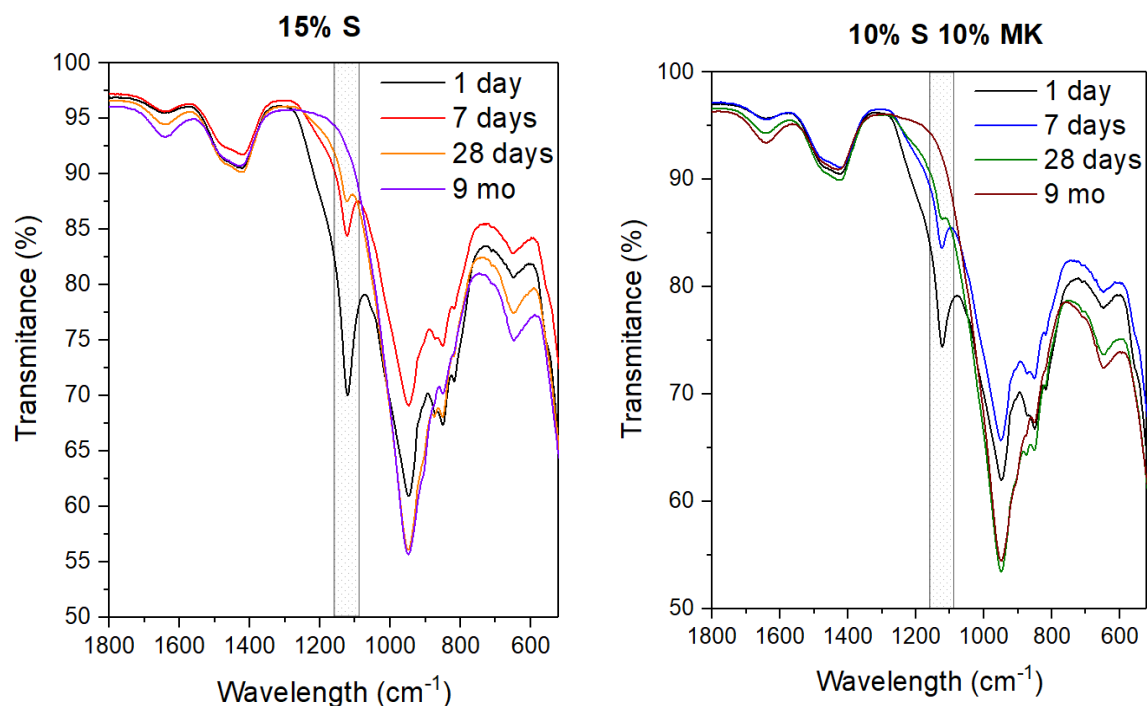
Figure 4-9. Fourier Transform Infra-red spectroscopy (FTIR) spectra for samples containing 15%S and 10%S10%MK cured for different ages
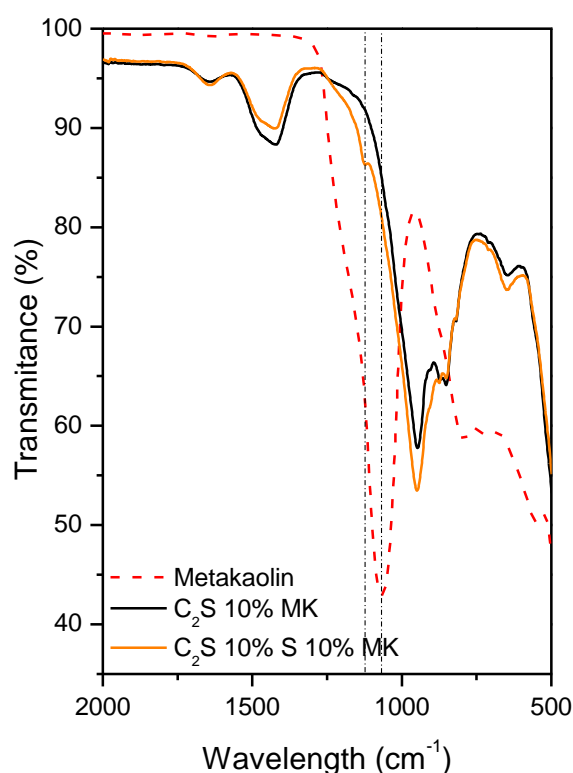
Figure 4-10. Fourier Transform Infra-red spectroscopy (FTIR) spectra for metakaolin and samples containing 10%MK and 10%S10%MK cured for 28 days
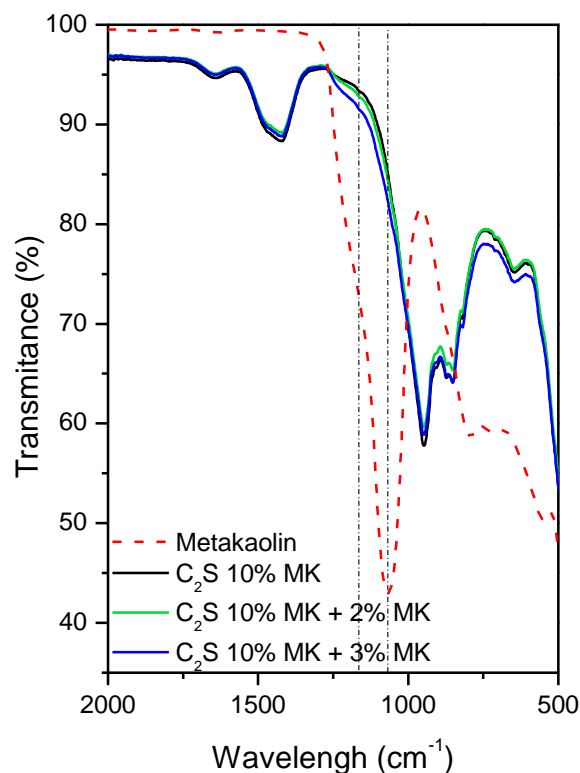
Figure 4-11. Fourier Transform Infra-red spectroscopy (FTIR) spectra for sample containing 10%S10%MK cured for 28 days with additional metakaolin

Figure 4-10 illustrates the FTIR spectra of samples containing 10% MK and 10%S 10%MK at 28 days hydration ages. Marked peaks corresponds to characteristic band for Si-O absorption free SiO_4

(1120 cm^{-1}). Only the sample containing silica presents the characteristic absorption band, for the sample with MK, this is not visible. In a study done by Cai and coworkers [104] on mixtures of Portland cement with up to 20 % metakaolin, the authors did not report any typical intensities of the silicate band from unreacted metakaolin, invoking the dilution effect which leads to absence of this band. To verify this possibility, mixtures of the sample with 10% MK at 28 days and additional MK have been prepared and the FTIR spectra are shown in Figure 4-11. Even with 3% more MK the absorption band does not become visible, but we observed a small shoulder at the characteristic wavelength becoming broader with more amount of MK added. FTIR signal given by unreacted silica or metakaolin could depend as well on the type of material used. Saez del Bosque and coworkers [105] studied using FTIR the effect of nanosilica on the nanostructure of C-S-H gel formed by hydrating tricalcium silicate. The FTIR spectra reported for mixture containint 10% nanosilica did not show any signal at the position of the main band in silica (1107 cm^{-1}) at early ages.

4.3.3. C-S-H characterization by BET & MIP

The BET specific surface area of C-S-H for the reference hydrated binder and the mixtures containing silica and metakaolin are given in Figure 4-12. The raw values of the s.s.a. of pastes are given in Table 4-2 in the Appendix of this chapter. The amorphous content from XRD was used for calculating the C-S-H content in each powder, as well as considering the estimated degree of reaction of silica and metakaolin from TEM data. The unreacted amount had to be subtracted from the total amorphous content, in order to obtain a more realistic composition. It was observed that the C-S-H at early ages in systems with silica and metakaolin has a lower s.s.a. than the hydrated C_2S.
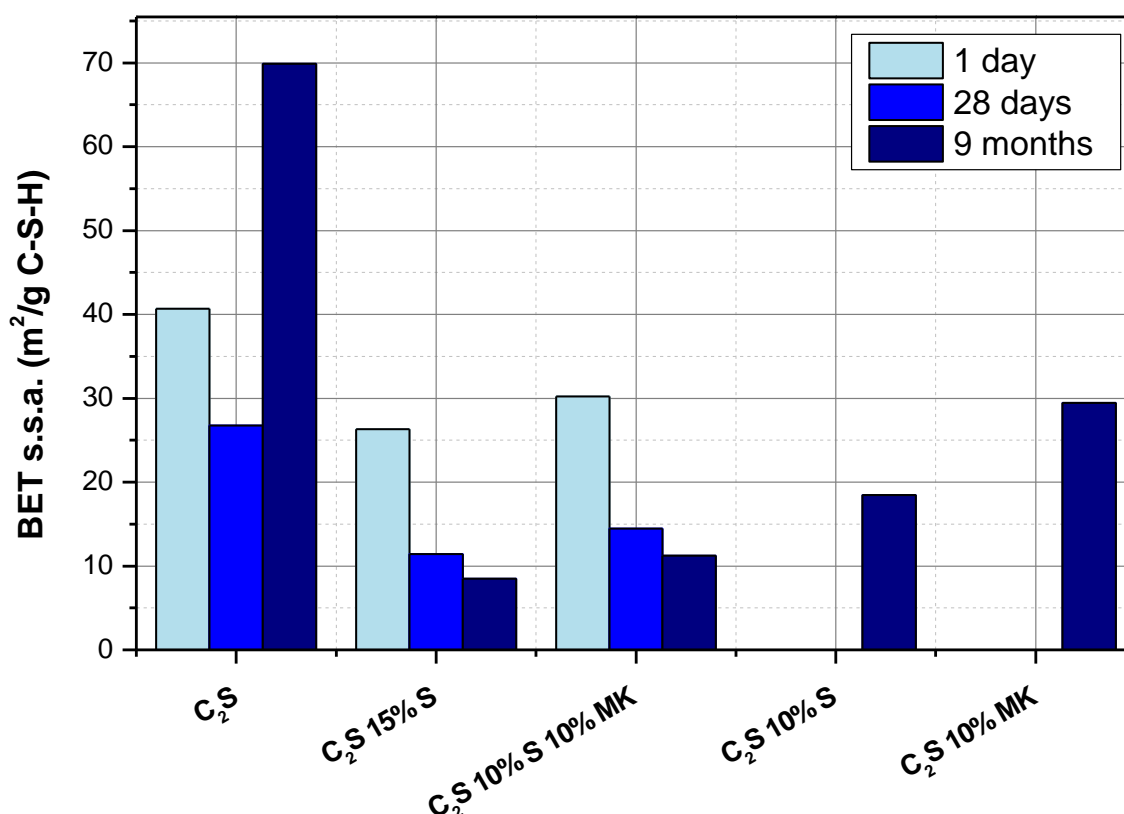
Figure 4-12. BET s.s.a. values for the hydrated C_2S, the mixture with silica and/or metakaolin at different age of hydration

Due to limited amount of sample, there were no duplicates measured. There was a general trend for the s.s.a. of C-S-H to decrease with hydration age, with one exception, the hydrated C_2S at 9 months, which had an inexplicably high value. When comparing only the 9 months values of the s.s.a. for all four samples containing silica and metakaolin, the values decreased in the following order: 10%MK > 10%S > 10%S10%MK > 15%S. The decrease seemed to be thus proportional with the amount of replacement of binder with silica or metakaolin. For the mixture with 15% S and 10%S10%MK, the values of s.s.a. are similar at all ages, with the metakaolin free sample having slightly lower values.

The MIP curves for all samples at 28 days hydration age are given in Figure 4-13. A refinement of pores for the pastes prepared with silica is observed, critical entry diameter is reduced to half and the total intruded volume decreases as well. Concerning the sample containing 10% metakaolin, the critical entry diameter is similar with the one of the reference sample, but total intruded volume is higher. When comparing the reference sample with the one with 10% MK and the sample with 10% S with the one having 10%S 10% MK, we observed that introduction of metakaolin increases the total porosity in both cases. Plate-like aspect and bigger particle size of metakaolin compared to silica could be factors responsible for the changes in porosities.

Porosity was assessed also at 9 months of hydration for pastes with 15%S, 10% MK and 10%S10%MK and the MIP curves are shown in Figure 4-14. For the paste with 15%S, there was no significant difference in porosity for the two ages (left image). In the case of the paste with 10%MK, with age there is a significant decrease of the total intruded volume, as well as the critical entry diameter. Concerning the paste with 10%S 10%MK, there is only a slight decrease in total intruded volume and critical entry diameter with age.

Further reaction of silica after 28 days seems to produce little or no changes in the porosity of the system, while by late reaction of metakaolin, more pores are filled with hydration products. Overall, the lowest critical entry diameter is for the sample containing both silica and metakaolin, although the total intruded volume of the sample is comparable with the one of the sample with 15%S. The system with 10%MK had at 9 months slightly higher total intruded volume and critical pore entry volume than the other two systems containing silica.
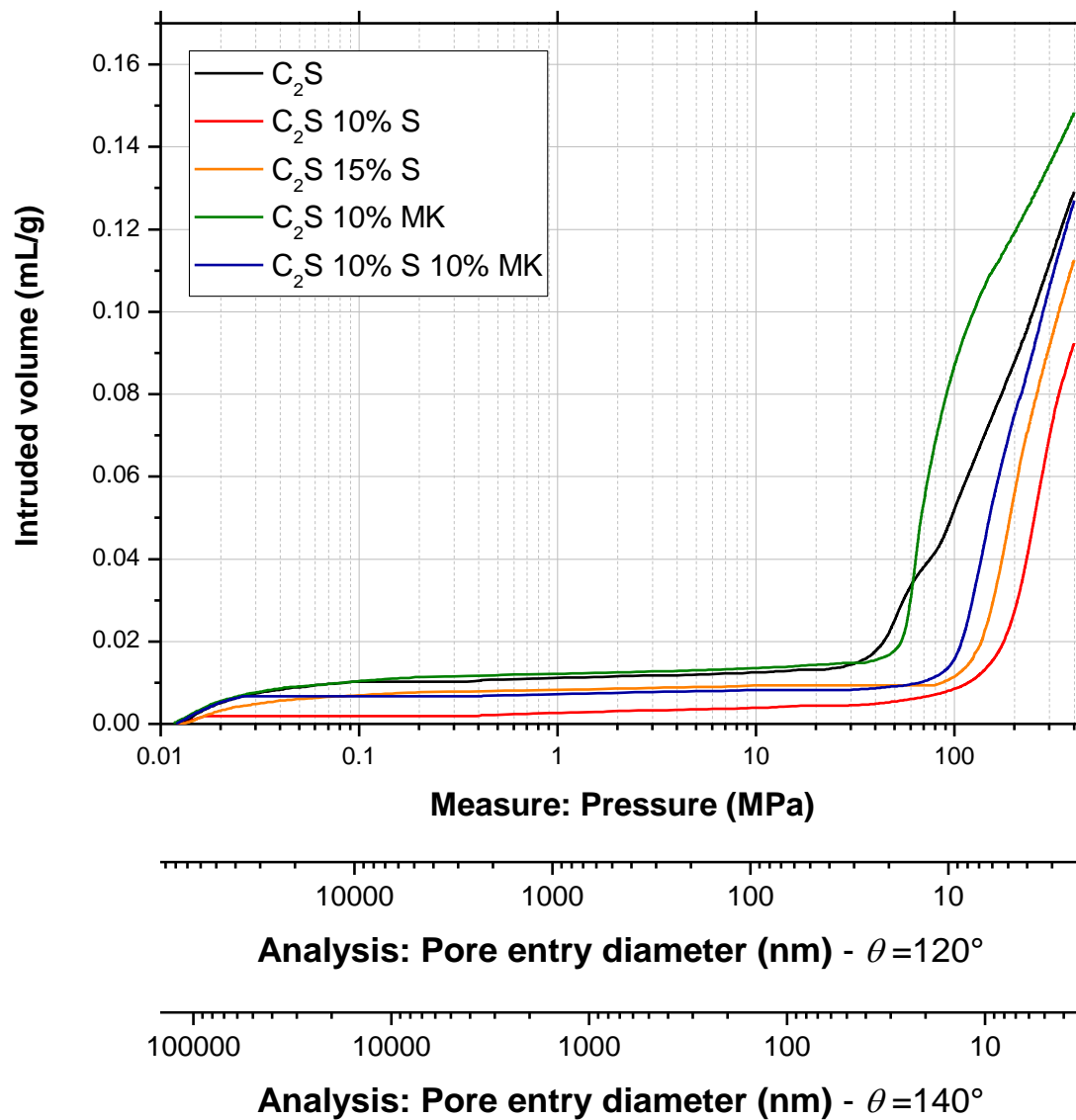
Figure 4-13. MIP curves for the hydrated C_2S and mixtures containing silica and metakaolin at 28 days of hydration
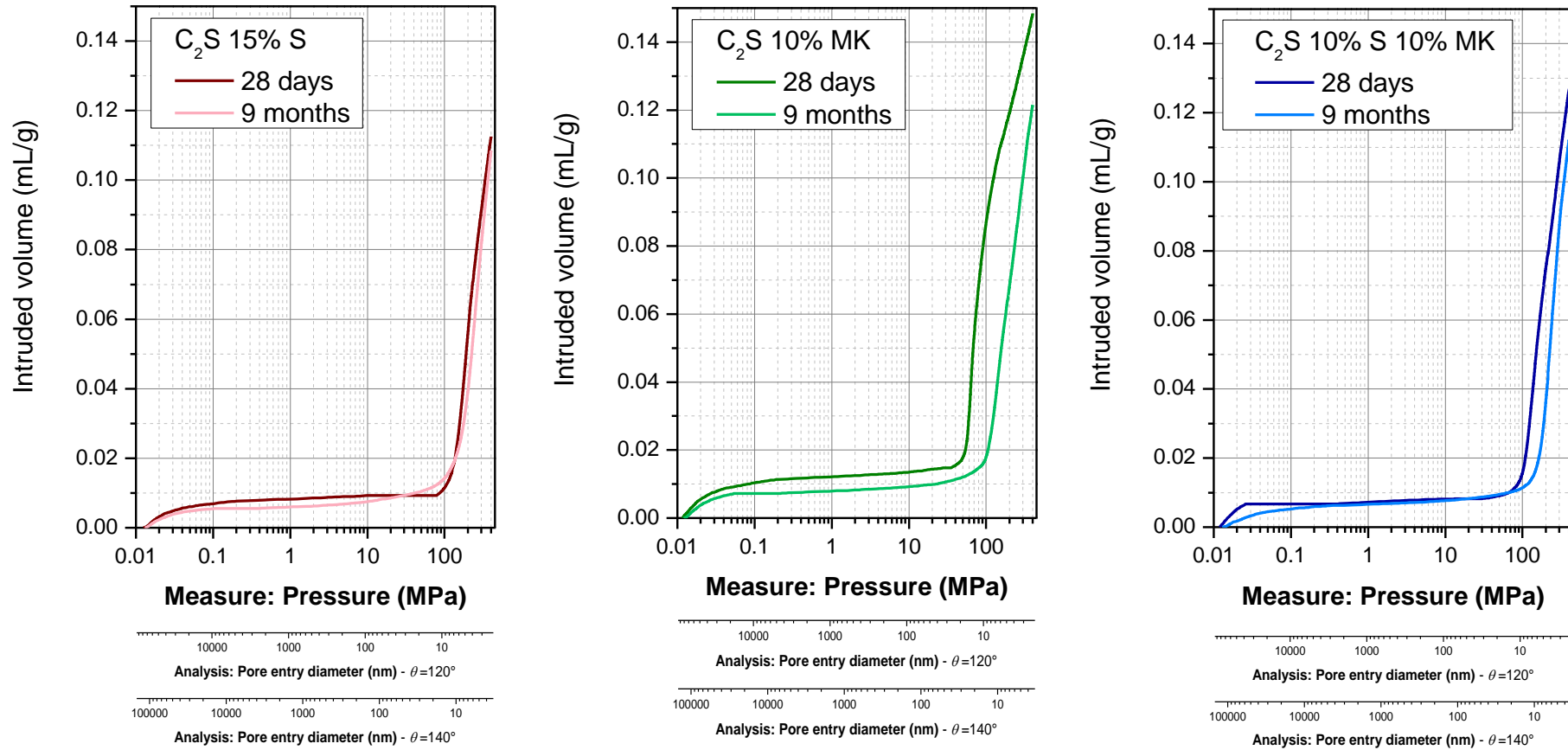
Figure 4-14. Total intruded volume given by MIP for the mixtures containing silica and metakaolin at 28 days and 9 months of hydration

4.3.4. Discussion on the reaction of silica and metakaolin

Analysis of the hydrated microstructure by SEM-EDS is strongly affected by the intermixing with small silica particles, leading to an underestimation of the Ca/Si ratio of C-S-H. This limitation is hard to overcome, as the hydrated matrix is formed of one type of C-S-H, which resembles to the outer product from the hydrated OPC pastes. Although in hydrated cement paste with increasing incorporation of silica, the Ca/Si ratio of both inner and outer product decreases with increasing content of silica [59], the measurement of the big inner product areas will limit the possibility of analysing highly intermixed volumes. TEM analysis was used to obtain a more realistic composition and the sample analysed had a Ca/Si ratio of almost 1.60. This is much lower than compared with the C-S-H formed in the plain hydrated C_2S (where Ca/Si ratio is 1.94), which proves that part of silica has reacted. FTIR showed progressive consumption of silica with hydration age, but metakaolin consumption could not be proved in the same manner using this method (although both SEM and TEM revealed that there is still unreacted MK present). Evidence from MIP shows that in samples with MK, the microstructure is slightly less porous at 9 months as compared to 28 days, signalling that the reaction advances beyond 28 days of hydration. This would lead to an even further decrease of the Ca/Si ratio and a possibly better agreement between TEM and SEM measured values. Concerning the s.s.a. of hydrated pastes, the trend of hydrated plain C_2S to have higher surface areas at later age agrees with observations for hydrated OPC systems [106]. There is no intuitive reason to why samples containing silica and metakaolin have a lower s.s.a. which decreases with time, although an explanation could be formulated based on the morphology changes. The TEM micrographs given in Figure 4-8 show no significant changes in the C-S-H morphology except the network becomes finer and denser. Nevertheless, this method provides just a 2D overview of a 3D network [9] and the if the elongated particles in the high Ca/Si ratio C-S-H undergo changes to become more thin wavey sheets in the lower Ca/Si ratio C-S-H [107], [108], this could lead to lower values of the measured s.s.a. . Another reason could be a more significant damage to gel pore structure due to solvent exchange and degassing protocol, resulting in a more 'closed' porosity for samples at later ages. Concerning the hypothesis of a different gel pore structure of the C-S-H, evidence from ^{1}H NMR showed that addition of silica to white cement does not change the gel pore sizes significantly [109].

XRD and TGA analysis of the plain hydrated C_2S showed very small CH content at all ages (as shown in Chapter 3). Given the absence of portlandite, we can propose that silica reacts exclusively with Ca which is coming out of the interlayer of the C-S-H with hydration age. This has been suggested even for mixtures of white cement-silica fume, where not all CH was consumed and necessary Ca for the reaction came from C-S-H [109]. As discussed in the Chapter 3, this process could be driven by the metastability of the high Ca/Si ratio C-S-H which tends to lose some of the additional Ca-OH groups from the interlayer when the supersaturation of the pore solution with respect to this phase decreases. Concerning the limiting factor of the silica and metakaolin reaction, since the availability of CH is out of discussion, the other two possibilities could be the dissolution of silica/metakaolin and the Ca release from the C-S-H. Concerning the dissolution of silica/metakaolin, it is known that the rate of the process is directly dependent on the pH value [110]. The reactive C_2S binder has a very low content of alkali, so the pore solution is expected to have a lower pH than in the case of OPC paste. Time constraints did not allow more experiments to be performed (for example with increasing alkali content). Additionally, absence of portlandite prevented the metakaolin to react with the calcite already present in the microstructure to form hemi- or monocarboaluminates. Atomistic simulations

have shown that only above the Ca/Si ratio 1.50, the surface Si-OH groups start to be deprotonated so that more Ca can be introduced in the structure. When the pH of the pore solution decreases, the high Ca/Si ratio C-S-H can be decalcified, providing Ca to react with the dissolved silica in the pore solution. This suggests that Ca/Si 1.50 might be the lower limit for C-S-H formed in the presence of silica. A further decrease in the Ca/Si ratio below this value, as reported in several studies [59], [109], [111], implies that other processes could happen, such as incongruent dissolution of C-S-H in the pore solution followed by reprecipitation at a lower Ca/Si ratio.

Concerning the Al uptake in the C-S-H, the high Ca/Si ratio does not favor a very high incorporation, as shown in [48]. But it was also observed by XRD that no other aluminate phases (hydroxide, katoite or strätlingite) are precipitating, which leads us to believe that all Al from the dissolved metakaolin is either found in the C-S-H or in the pore solution.

4.4. Conclusions

Mixtures of the reactive C_2S binder with micro silica and metakaolin were used to produce microstructures where the Ca/Si ratio of C-S-H decreased. SEM-EDS analysis showed decreasing trend of the Ca/Si ratio with increasing content of silica, but the results were strongly affected by intermixing with unreacted material. Results from TEM were used to correct the values and the expected Ca/Si ratio were in the range 1.85 – 1.60. The Al/Si ratio of the samples containing metakaolin were in the range 0.07 – 0.10, indicating a rater low degree of reaction of metakaolin. The microstructure is refined but the specific surface area of C-S-H decreases in the samples containing silica and metakaolin, as compared to the reference system. Besides Al uptake observed by chemical analysis through electron microscopy, other significant fundamental changes in the C-S-H structure and formation of C-A-S-H could not be reported by using XRD or FTIR. A more thorough characterization by ^{29}Si MAS NMR or ^{1}H NMR should be used to obtain more evidence on the reaction with silica and metakaolin and the features of the C-S-H with lower Ca/Si ratio. Overall, this study suggests that in the absence of portlandite, C-S-H can act as Ca source for the reaction with silica and metakaolin to produce additional C-S-H, although the driving factors of the reaction are expected to be very different from the hydrated cement paste scenario and require more investigation.

Appendix

Table 4-2. BET s.s.a. (m^2/g) of the investigated dried pastes, used for the calculation of the C-S-H s.s.a., represented in Figure 4-12

Sample → Age ↓	C_2S	C_2S 10 % S	C_2S 15% S	C_2S 10% MK	C_2S 10% S 10% MK
1 day	28.9	-	17.9	-	19.0
28 days	24.6	-	9.8	-	11.9
9 months	64.4	16.0	7.4	25.4	10.3

Chapter 5.   Chloride uptake by C-S-H microstructures

5.1. Introduction

Chloride induced corrosion is considered the major cause for degradation of steel reinforcement in concrete [112]. Corrosion of steel reinforcement is mainly induced by the ingress of chlorides upon exposure to seawater or deicing salts. In the saturated state, chloride ions enter concrete by ionic diffusion due to concentration gradient between the exposed surface and the pore solution inside concrete [112]. Chloride diffusing inside concrete can end up being dissolved in the pore solution or bound to the cement hydrates along the diffusion path. Therefore, the total chloride inside concrete is composed of free chloride and bound chloride. As free chloride can be transported through the microstructure of concrete, it is the one that reaches the steel rebar and causes corrosion. It has been accepted that chloride uptake in hydrated products does not lead to the formation of detrimental new phases that can cause expansion or cracking [113]. Chloride binding in hydrates can have a beneficial impact on the durability of reinforced concrete since it slows down the rate of ingress toward reinforcing steel.

In hydrated cement pastes, chlorides may either react with the aluminate phases in the paste (chemical binding) or they can be physically adsorbed on the calcium silicate hydrate gel (C-S-H). Chemical binding involves formation of Friedel's salt ($3CaO \cdot Al_2O_3 \cdot CaCl_2 \cdot 10H_2O$), which is stable over a wide range of chloride concentrations; in some cement systems also Kuzel's salt was observed ($3CaO \cdot Al_2O_3 \cdot 1/2CaCl_2 \cdot 1/2CaSO_4 \cdot 10H_2O$) [113]. Early research done by Tang et al [114] showed that the chloride binding capacity of concrete strongly depends on the content of C-S-H gel in the concrete (expressed as unit weight). For cement pastes and mortars, regardless of the water-cement ratio, chloride binding isotherms were found to be identical, as chloride binding mainly occurs through the interface between pore solution and hydrated products in concrete. Similar findings were reported by Delagrave et al [115]. To study the binding capacity of various cement systems, the chloride was either introduced in the mixing water [116]–[118] or the equilibrium method was used, which is based on storing samples of paste or mortar in chloride solutions until equilibrium is reached between the external solution and the pore solutions of the samples [114], [115], [127], [119]–[126].

There are several factors which can influence the chloride binding capacity of cement pastes. The chloride content of the pore solution of cement paste can increase with higher amounts of admixed chloride, until it reaches a plateau, as reported by Anders et al [117]. Delagrave et al [115]

showed how the total amount of bound chloride is higher when lime saturated solution is used instead of alkaline solution and the amount of bound chloride is as well enhanced for samples immersed in calcium chloride solutions, as compared to using sodium chloride solution. Concerning the cement composition, the C_3A and C_4AF content play a decisive role in the chloride binding capacity at high concentrations, but not at low concentrations of free chloride [122]. Additionally, the sulfate content was found to have a negative influence on the binding capacity [122], [124]. It was reported in several studies that partial substitution of OPC with silica fume caused a reduction in the binding capacity [116], [122]. The partial substitution of OPC with metakaolin increases the binding capacity, due to high alumina content of the metakaolin [122], [125], [127], [128]. The pH of the pore solution was also found to influence the amount of bound chloride. An increase in pH was found to reduce the binding capacity, as a competition exists between hydroxyl and chloride ion for adsorption sites on cement surface [129].

Compared to C_3A, much less studies were focused on binding capacity of hydrated C_3S and C_2S. C–S–H gel, as the main hydration product of Portland cement, dominates the physical binding of chloride [129]. Ramachandran proposed that besides the chemisorbed layer on the C-S-H, chloride can exist as well in the interlayer and also intimately bound in the lattice [118]. A comparative study done by Hirao et al [120] on hydrated C_3S and AFm showed that through chemical binding, almost double the amount of chloride was retained, compared to physical binding on C-S-H. On the other hand, Lambert et al [130] reported that hydration of a C_3S showed no detectable capacity to bind chloride ions, which were introduced in the form of the sodium salt, dissolved in the mix water of pastes. Synthetic C-S-H was as well used to study the chloride physical binding. By using synthetic C-S-H with Ca/Si ratio ranging from 0.6 to 1.4, Beaudoin et al [126] showed that the amount of chloride held by C-S-H increased with Ca/Si ratio and decreased with surface area. The chloride content considered in this study was the chloride insoluble in alcohol, but which could be removed by washing with water. In a different experiment, Plusquellec et al [56] measured the conductivity of suspensions containing synthetic C-S-H with increasing amounts of chloride and bromide. They concluded that there were no interactions between the surface of C-S-H and the anionic species or these interactions were not measurable.

Except few studies done on alite and synthetic C-S-H, the common approach to quantify the physical binding is to determine the total amount of bound chloride and then subtract the free chloride and chloride chemically bound in AFm [121], [125], [127]. In this study, the chloride binding capacity of the reactive C_2S was investigated using the equilibrium method. This allows the direct quantification of the chloride bound in a matrix containing only C-S-H and no other hydration product. The influence of gypsum, alkali, silica and metakaolin was investigated and the results were compared to other types of C-S-H from hydrated white cement and synthetic C-S-H.

5.2. Materials and methods

Pastes were prepared from the hydrated C_2S or from mixtures of it with silica (ELKEM micro-white), metakaolin (Metastar^{TM}501) or REA gypsum. For two of the pastes, a 0.1N solution NaOH was used instead of the distilled water. The plain binder was hydrated at different water-to-binder ratios, while all the mixtures had the same w/b. The powders were dry mixed for 1 hour in a Turbula Mixer and then pastes were prepared by mixing for 2 mins at high speed and at a high shearing rate using

ULTRA-TURRAX® - IKA. A superplasticizer admixture BASF ACE30 was added as 1% of the mass of the binder to improve workability. All samples were kept sealed for 24 hours, then were demolded and cured in lime water, in plastic recipients having the diameter slightly bigger than the samples. White cement pastes were prepared by hydrating mixtures of white clinker (Aalborg White) with 5.5% REA gypsum and 10% silica (ELKEM micro-white) at w/b 0.70. The pastes were cured sealed for minimum 3 months at two different temperatures, 5 and 55 °C. Prior to the binding experiment, the samples were equilibrated in saturated lime water for 2 months, to ensure that all pores are saturated. Synthetic C-S-H samples were prepared via the dropwise method from sodium silicate solution and calcium nitrate solution [50], [131]. The targeted Ca/Si ratio were 1.80, 1.50 and 1.20. The gels were filtered under N_2 pressure at 7 bar using a stainless steel cylinder with a 47 mm diameter nylon filter with 0.45 μm pore size (Sartorius Filter Holder). The gels were washed with approx. 200 mL deionized water and filtered again. The samples were kept in desiccator under medium vacuum until start of the test. All the investigated compositions are described in Table 5-1.

Hydrate characteristics were observed at different hydration ages by stopping the hydration reaction using the solvent exchange technique, using isopropanol followed by a quick washing with petroleum ether [81]. For MIP measurements, bulk hydrated samples were crushed and the fraction 1-2 μm was selected. The analysis was performed using a Pascal 140/440 Porosimeter from Thermo Scientific up to a maximal pressure of 400 MPa. Thermogravimetric analysis was carried out on ground hydrated binder using a NETZSCH STA F449 device. The weight loss was monitored while heating up a 30±1 mg sample until 1050 °C at 20°C/min in N_2 atmosphere. The SSA_{BET} was determined by five-point N_2 absorption / desorption isotherm measurements using a NOVA Touch NT4LX-1 from Fa. Quantachrome using the BET-equation (BET = Brunauer, Emmett and Teller). Dried powders specimens were ground to < 63 μm and a gentler degassing protocol was used, 24 hours at 30 °C under constant N_2 flow and medium vacuum.

Table 5-1. Investigated mixtures composition

Investigated systems		
C_2S − w/b=0.25	C_2S + 10% S − w/b=0.35	W.C. 10% S − w/b=0.70, 5°C
C_2S − w/b=0.30		W.C. 10% S − w/b=0.70, 55°C
C_2S − w/b=0.35	C_2S + 15% S − w/b=0.35	
C_2S + 5% G − w/b=0.35	C_2S + 10% MK − w/b=0.35	C-S-H, Ca:Si = 1.8
C_2S + 0.1N NaOH − w/b=0.35		C-S-H, Ca:Si = 1.5
C_2S + 5% G + 0.1N NaOH − w/b=0.35	C_2S + 10% S 10% MK− w/b=0.35	C-S-H, Ca:Si = 1.2

For the recording of the binding isotherms, five solutions of laboratory grade NaCl (Merck) were prepared, having concentrations 0.1M, 0.3M, 0.5M, 1.0M and 2.0M. Slices from hydrated pastes with thickness of 2.5 mm were immersed in NaCl solutions, at a liquid/solid volume ratio of 4. Concerning the synthetic C-S-H gels, 2-3 g of each sample were immersed in a two times bigger volume of solution. The small plastic containers were kept sealed for 10 months for the paste and 6 months for the synthetic C-S-H. Due to the limited amount of sample, replicates could not be prepared for all systems. The chloride content of the equilibration solutions was determined before and after the test and the amount removed from the solution was attributed to binding. The chloride concentration in the solutions was determined by potentiometric titration. Small volumes between 30 − 150 μL (depending on the chloride concentration of the equilibration solution) were collected using a micropipette and introduced in a measurement beaker, to which 10 mL HNO_3 (65% supplied by Merck

and diluted 1:1) and approx. 90 mL of deionized water were added. The chloride content was determined with a T90 titrator from Mettler Toledo equipped with Rondo autosampler, using 0.1 M or 0.01 M AgNO₃ solution (Merck, Titrisol).

The amount of chloride retained by the samples was determined using Eq. (1).

$$m_{bound\ Cl} = \frac{(c_{Cl,i} - c_{Cl,eq})*V_{sol}/1000*M_{Cl}}{w_{paste}}, mg\ Cl/g\ paste \qquad (1)$$

where $c_{Cl,i}$ is the initial concentration of the equilibration solutions (0.1 M – 2.0 M), $c_{Cl,eq}$ is the concentration of the solution after 10 month (6 months for synthetic C-S-H), V_{sol} is the volume of equilibrating solution used for the test, M_{Cl} is the molar mass of chlorine (35.45 g/mol) and w_{paste} is the weight of the sample.

After the equilibration time, several samples were tested using SEM-EDS to determine the atomic ratios and quantify the adsorption of Cl by C-S-H. Slices were removed from the equilibration solutions and the pore solution was removed by the solvent exchange method. A scanning electron microscope Zeiss EVO LS10 with a Quantax400 Detector from Bruker was used to investigate the microstructure of the hydrated specimens. For chemical analysis of the C-S-H, EDS point analysis and mapping were carried out on selected areas. All samples for SEM investigations were impregnated under vacuum with a spectrally transparent epoxy resin (EpoTek® 301), gradually polished down to 1 µm with a diamond spray and petrol as a lubricant and coated with a thin conductive layer of carbon (15 nm).

Three of the samples were tested for desorption: C₂S – w/b=0.35, C₂S + 10% S 10% MK– w/b=0.35 and W.C. 10% S – w/b=0.70, 55°C. The samples were crushed in a mortar and then rapidly introduced in the NaCl solution. To avoid carbonation, the samples were ground for less than a minute. After equilibration for 7 months, the amount of bound chloride in the crushed samples was determined. The samples were removed from the equilibrating solution, were filtered by gravitational filtration, then introduced in 8 mL deionized water, shaken for 1 minute and filtered again. The removed water was tested for chloride concentration and the amount of chloride left in the samples was determined using Eq. (2).

$$m_{residual\ Cl} = m_{bound\ Cl} - m_{desorbed\ Cl}, \ mg\ Cl/g\ paste \qquad (2)$$

$$m_{desorbed\ Cl} = \frac{(c_{des}*(V_{H_2O}+V_{free\ w}) - c_{eq}*V_{free\ w})/1000*M_{Cl}}{w_{sample}}, \ mg\ Cl/g\ paste \qquad (3)$$

where the c_{des} is the concentration of the solution after washing the samples for 1 min, V_{H_2O} is the volume of water used (8 mL), $V_{free\ w}$ is the amount of free water in the ground samples, c_{eq} is the concentration of the NaCl solutions from which the samples were removed and w_{sample} is the weight of the sample.

5.3. Results and discussion

5.3.1. Adsorption of chloride

The binding isotherms for selected samples described in Table 5-1 are given in Figure 5-1. One can observe the characteristic evolution of adsorption process, with increased amount of chloride at higher concentrations of NaCl. At low concentration of NaCl (0.1M), the total amount of Cl is quite similar for most of the samples. The error bar represents the scatter of experimental points from several titrations of the same sampled solution. Bigger differences between systems are observed starting with 0.5M NaCl concentrations. Even at the lowest NaCl concentration, there were still chlorides in the equilibrating solutions after the exposure time, so the similarities between samples are not due to all chlorides being adsorbed. Overall, the synthetic C-S-H retained the most amount of Cl from the equilibration solutions and hydrated white cement samples retained more that all the hydrated C_2S pastes. Amongst the hydrated C_2S systems, the amount of chloride retained was lower for samples containing silica and metakaolin, compared to the plain C_2S systems.
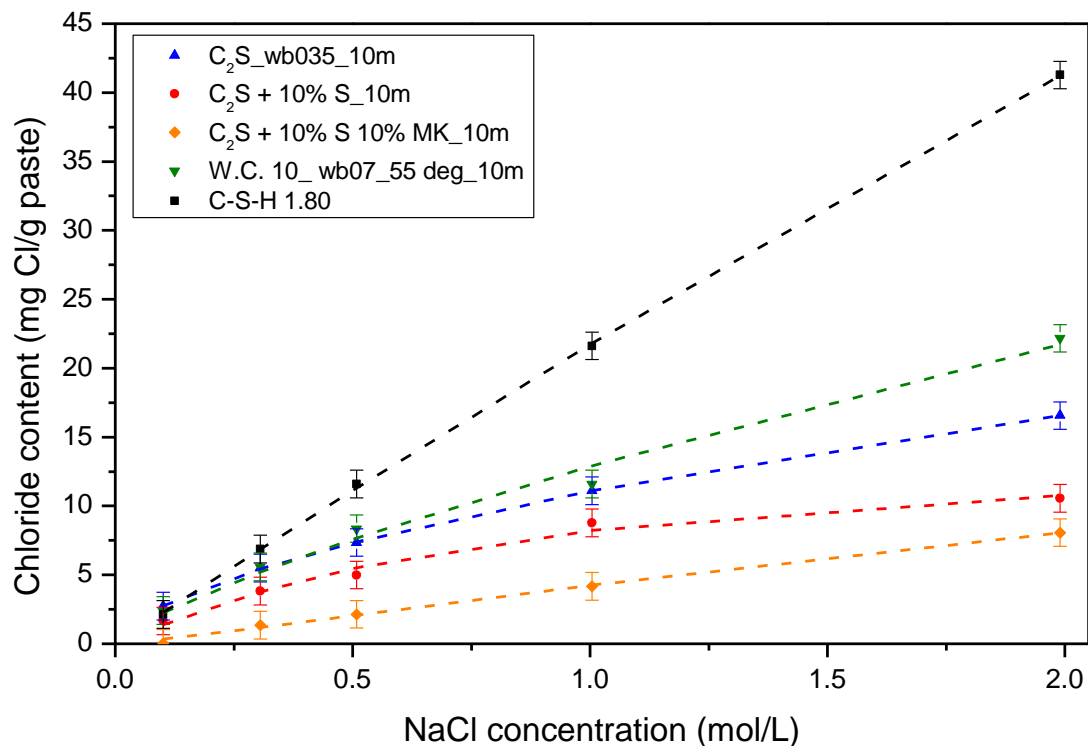
Figure 5-1. Chloride binding isotherms for selected samples

For comparison purposes, the amount of Cl retained by all the samples, except the synthetic C-S-H, at 0.5M NaCl was represented in Figure 5-2. Vertical lines were used to separate the samples into four smaller groups that will be further described. One of the microstructure features that can influence to some extent the chloride binding capacity of pastes is the pore network, as a certain amount of chloride is found in the pore solution. The MIP curves of the four groups are given in Figure 5-3. For the first two samples in Figure 5-2, the influence of the w/b is reflected in the amount of chloride retained. A lower w/b leads to a lower total porosity and critical entry diameter, as seen in Figure 5-3a. This can also be associated with a lower total amount of chloride retained. The samples

55

with 5% gypsum and 0.1N NaOH have w/b ratio 0.35, but the chloride content is different from the C_2S paste with same w/b but free of gypsum and alkali. While presence of gypsum decreased the critical entry diameter (Figure 5-3b) and also lead to lower chloride content, NaOH lead to higher total porosity in the microstructure and slightly higher content of chloride. Mixtures containing silica and metakaolin lead to refinement of porosity (Figure 5-3c), which could be as well linked to lower chloride retention. When different types of binders are compared (C_2S binder and white cement), we clearly see how porosity does not play the biggest role anymore. The white cements paste have a much coarser porosity than the C_2S pastes (due to the higher w/b used), nonetheless the amount of chloride retained is comparable at this NaCl concentration. The amount of porosity from MIP is further used to determine the volume of pore solution and to quantify the amount of Cl in C-S-H, which due to its surface area and chemical composition, is expected to play a more important role.
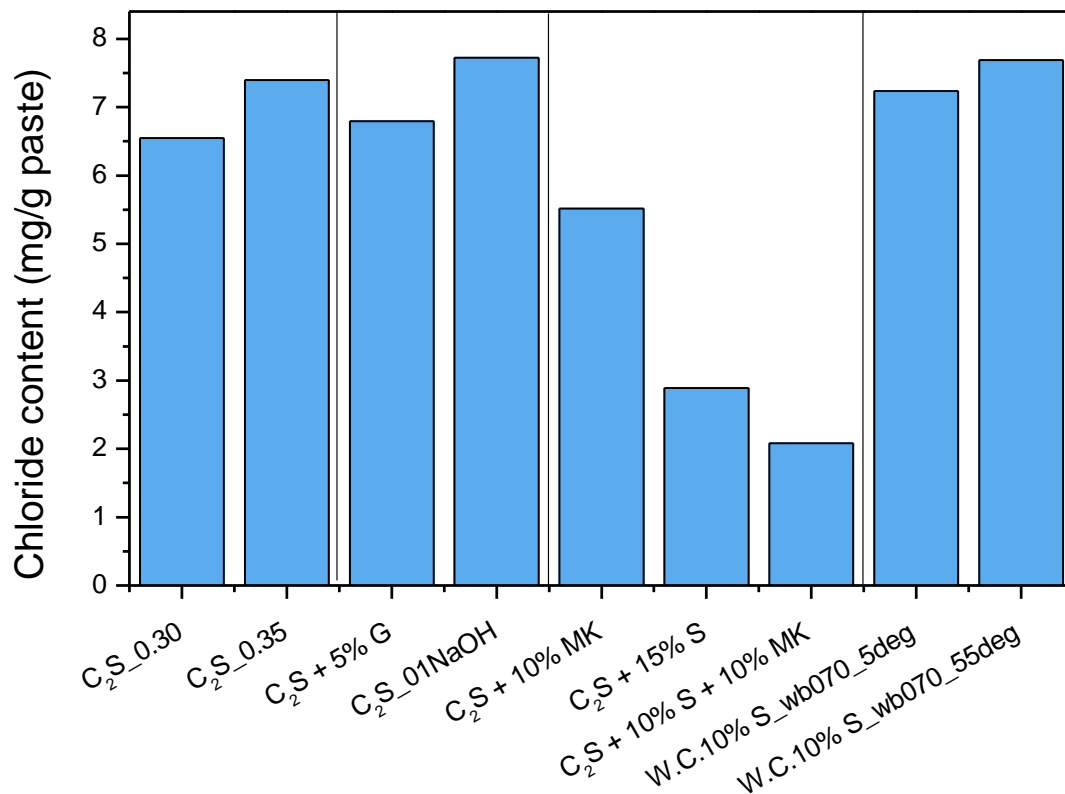
Figure 5-2. Amount of total chloride in samples equilibrated in 0.5M NaCl solution

Two methods of determining the pore solution volume (via solvent exchange and via MIP curves) were used to quantify the C-S-H – Cl and pore solution – Cl. The results are shown in Figure 5-4 (a – for the pore solution method and b – for the MIP method). The values used for the calculation are given in Table 5-3 in the Appendix of this chapter. The two methods give similar results for most samples, except for the samples with 15%S and 10%S10%MK. For the hydrated C_2S pastes, the amount of chloride in the pore solution is very small compared to the amount of chloride in the C-S-H. In the case of samples with silica and metakaolin, the same observation does not hold, as a lower total amount of chloride retained resulted in low amount of Cl in the C-S-H. Concerning the white cement paste, due to the high porosity, the amount of chloride in the pore solution was higher than the amount of chloride in the C-S-H. The value considered here might even be overestimated, as chemical binding in AFm phases was not determined.
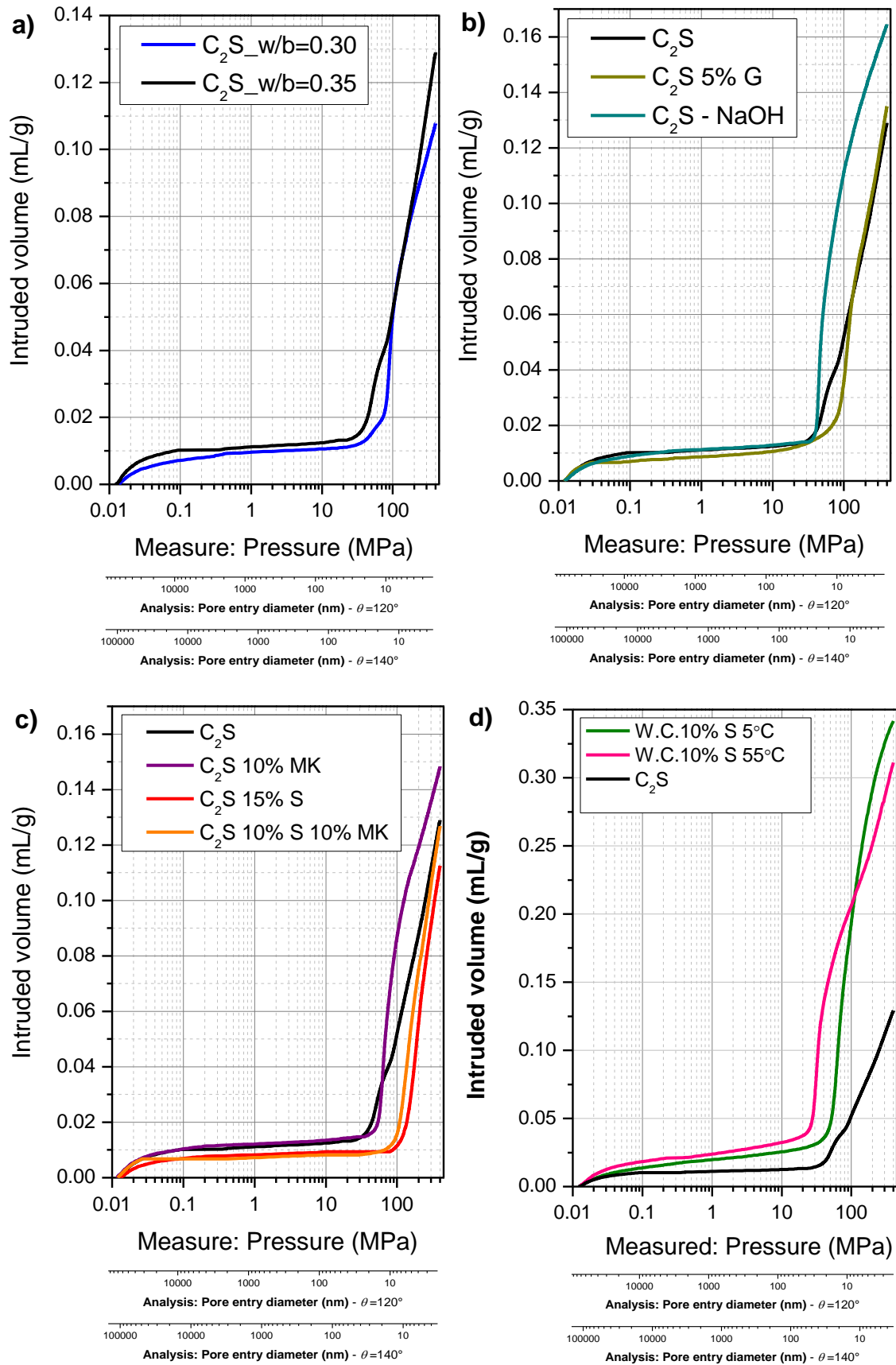
Figure 5-3. MIP curves of the investigates systems at 28 days of hydration: (a) plain hydrated C_2S samples with different w/b ratios, (b) pastes prepared with gypsum or NaOH solution, (c) pastes containing silica or/and metakaolin and (d) white cement paste with 10% silica
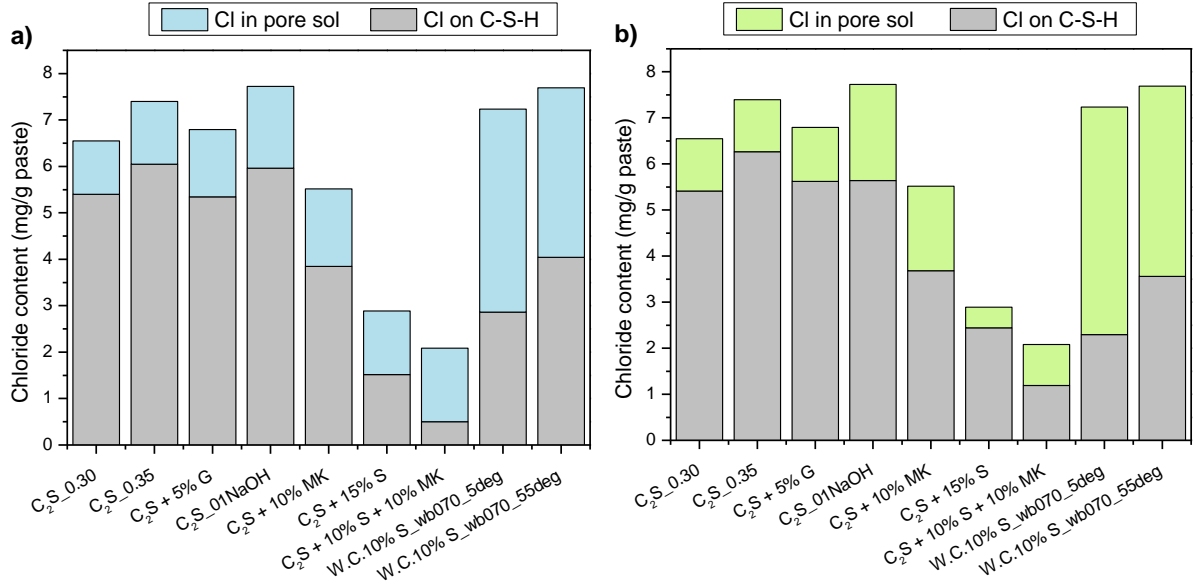
Figure 5-4. Amount of chloride in the pore solution and adsorbed on C-S-H for samples, the volume of pore solution was determined using solvent exchange data (a) and MIP pore distribution (b)

The influence of the C-S-H surface on the amount of adsorbed chloride was considered for selected samples with known s.s.a. (described in subchapter 4.3.3.) and the isotherms are presented in Figure 5-5. In both cases, the amount of chloride adsorbed on the C-S-H, determined by removing from the total chloride content, the free chloride in the pore solution is considered. In subfigure a), the chloride amount is normalized per amount of C-S-H in the wet pastes, while in subfigure b), the chloride amount is represented per unit area of C-S-H, calculated using Eq (4):

$$m_{Cl}^* \left[{}^{mg}/_{m^2} \right] = \frac{m_{Cl}[{}^{mg}/_{g_{C-S-H}}]}{s.s.a. \ [{}^{m^2}/_{g_{C-S-H}}]} \tag{4}$$

where m_{Cl}^* is the amount of chloride per unit area of C-S-H, m_{Cl} is the amount of chloride per amount of C-S-H and s.s.a. is the BET specific surface area of C-S-H, determined by nitrogen adsorption.

The s.s.a. values used in the equation correspond to samples hydrated for 9 months (for all samples containing silica or metakaolin) or 28 days, when measurements were not carried out at 9 months (sample containing NaOH). For the reference C$_2$S sample, the s.s.a. of the 28 days paste was as well considered, as the 9 months s.s.a. was inexplicably high and it would lead to a very low content of chloride per unit area of C-S-H (this is represented by the grey dashed line in subfigure b).

When looking at the subfigure a), one can observe that the isotherm of the sample prepared using NaOH is comparable to the one of the reference C$_2$S at lower NaCl concentrations, but at higher concentrations, the amount of chloride in C-S-H is lower. When it comes to the C-S-H formed in presence of silica and metakaolin, the samples with 10% S have retained slightly less Cl than the reference C$_2$S while the hydrates formed in the mixtures with 15% S and 10% S 10% MK have adsorbed the lowest amount of chloride at all NaCl concentrations. Concerning the subfigure b), one can again observe differences between the reference C-S-H and the hydrates formed in the other systems. The alkali containing sample has adsorbed similar amounts of Cl per unit area of C-S-H at lower NaCl concentrations, but lower amounts were adsorbed at higher concentrations. The two C-S-H in the mixtures containing metakaolin retained lower Cl/m^2 of C-S-H than the reference at all NaCl

concentrations. Surprisingly, in the two mixtures containing silica, the C-S-H seemed to have bound more Cl per unit are than the reference C-S-H. Ideally, if the amount of adsorbed Cl would be a function of only the available surface, all C-S-H samples should have very similar isotherms. In this case, we clearly see how samples with different s.s.a. can, at the same time, retain different amounts of chloride per unit area.
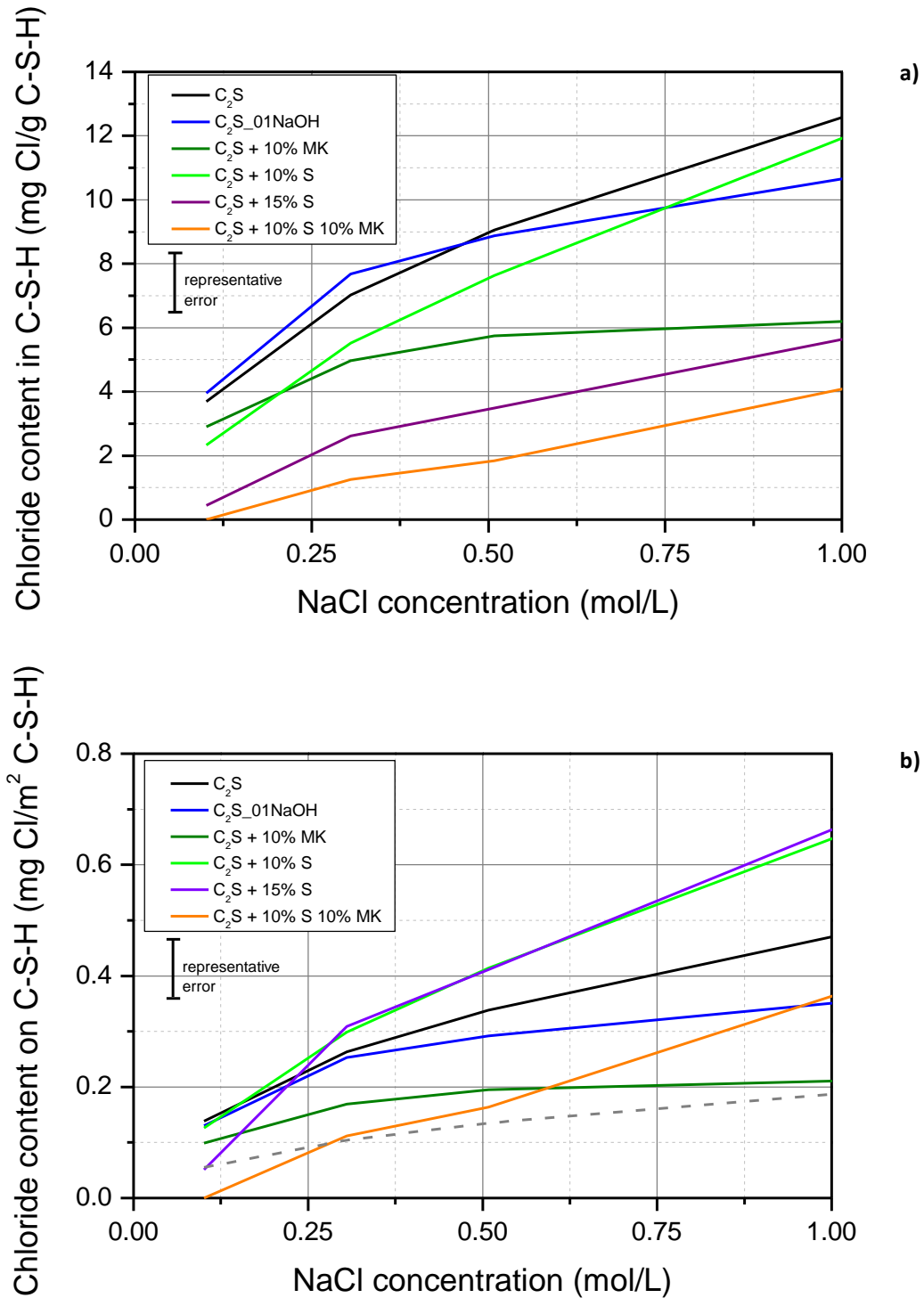
Figure 5-5. Chloride isotherms for selected C-S-H samples, expressed per weight of C-S-H (a) and unit area of C-S-H (b)

In Figure 5-6, the amount of chloride in C-S-H expressed in Figure 5-4b was plotted as function of the amount of Ca in C-S-H for the samples. It was considered that Ca goes almost exclusively in the C-S-H, the portlandite amounts are insignificant (see Chapter 3). This allows for a visualization of the role of Ca content on the amount of chloride retained. Additionally, the Cl is exclusively bound in C-S-H as no other phases were formed during the equilibration in NaCl chloride (see Figure 5-11 in the Appendix of this chapter).
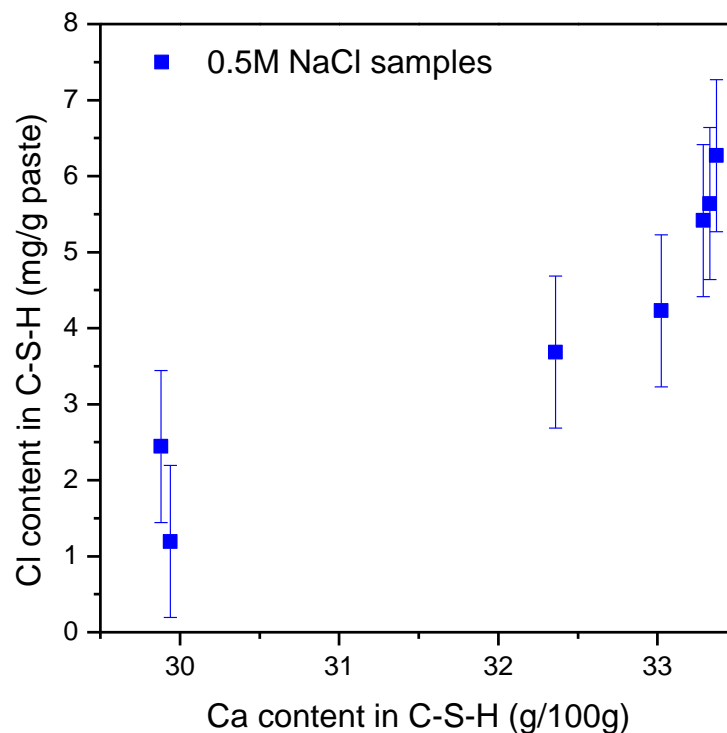
Figure 5-6. Cl content in C-S-H as function of the Ca content in the C-S-H for the hydrated C_2S systems

One can observe that with decreasing Ca content in the C-S-H, the content of Cl is decreasing as well. The samples with higher Ca content in C-S-H (which translates in higher Ca/Si ratio) have adsorbed comparable amounts of chloride. When the binder was hydrated with silica and/or metakaolin, the Ca/Si ratio decreases, thus the total number of Ca adsorption sites is decreasing, leading to a lower adsorption of chloride negative ions per molecule of C-S-H.

Illustrating the effect of Ca content in C-S-H on the amount of adsorbed chloride was attempted by recording the binding isotherms of the three synthetic C-S-H samples having different Ca/Si ratio (1.20, 1.50 and 1.80). The results are shown in Figure 5-7. For comparison purposes, the binding isotherm of the C_2S paste with w/b 0.35 was added as well. It can be seen how the synthetic C-S-H retained more Cl at almost all NaCl concentrations. A challenging process is to correctly quantify the amount of Cl in the C-S-H solid, as the plotted values correspond to the amount of Cl in the whole C-S-H gel samples, which includes the C-S-H solid together with a certain amount of free water.
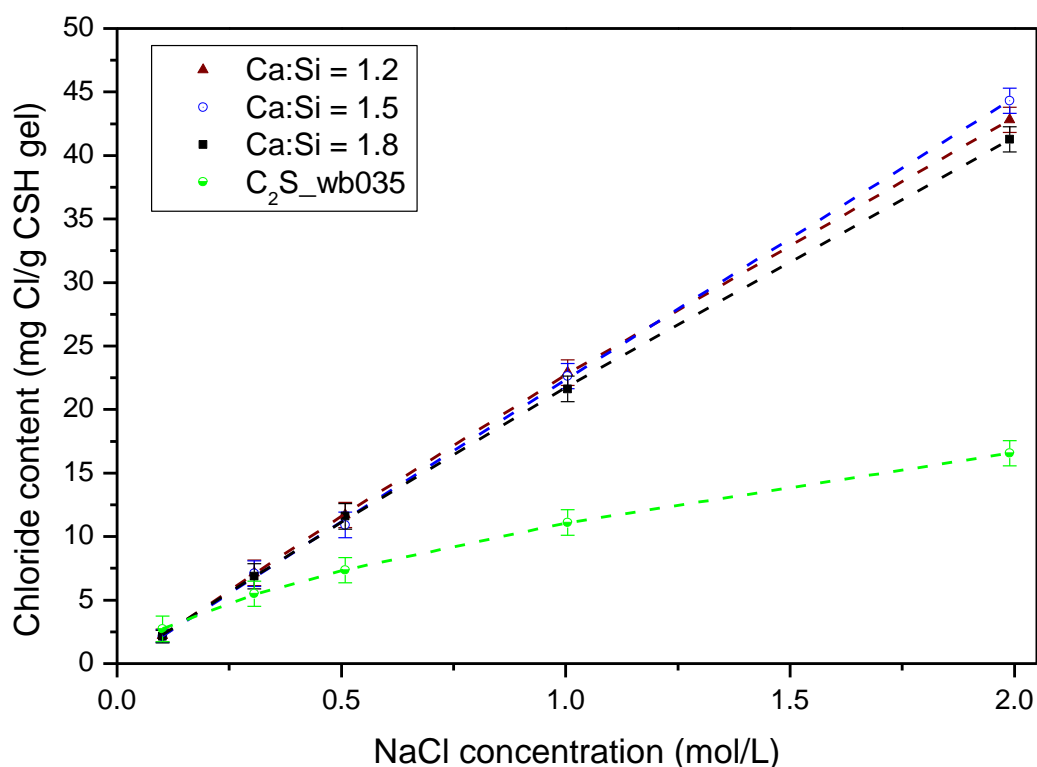
Figure 5-7. Chloride binding isotherms for synthetic C-S-H samples as compared to one hydrated C_2S system

The quantification of the free water is challenging due to the nature of synthetic C-S-H, which is prone to carbonation when exposed to air. Freeze-drying was chosen as a technique to record the amount of water in the gel which is not part of the C-S-H solid. Because the measurements were carried out in a different facility, the filtration technique described in Section 2 was not available, so before being introduced in the freeze-dryer, the gels were filtered by conventional vacuum filtration. The amount of free water for the three types of C-S-H is given in Table 5-2. There is a decreasing trend of the free water content with increasing Ca/Si ratio. After subtracting the free water content from the sample weight, the amount of chloride in the free water was as well subtracted from the total amount of chloride retained from the solution, thus the corrected values for the chloride adsorbed on the C-S-H were obtained.

Table 5-2. Corrected amount of chloride on synthetic C-S-H surface

NaCl concentration	C-S-H, Ca:Si = 1.2		C-S-H, Ca:Si = 1.5		C-S-H, Ca:Si = 1.8	
	free water = 61.55 g/100g dry C-S-H		free water = 55.52 g/100g dry C-S-H		free water = 50.60 g/100g dry C-S-H	
	Chloride content	Corrected chloride content	Chloride content	Corrected chloride content	Chloride content	Corrected chloride content
mol/L	mg/g gel	mg/g C-S-H	mg/g gel	mg/g C-S-H	mg/g gel	mg/g C-S-H
0.1	2.20	2.03	2.15	1.96	2.13	1.93
0.3	7.14	7.07	7.08	6.97	6.88	6.61
0.5	11.70	11.39	10.91	9.98	11.59	11.25
1.0	22.91	22.14	22.63	21.71	21.62	20.01
2.0	42.80	38.86	44.31	42.16	41.28	36.87

At almost all NaCl concentrations, the reduction in adsorbed chloride content is rather small and comparable even to the experimental error given by the method. No clear relationship with the Ca/Si ratio could thus be established. Further characterization of these gels is needed, as the amount of sodium nitrate left in the gel after washing and filtering in an unknown variable. It cannot be excluded that the C-S-H precipitated through this method contains a certain amount of alkali adsorbed, which could contribute to the chloride adsorption through their positive charges. Another unknown variable is the surface area of the synthetic C-S-H gel, although a variation with Ca/Si ratio has not been mentioned in previous publications.

Direct quantification of the amount of chloride adsorbed on C-S-H was attempted by SEM-EDS measurement. The values determined for the Cl/Ca and Ca/Si of C-S-H for two samples, one C$_2$S paste cured in lime water and another one equilibrated in NaCl solution are plotted in Figure 5-8a. As it can be observed, there is a small amount of Cl in the sample which was not in contact with NaCl solution, due to the resin used for impregnation. Overall, the Cl/Ca ratios of the sample equilibrated in 2.0M NaCl solution were higher.
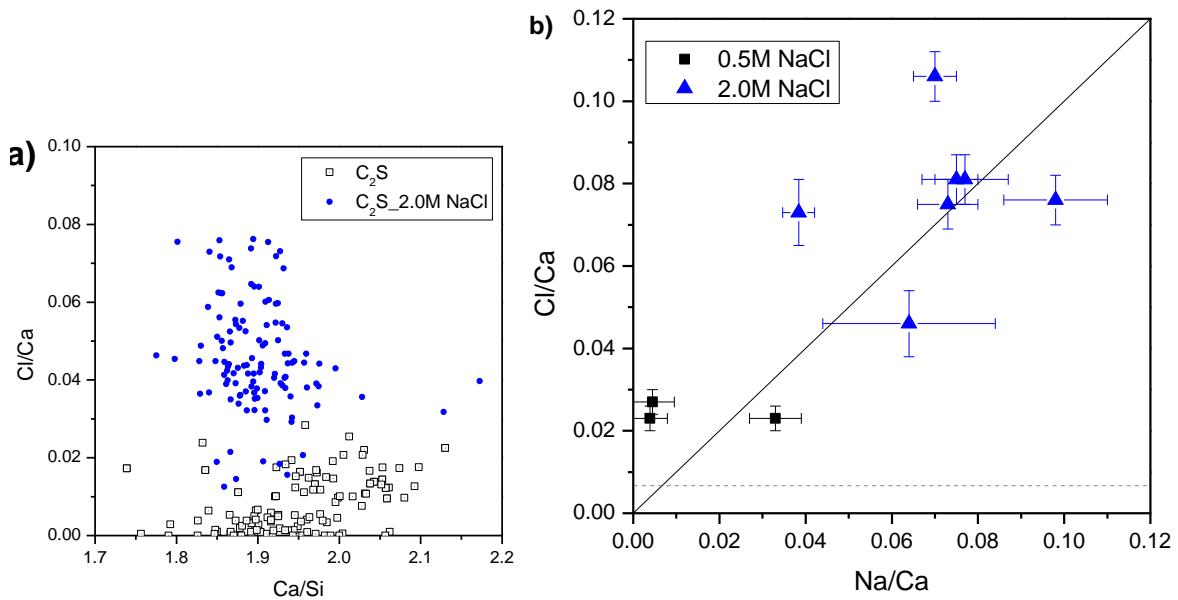
Figure 5-8. (a) Cl/Ca vs Ca/Si atomic ratios from SEM-EDS for C$_2$S samples cured in limewater and sample equilibrated in 2.0M NaCl solution; (b) Ca/Ca and Na/Ca atomic ratios for all selected samples equilibrated at 0.5M NaCl, horizontal dash line represents Cl signal than can be expected due to the resin used for impregnation

The resulting Ca/Si ratios and the Na/Ca ratios are plotted in Figure 5-8b, where the average Cl/Ca expected as background signal due to resin is plotted as a reference line at Cl/Ca 0.065. Samples equilibrated at higher NaCl concentrations have higher Cl/Ca ratios, the maximum value corresponding to the white cement sample. Amongst the group of samples equilibrated at the same NaCl concentrations (0.5M or 2.0M), one can observe that the distribution of the values is comparable to the scatter of values within the same sample (given by the error bars). For this reason, the values could not be used to accurately quantifying the amount of Cl in each sample. A common process that can interfere with this method is the precipitation of NaCl from the pore solution when the hydration is stopped by the solvent exchange method. Additionally, there is no evidence of how chloride ions bound to the C-S-H surface behave when the pore solution is removed, whether desorption occurs and to which extent the partial desorption happens.

5.3.2. Desorption of chloride

The results of the desorption experiment are shown in Figure 5-9. For both the hydrated C_2S pastes and the white cement paste, there is a significant decrease in the Cl content (more than 50%) after the 1-minute washing step. This is suggesting that there is probably a fast exchange between the pore solution and the bulk water, with part of the Cl desorbing from the surface. The interaction of Cl with the adsorption sites must therefore be a weak one. Given the small amount of sample used for this test, differences between the systems are disregarded, as it is not clear at this point if the remaining Cl in the C-S-H can be a function of the Ca/Si ratio or of the type of binder used.
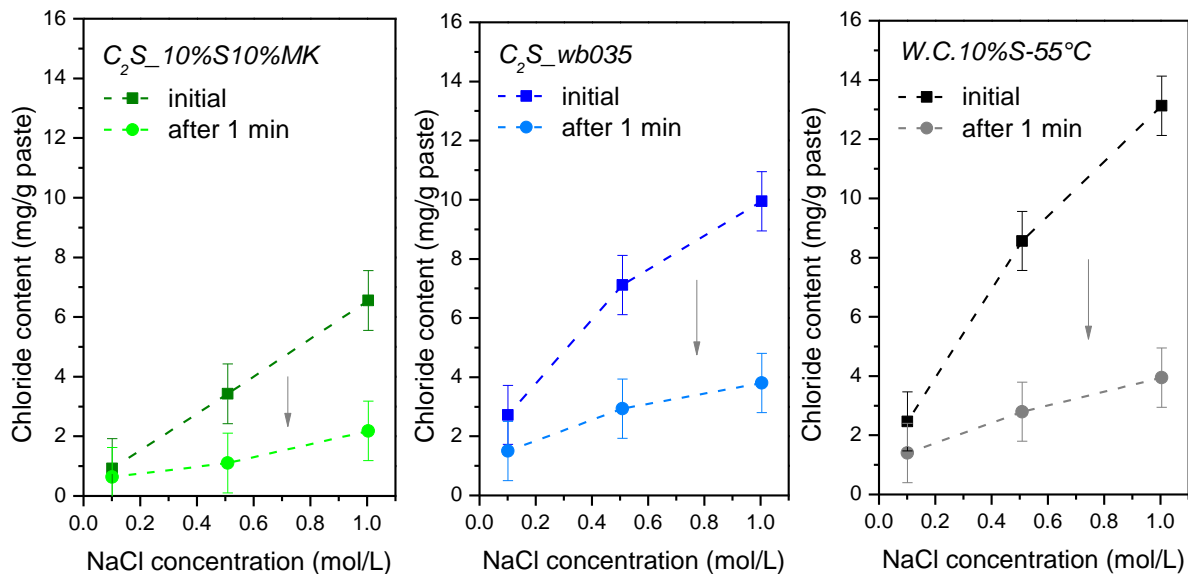
Figure 5-9. Chloride content in three of the samples before and after 1 minute washing with distilled water

5.3.3. Discussion

As seen in Figure 5-1, the amount of chloride that was bound in the various hydrated C_2S systems is by all means not negligible. For the determination of the adsorbed chloride on the C-S-H, the pore solution volume was determined by two separate methods and the results were in good agreement. The physical adsorption on the surface of C-S-H can be understood when two important parameters that characterize the C-S-H are considered: the s.s.a. and the surface chemistry. Neither of these two parameters alone can account for the different amounts of chloride bound in the different samples presented here. If the amount of available adsorption sites would be the only parameter influencing the adsorption, all the C-S-H microstructures would retain the same amount per unit area. On the other hand, if the surface chemistry itself would govern the binding process, we should observe a simple and direct relationship between the amount of chloride and the Ca/Si ratio (or the amount of Ca in the C-S-H, as the surface chemistry is a function of the chemistry of C-S-H). Two important aspects need to be kept in mind when comparing the amount of chloride normalized per unit area of each sample. The notions of "surface" considered in the two experiments can be somehow different. The s.s.a. determined by nitrogen adsorption and BET method records the available surface of a dry powder after performing solvent exchange. This itself questions the nature of the surface being measured, as this process is dynamic and the obtained information reflects a microstructure that does not correspond to the saturated state. Additionally, the microstructure can

be modified as a result of the drying step, with some part of finer porosity collapsing. The very fine internal structure of C-S-H and its surface area can only be measured by X-ray in techniques such as small angle X-ray scattering (SAXS). Unfortunately, due to their limited availability and high complexity, such methods are not yet widely used to study the C-S-H structure and surface. On the other hand, during the adsorption experiment, the microstructures are saturated at all times and chloride can access all the pores, as they are all filled with pore solution. Therefore, some surfaces might be accessible to chloride during the uptake experiment, but the same surfaces might become inaccessible during nitrogen adsorption, if they were found to be in the collapsed pores. This could explain why some samples seem to have adsorbed more chloride per unit area than others. Although one cannot ignore the surface chemistry factor, given that the interaction between chloride and C-S-H surface is due to charge balance and larger surfaces would not necessarily lead to more bound chloride if the surface charge density were decreased.

The values obtained for the C_2S samples with higher Ca/Si ratio agree well with values mentioned in [121] and [123], approx. 5 mg Cl/g C-S-H. It is worth mentioning as well that the OPC systems studied in [121] had a Ca/Si ratio of C-S-H of 1.85. Concerning the white cement paste, despite having very high porosity, a quite low amount of Cl was bound in the microstructure. Since it was not accounted for the chemical binding in AFm phases, this would lead to even lower values for the chloride adsorbed on C-S-H. As reported in [121] the chemical binding and physical binding were of the same order of magnitude for hydrated OPC. This would bring the real Cl content on C-S-H to values very close to those of the hydrated C_2S with 15% S and 10%S 10% MK. These mentioned systems all have a much lower s.s.a. and lower Ca/Si ratio in C-S-H than the plain hydrated C_2S binder. For the white cement sample cured at 5°C, the average Ca/Si ratio measured by SEM-EDS was 1.41 ± 0.05, while the C_2S sample with 10%S 10%MK had 1.20 from SEM-EDS and 1.59 from TEM at 28 days hydration. It is likely that more of silica and metakaolin react and the Ca/Si ratios of the two systems might be more similar, since the chloride measurement was started after 6 months of curing and samples were left to equilibrate for 10 months. The trend observed for the chloride content in the C-S-H to decrease with Ca content (Figure 5-5) gives an indication of the role of Ca/Si ratio in the adsorption process. This agrees well with results reported in [126], where the chloride content is decreasing with Ca/Si ratio for synthetic C-S-H samples which has similar surface areas. The implications of this are intriguing, as there might be a value of Ca content in C-S-H (or Ca/Si ratio) at which the physical binding becomes insignificantly low. As suggested in [83], below the Ca/Si ratio 1.50, the surface is covered in Si-OH groups. Above this value, they groups are deprotonated and Ca is introduced in the interlayer. This could indicate that around this Ca/Si ratio, the adsorption capacity might change significantly.

Decoupling the influences from the two factors is not an easy task, especially when they vary at the same time for one considered C-S-H sample. The addition of SCMs such as silica and metakaolin have become so common because it leads to an improvement of several properties simultaneously. Variation of C-S-H chemistry without changing the microstructural parameters is not possible, while changing the C-S-H properties and not affecting the chemical composition is as well not a desired approach, since usage of all SCMs has always an impact on the different atomic ratios of the C-S-H.

The SEM-EDS method to directly quantify the amount of chloride in C-S-H was shown not to be sensitive enough to compare different samples equilibrated at the same NaCl concentration. As suggested in [121], there is a relatively large variation in Cl concentrations in the microstructure at the

volume analyzed by SEM-EDS. Nevertheless, the Cl/Ca ratio for samples equilibrated at 2.0M NaCl is 2-3 times higher than the Cl/Ca ratio for the samples equilibrated at 0.5M NaCl. When considering the amount of chloride in the pastes determined by titration at these 2 concentrations, a similar ratio of the two chloride contents was obtained for most samples.

Concerning the desorption process, the isotherms of the samples in Figure 5-9 are shown again in Figure 5-10, but in this case, for the washed samples, the amount of chloride was plotted function of the concentration of the solution after 1 minute of contact. This method allows a better visualization of changes between both the retained chlorides by the pastes and the equilibration bulk solutions in which these pastes were kept.
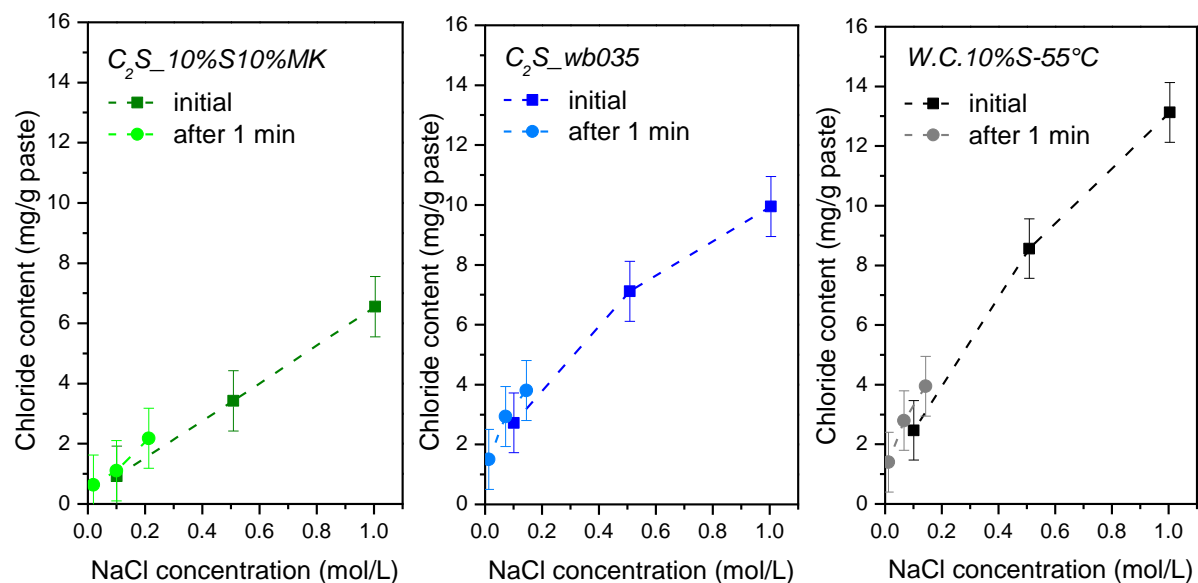
Figure 5-10. Chloride content in three of the samples before and after 1 minute washing with distilled water, for the washed samples the concentrations of the resulting solutions were used instead of the initial ones

Although a major part of the physically bound chloride in all three pastes paste was released in the water, the resulting concentration of the solutions remained very low. A very different outcome was reported by Zibara in [122], where almost 80% of the initial bound chlorides were still retained after equilibrating samples at a liquid/solid ratio of ≈ 10, while the ratio adopted in this study was 4. Additionally, in their study, the water was saturated with $Ca(OH)_2$ and they mentioned it was possible that the released Cl$^-$ ions were replaced by OH ions through an ion exchange mechanism. Distilled water was used for this study so it is clear that just the reduction in the chloride concentration in the pore solution of the pastes resulted in the partial release of bound chloride. These plots also serve as visual indication on how small the amounts of chlorides were retained from the initial equilibrating solutions, since after 1 minute of contact, the released chloride only led to concentrations of solutions approx. 10 times lower. Nevertheless, the amount that could be removed after a 1 min washing with distilled samples was very high. This indicates that desorption is a relatively fast process and one can expect that remaining amount of chloride can be easily removed as well. Beaudoin et al [126] showed that after washing synthetic C-S-H samples with a large volume of water for 1 day, the amount of chloride still left in the sample, which he called tightly held chloride, is an order of magnitude lower than chloride that was removed by washing.

As illustrated in Figure 5-4, the amount of chloride that was found in the pore solution is much lower than the amount of chloride adsorbed on the C-S-H. This is mainly due to the low w/b ratio used for preparing the pastes. In practice, the conventional value for the water-to-cement ratio can be as well lower than 0.4 and with increasing amounts of SCMs used, the total porosity can be even lower than in the C_2S pastes described in this study. Most of the total amount of bound chloride by a paste can be thus attributed to the C-S-H and the other hydrates. The physical binding only serves to balance positive charges on the surface. For this, two conditions need to be fulfilled: the surfaces are accessible (the porosity is not mostly closed) and the C-S-H has an excess of calcium ions on its surface. For the usual hydrated OPC this is always the case, but for systems containing certain SCMs, it would be possible that physical binding becomes insignificantly low when compared to the chemical binding.

5.4. Conclusions

The amount of chloride adsorbed on C-S-H was determined for various hydrated C_2S systems free of AFm (which translates in no chemically bound chloride). The role played by the pore structure, available surface of C-S-H and Ca content of C-S-H in the amount of Cl that was adsorbed in each system was discussed. A direct consequence of replacing part of the binder with micro-silica or metakaolin is the simultaneously reduction of total porosity, s.s.a. and Ca/Si ratio of C-S-H, this leading to lower amounts of physically bound chloride at all NaCl concentrations, when compared to the reference C_2S. A similar observation can be made regarding the white cement pastes, which seemed to have retained as well less chlorides in the C-S-H, compared to the reference C_2S. Besides the significant differences in porosity, there were also differences in the Ca/Si ratio of the C-S-H, although the C-S-H surface of the white cement pastes was not characterized.

Desorption experiment performed on selected crushed samples showed that in just 1 minute of equilibrating the samples in distilled water, significant amount of Cl can be removed, thus indicating there is a weak interaction between the Cl and C-S-H surface.

Role of silica and metakaolin could be better understood if, in future studies, reference mixtures with an inert material (such as quartz) are used for comparison. Additional information of the surface charges (Zeta potential measurements) could give a better indication of the role C-S-H surface has in the uptake process.

Acknowledgments

Appendix

Table 5-3. Pore volume of investigated mixtures

Nr.crt.	Sample	Volume of pore solution removed by solvent exchange, mL/g solid	Total volume of pores with diameter > 10nm, obtained from MIP curve, mL/g solid
1	C_2S – w/b=0.25	4.93	2.27
2	C_2S – w/b=0.30	7.30	7.2
3	C_2S – w/b=0.35	8.58	7.28
4	C_2S + 5% G – w/b=0.35	9.12	7.5
5	C_2S + 0.1N NaOH – w/b=0.35	11.15	13
6	C_2S + 5% G + 0.1N NaOH – w/b=0.35	10.95	12.86
7	C_2S + 10% S – w/b=0.35	6.21	1.44
8	C_2S + 15% S – w/b=0.35	7.63	2.6
9	C_2S + 10% MK – w/b=0.35	10.00	10.88
10	C_2S + 10% S 10% MK– w/b=0.35	8.58	4.99
11	W.C. 10% S – w/b=0.70, 5°C	23.12	25.6
12	W.C. 10% S – w/b=0.70, 55°C	20.82	23.1
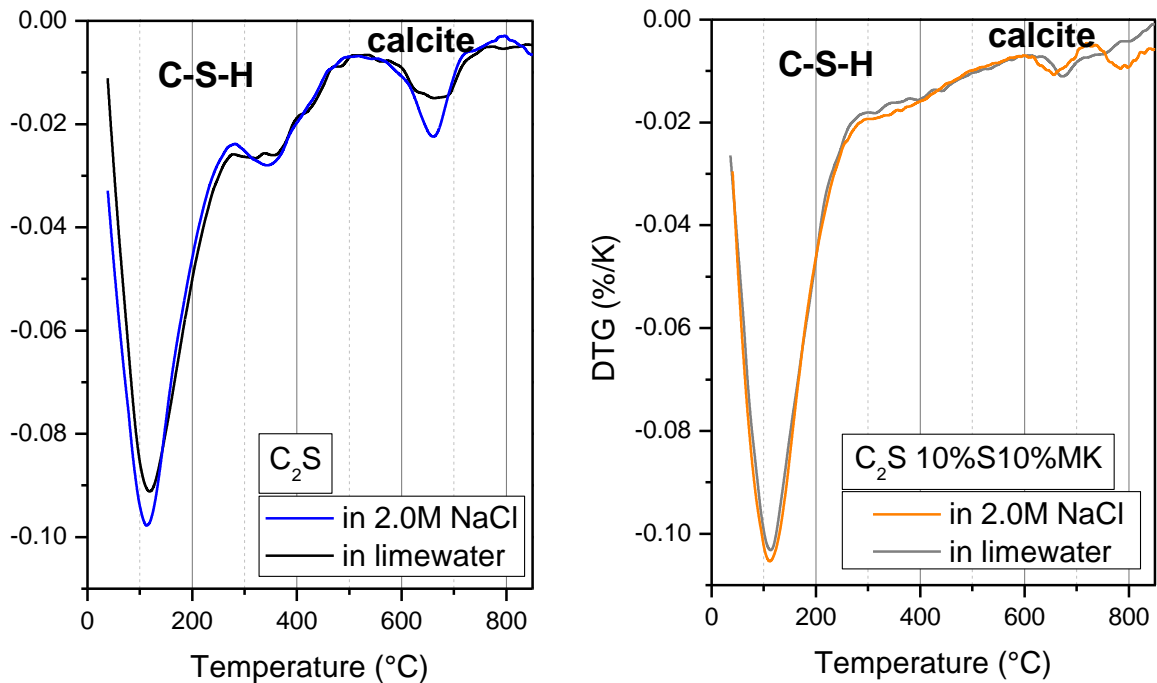
Figure 5-11. DTG curves for two samples (hydrated C_2S and mixture C_2S + 10%S 10% MK) cured in lime water and after being equilibrated in 2.0M NaCl solution for 10 months, showing there are no additional phases formed in the chloride environment

Chapter 6. Chloride migration through C-S-H microstructure

6.1. Introduction

In reinforced concrete, transport of chloride ions through the hydrated cement matrix to the steel reinforcement leads to pitting corrosion and deterioration of the surrounding area. Research studies have focused on this process with the purpose of ranking the chloride resistance of concrete and to obtain input parameters for the prediction of service life of concrete structures subjected to chloride environments [132]–[135]. To obtain information about the transport of chloride through concrete structures, diffusivity tests are performed. The rate of diffusion of an ion through a network is characterized by diffusion coefficient, often referred as diffusivity. Experimental setups to determine diffusivity of cementitious materials can be divided into four categories [136]:

    a)   through-diffusion based on measuring fluxes;
    b)   in-diffusion based on measuring concentration profiles in the sample;
    c)   electro-migration experiments, ion diffusion being accelerated by an electric field;
    d)   techniques in which proxy variables are used to determine diffusivity (e.g. electrical resistivity techniques).

The experimental setups can vary from easy to complex and the test duration can vary from few days (electro-migration tests) to even few years (through-diffusion experiments). Various diffusing species can be considered for diffusivity measurements: water, ions or dissolved gases [136]. In steady state diffusion/migration tests (with a constant chloride flux), the effective diffusion/migration coefficients are determined. They refer to the diffusivity of chlorides in the pore solution by taking into account the volume fraction of the permeable pores in the entire volume of concrete. The apparent diffusion/migration coefficients obtained in the non-steady-state tests represents the diffusion/migration of chlorides in the pore solution of concrete, taking into account the reaction between the chlorides and the porous medium (so-called chloride binding) [137].

Accelerated tests where an electric field is applied have gained a lot of interest due to shorter time needed to determine the diffusion coefficient [138]. It is assumed in these tests that convection does not operate inside the concrete and that diffusion is negligible compared to migration [139]. In an electric field, positive ions will move preferentially to the negative electrode and negative ions to the positive one. The chloride conductivity test therefore provides an indication of overall diffusivity, being sensitive to changes in pore structure and concrete chemistry [132]. In a study done using the

Rapid Chloride Migration Test (RCM), described in the guideline NT Build 492 [140], it was concluded that the voltage in the investigated range was not influencing the chloride migration coefficients significantly [141]. While in steady state, the diffusion equation can be expressed by Fick's first law (Eq. (1)), for the accelerated migration, the Nernst-Plank equation is usually used – Eq. (2). To characterize the chloride flux, chloride ion concentration of the downstream solution must be periodically monitored to ensure that only the movement of chloride ions will be used to evaluate the diffusion coefficient [138].

$$J = -D \frac{\partial c}{\partial x} \tag{1}$$

where J is the flux, D is the diffusion coefficient., c is the chloride concentration and x is the depth.

$$J = \frac{zFDc}{RT} \frac{\partial E(x)}{\partial x} \tag{2}$$

where z is the ion valency (-1 in the case of chloride), F is the Faraday constant, E(x) the external electrical field applied on the system as a function of the location x, R the universal gas constant, T the temperature in Kelvin and c the chloride concentration in the upstream compartment.

Several studies have tried to establish a relationship between the of type of cement and resulting microstructure and the transport properties. Sakai et al [142] reported that a good correlation between total porosity and chloride diffusion was found when the sample did not include admixture materials and the chloride diffusion test was conducted without acceleration. When limestone was used in ternary blends with calcined clay, the chloride resistance was improved [143]. The pore solution plays a very important role in chloride transport as well [143], [144]. The relationship between several microstructure parameters and the effective chloride diffusion coefficients has been described by Wilson et al [144]. The pore solution conductivity plays a significant role in diffusion, but when the bulk conductivity is also used (and the pore connectivity parameter is determined β), the relationship is not straight-forward. The pore connectivity parameter can be obtained from the formation factor F, which may be expressed in terms of resistivity or conductivity of the pore solution and bulk concrete, as given in Eq. (3) [144]–[146]. Overall, the incorporation of supplementary cementitious materials in blended-cements pastes increased the resistance to chloride ingress by reducing the pore connectivity parameter and/or the pore solution conductivity [144]. Shekarchi et al [95] reported that transport properties measured in terms of water penetration, gas permeability, water absorption, electrical resistivity, and ionic diffusion were improved in mixtures containing metakaolin.

$$F \equiv \frac{\rho_b}{\rho_0} = \frac{\sigma_0}{\sigma_b} \cong \frac{1}{\emptyset\beta} \tag{3}$$

where ρ_b is the resistivity of the bulk concrete, ρ_0 is the resistivity of its pore solution, σ_0 the conductivity of the bulk concrete, σ_b the conductivity of its pore solution and $\emptyset$ the porosity.

Studies have usually focused on studying the overall transport process of different liquids or gases through the hydrated matrix of cement, which is composed of C-S-H and other hydrates (portlandite, aluminum sulfate phases). Therefore, the contribution of C-S-H and the influence of its

chemical composition to the overall transport process is not always easy to separate from the contribution of the other phase. In this work, a hydrated C_2S microstructure composed of only C-S-H was studied in terms of chloride migration. Another type of C-S-H microstructure, formed by hydrating white cement with micro-silica was used to reveal the impact the nature of the C-S-H has on chloride resistance.

6.2. Materials and methods

The composition of the systems investigated in this Chapter are given in Table 6-1. The pastes were prepared exactly as described in Chapter 5 and cured in lime water for at least 6 months prior the test. The mini-migration approached described in [144] was used, since a small paste sample could be tested (as opposed to big concrete specimens) and the measurement time is reduced to maximum 14 days. Slices of 10 mm thickness were cut from the bulk cylinder pastes, gently polished on both sides and glued on a plastic holder. After the glue has hardened, the sample is kept overnight in lime water, to ensure complete saturation of pores. The sample was then placed between the two compartments of the mini-migration setup, upstream and downstream (see Figure 6-1). The upstream compartment was filled with lime water prepared using laboratory grade $Ca(OH)_2$ (Merck) and had a concentration of 0.5 M NaCl (Merck), while the downstream contained just lime water.
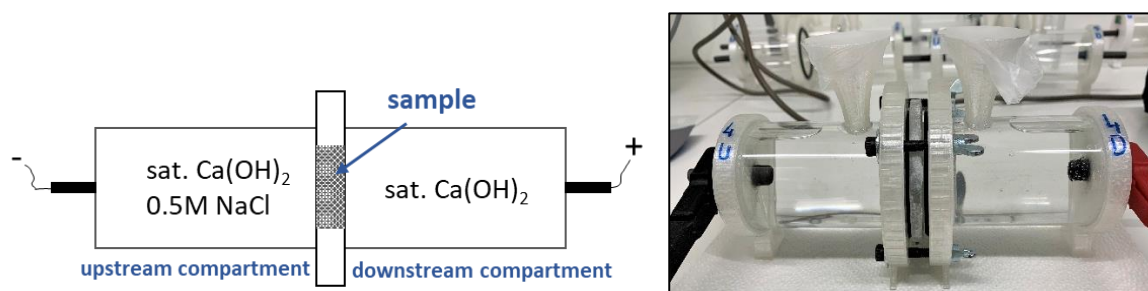
Figure 6-1. Schematic representation of the mini-migration setup (left) and image of the setup used (right)

An electrical voltage was applied using a power source (Farnell D30 2T 30V 0-2A Dual Output Power Supply) and the intensity through the circuit was measured using multimeter (Benning mm2 digital multimeter). The downstream compartment was sampled 2-3 times every day by collecting 5 mL of the solution and replacing it with 5 mL of lime water. The concentration of the sampled solutions was determined without dilution. 1-2 mL were introduced in a measurement beaker, to which 10 mL HNO_3 (65% supplied by Merck and diluted 1:1) and approx. 90 mL of deionized water were added. The chloride content was determined with a T90 titrator from Mettler Toledo equipped with Rondo autosampler, using 0.1 M or 0.01 M $AgNO_3$ solution (Merck, Titrisol).

Table 6-1. Investigated mixtures composition

Investigated systems	
C_2S − w/b=0.25	C_2S + 10% S − w/b=0.35
C_2S − w/b=0.30	C_2S + 15% S − w/b=0.35
C_2S − w/b=0.35	C_2S + 10% MK − w/b=0.35
C_2S + 5% G − w/b=0.35	C_2S + 10% S 10% MK− w/b=0.35
C_2S + 0.1N NaOH − w/b=0.35	W.C. 10% S − w/b=0.70, 5°C
C_2S + 5% G + 0.1N NaOH − w/b=0.35	W.C. 10% S − w/b=0.70, 55°C

The diffusion coefficient was determined using a modified Nernst-Plank equation [144], which was adapted for the migration experiment as proposed in [139]:

$$D_{eff} = \frac{J}{c_{up}} \frac{RT}{F} \frac{l}{\Delta E} \tag{4}$$

where D_{eff} is the chloride effective diffusion coefficient (during the steady state regime), R is the gas constant, T is the temperature, F is the Faraday constant, l is the specimen thickness, c_{up} is the chloride concentration in the upstream reservoir, ΔE is the voltage drop across the specimen, and J is the chloride flux through the specimen [mol/m^{2}s]. Experimentally, J can be determined from the slope $\dot{m}_{Cl^-}$ of the chloride mass in the downstream reservoir as a function of time:

$$J = \frac{\Delta c_{down} V_{down}}{\Delta t A} = \frac{\dot{m}_{Cl^-}}{M_{cl}} A \tag{5}$$

where Δc_{down} is the variation of the chloride concentration in the downstream reservoir per time interval Δt, V_{down} is the volume of the downstream reservoir, A is the specimen surface area, and M_{Cl} is the molar mass of chlorine (35.45 g/mol).

Hydrate characteristics were observed before testing at different hydration ages by stopping the hydration reaction using the solvent exchange technique, using isopropanol followed by a quick washing with petroleum ether [81]. For MIP measurements, bulk hydrated samples were crushed and the fraction 1-2 μm was selected. The analysis was performed using a Pascal 140/440 Porosimeter from Thermo Scientific up to a maximal pressure of 400 MPa. The C-S-H content of the microstructures was determined by XRD-Rietveld refinement analysis [147]. The XRD patterns of the powders were obtained at room temperature using a Bruker D-8 Advance diffractometer in a θ-θ configuration with CuKα radiation (λ = 1.54059 Å) and for the Rietveld analysis the external standard method was used, using quartzite. A scanning electron microscope Zeiss EVO LS10 with a Quantax400 Detector from Bruker was used to investigate the microstructure of the hydrated specimens. For chemical analysis of the C-S-H, EDS point analysis and mapping were carried out on selected areas. All samples for SEM investigations were impregnated under vacuum with a spectrally transparent epoxy resin (EpoTek® 301). Thin slices from hydrated specimens were used, except for the samples hydrated in suspension, where hydrated powders impregnated. The impregnated samples were gradually polished down to 1 μm with a diamond spray and petrol as a lubricant and coated with a thin conductive layer of carbon (15 nm). The SSA$_{BET}$ was determined by five-point N$_2$ absorption / desorption isotherm measurements using a NOVA Touch NT4LX-1 from Fa. Quantachrome using the BET-equation (BET = Brunauer, Emmett and Teller). Dried powders specimens were ground to < 63 μm and a gentler degassing protocol was used, 24 hours at 30 °C under constant N$_2$ flow and medium vacuum.

6.3. Results and discussion

6.3.1. Parameters of the mini-migration cell

The applied external voltage and the measured initial intensities of the mini-migration cells containing the samples are given in Table 6-2. The approach was to use similar values for the external applied voltage for all investigated systems. The intensity of the current was then measured at the beginning of the test. As a general observation, at the same applied voltage, the intensity measured trough the setup for different systems varied. According to Ohm's law, the ratio between the voltage and intensity is the resistance of the setup [148]. Given that the setups and solutions used are constant, a change in the intensity of the current/resistance of the setup would be due to different samples. For samples containing silica and metakaolin, higher values of the external voltage had to be used, as the measured intensity was in some cases very low (see values in Italic). This translates in a higher resistance than for the plain hydrated C_2S binder, which means the electric current cannot pass as easily through the sample. Note that these parameters do not contribute to the calculation of the D_{eff}, it is the measured voltage between the two compartments which can directly affect the value of the D_{eff}.

Table 6-2. Initial parameters from mini-migration setup for the investigated samples

Nr.crt.	Sample	External applied voltage (V)	Measured initial intensity (mA)
1	C_2S – w/b=0.25	5.5	6.5
2	C_2S – w/b=0.30	5.5	7.5
3	C_2S – w/b=0.35	5.0	9.0
4	C_2S + 5% G	5.5	8.0
5	C_2S + 0.1N NaOH	5.5	9.0
6	C_2S + 5% G + 0.1N NaOH	5.5	8.0
7	C_2S + 10% S	*10.0*	*4.5*
8	C_2S + 15% S	*10.0*	*< 1.0*
9	C_2S + 10% MK	*10.5*	*< 1.0*
10	C_2S + 10% S 10% MK	*10.0*	*< 1.0*
11	W.C. 10% S, 5°C	5.5	8.0
12	W.C. 10% S, 55°C	6.0	7.5

The evolution of mass of chloride in the downstream compartment as function of time for two different samples is illustrated in Figure 6-2. In the first 1-2 days, usually no significant amount of chloride passed in the downstream compartment. After the breakthrough point, the chloride started to pass though the sample and the concentration in the downstream compartment increased. The steady state was then achieved, the slope of the evolution curve was determined and used for the calculation of the D_{eff} value. The values for the slope of the curve are mentioned in Figure 6-2 for the two samples. The peak chloride content was usually achieved in 5-6 day, afterwards the migration was not in steady state anymore. Due to increased concentration of chloride in the solution, chemical reactions occur at the anode and sometimes chlorine starts to evaporate, making the concentration to decrease.
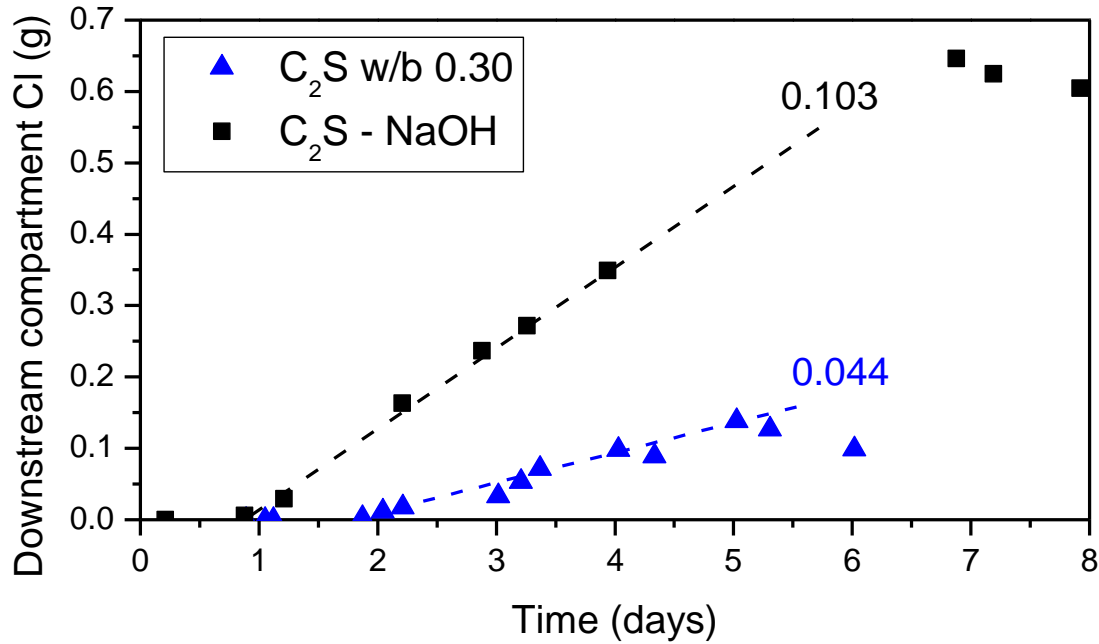
Figure 6-2. Evolution of the mass of chloride in the downstream compartment as function of time for hydrated C$_2$S at w/b 0.30 and hydrated C$_2$S with 0.1N NaOH solution at w/b 0.35. The indicated number on the trendlines represent the slope of the chloride mass in the downstream reservoir as a function of time ($\dot{m}_{Cl^-}$) used for the determination of D$_{eff}$

6.3.2. Chloride diffusion coefficients

The chloride effective diffusion coefficients calculated with Eq (4) for the various investigated systems are illustrated in Figure 6-3. Vertical lines were placed to separate the four different groups of samples: hydrated C$_2$S at different w/b ratio, hydrated C$_2$S in presence of gypsum or alkali, mixtures of hydrated C$_2$S containing silica or metakaolin and hydrated white cement with silica. There are two main observations one could make from the D$_{eff}$ values. The first one is that the diffusion coefficient for the plain hydrated C$_2$S samples decreases with decreasing w/b and the second one, the sample containing silica and metakaolin have D$_{eff}$ one order of magnitude lower than the hydrated C$_2$S prepared with the same w/b ratio. Some factors were considered to decouple the influences of the microstructure on the D$_{eff}$ value.

The pore network was the first microstructure feature to be associated with variations of the D$_{eff}$. As the diffusion constant is only determined for the steady state part of the experiment, the physical binding of chloride in C-S-H is not considered. Undoubtedly, the C-S-H also plays a role in the migration of chloride ions and that will be covered as well. The MIP analysis was used to obtain the total pore volume and the critical pore entry diameter of the analyzed samples, as these can provide information about the percolating network of spaces that can enable the chloride transport.
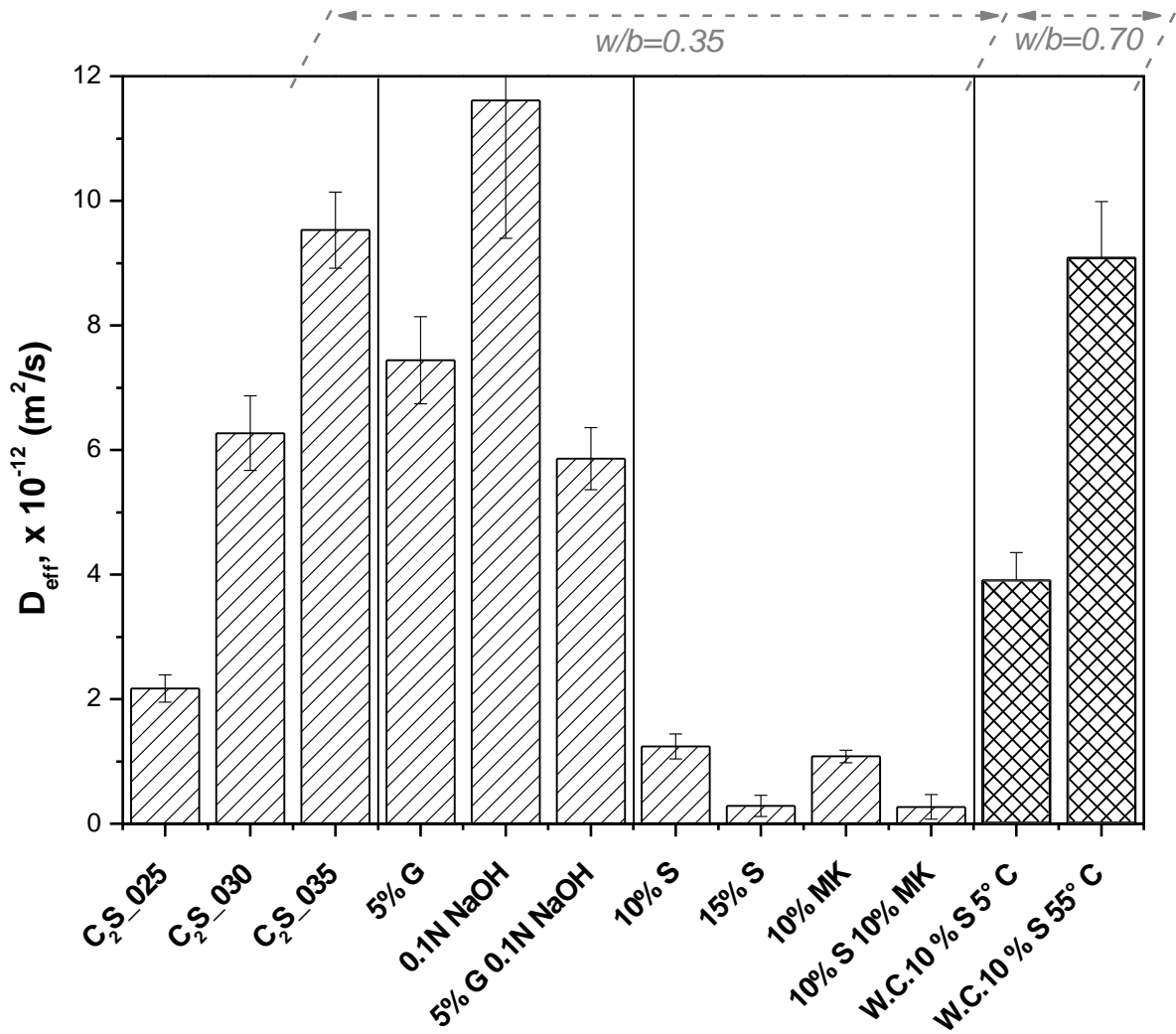
Figure 6-3. Effective chloride diffusion coefficients D_{eff} of the investigated systems

The diffusion coefficients were plotted as function of the total intruded volume by MIP (Figure 6-4a) and the critical entry diameter (Figure 6-4b). There is a clear trend for the plain hydrated C_2S sample (black squares) to show a lower diffusion coefficient with lower total porosity, as a result of a lower w/b. This relationship is not as direct for the other samples. Despite being hydrated at the same w/b ratio, the distribution of total pore volumes is wide. The samples prepared with silica and metakaolin have total pore volumes comparable with the hydrated C_2S at a lower w/b (0.30) but the D_{eff} value is six times lower. An interesting observation is related to the samples containing gypsum. The hydrated C_2S and $C_2S+5\%G$ have the same total pore volume and so do the samples C_2S-NaOH and $C_2S+5\%G$-NaOH. In both cases, the sample containing gypsum had lower D_{eff} coefficients than the samples without, the reduction being more significant for the pair of samples containing alkali. The relationship between the total pore volume of the hydrated white cement samples and their D_{eff} values is not intuitive, as the D_{eff} was higher for the paste having lower total porosity. Addition understating of these variations come from analyzing the dependency of the D_{eff} on the critical pore entry diameter. Once again, there is a good agreement for the hydrated pastes containing only C_2S at various w/b. The D_{eff} value decreased with decreasing critical pore entry diameter. The group of samples containing gypsum and/or alkali do not seem to have any clear relationship. Nevertheless, the sample containing alkali fits the trend given by the three hydrated C_2S samples (grey dashed line).
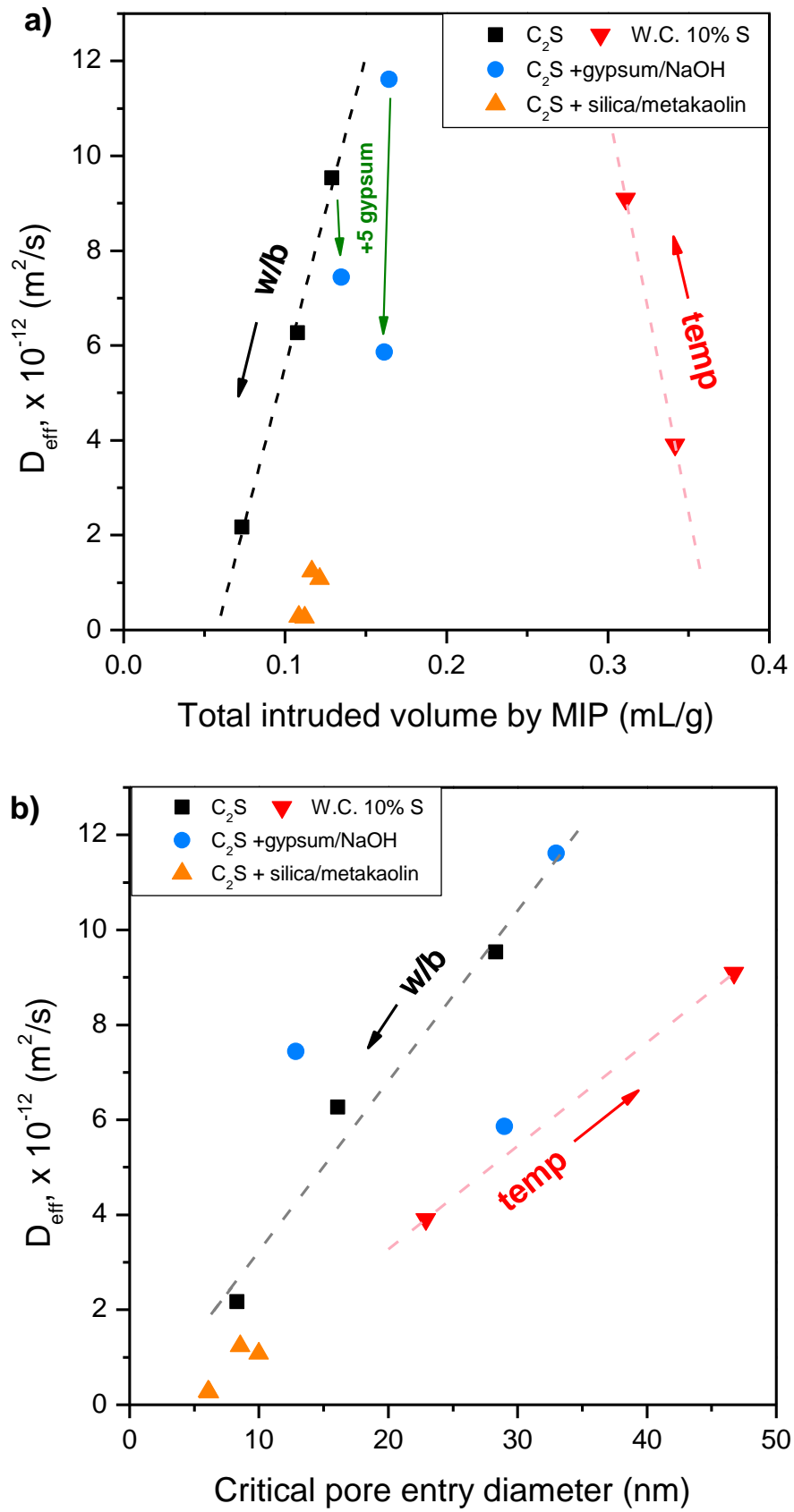
Figure 6-4. Effective chloride diffusion coefficient, D_{eff}, as function of (a) total intruded volume and (b) critical entry pore diameter, determined by MIP. For simplicity, groups of samples are represented with the same symbol, instead of labeling each point in the plots. For the D_{eff} value of each sample, the reader is referred to Figure 6-3

Both samples containing gypsum (with and without alkali) have lower D_{eff} that the hydrated C_2S without gypsum at the same w/b ratio, but only for the sample with gypsum and no alkali was the porosity refined. From the group of four samples with silica and metakaolin, two of them had similar critical pore entry diameter with the C_2S hydrated at low w/b (0.25), while the D_{eff} was slightly lower. In the case of samples with 10%S 10%MK, they had both the lowest critical entry pore diameter and the lowest D_{eff}. For the two white cement sample, the correlation between D_{eff} and the critical entry diameter is showing that at higher curing temperature (55°C), the microstructure is coarser and thus the D_{eff} is increased. The slope given by these two samples is flatter than the one given by C_2S at three w/b ratio. The white cement sample cured at lower temperature (5 °C), showed a comparable critical entry diameter when compared to hydrated C_2S with w/b 0.30, but the D_{eff} value was half.

6.3.3. Discussion

Since the hydrates are a very porous phase, their contribution to the chloride migration has to be considered as well. Theoretical work has shown that the time dependence of the effective diffusion constant in porous media contains information about the surface-to-pore volume ratio, the tortuosity and other parameters of the analyzed inert substrate [149].

Two types of surface-to-volume (S/V) ratios were considered in this study and for both of them, the s.s.a. of samples was used, as it was considered an interface between the solid and the liquid phase. The first determined ratio relied on the total pore volume > 10 nm from MIP analysis (mentioned in Table 5-3 in Chapter 5). The second S/V considered the total solid volume in a paste, calculated by subtracting from the sample volume, the total pore volume > 10 nm from MIP analysis, according to the following equations:

$$S/V \ [1/m] = \frac{m_{C-S-H}\left[\frac{g_{C-S-H}}{g_{paste}}\right] \times (w_{sample} - V_{pores})[g_{paste}] \times s.s.a.\left[\frac{m^2}{g_{C-S-H}}\right]}{V_x[m^3]} \qquad (6)$$

$$V_x = V_{pores} \ \text{or} \ V_x = V_{solid} = V_{paste} - V_{pores} \qquad (7)$$

where S/V is the surface-to-volume ratio, m_{C-S-H} is the C-S-H content of the pastes, w_{sample} is the weight of the sample subjected to testing, V_{pores} is the total volume of pores > 10 nm, according to Table 5-3, $s.s.a.$ is the BET specific surface area of C-S-H, determined by nitrogen adsorption, V_{solid} is the volume of the solid phase in the tested sample and V_{paste} is the total volume of the sample, calculated using the formula for the volume of a cylinder:

$$V_{paste} = \frac{\pi d^2 h}{4} \qquad (8)$$

where d is the diameter and h is the thickness of the samples.

The representation of the D_{eff} as function of the two S/V ratios is given in Figure 6-5.
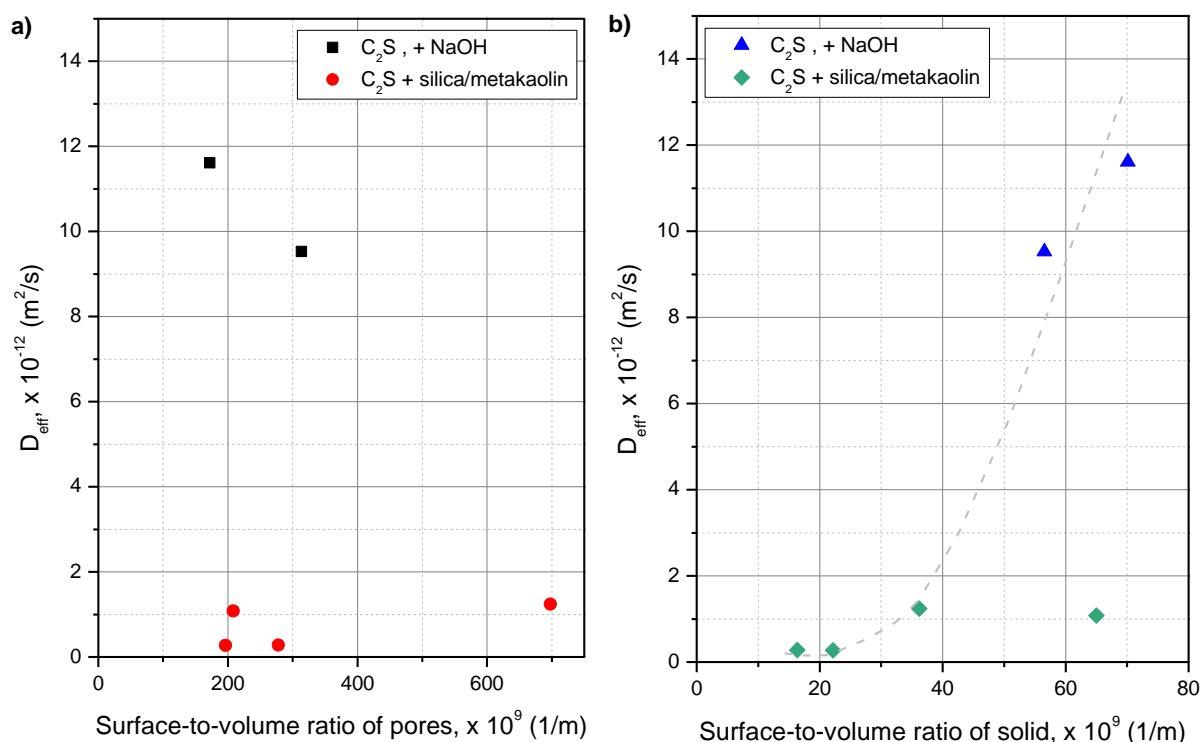
Figure 6-5. D_{eff} values for selected samples, plotted against the surface-to-volume ratios, considering either the total pore volume (a) of the total solid volume (b)

One can observe in Figure 6-5 a) that when the D_{eff} and the S/V ratio of pores are plotted together, no clear relationship can be established between the two. Furthermore, most of the analyzed samples had very similar S/V ratios, as a consequence of decrease of s.s.a. when the pore volume decreased as well. The outlier in the Subfigure a) is the sample containing 10% silica, for which there was a more significant decrease in the total pore volume than in s.s.a., when compared to the other samples. This is a good indication that at the same surface-to-volume ratio of pores, migration can occur at different speeds. In other words, there are other influencing factors affecting the diffusion when pore structure above a certain value of pore radius is similar. When looking at Subfigure b), we observe that the S/V ratio of C-S-H in all samples is not very similar anymore. In this case, the D_{eff} seems to increase with increasing the S/V ratio, although this relationship is linear only when maximum three points are considered. The two C-S-H microstructures formed with maximum content of silica and metakaolin (15%S and 10%S10%MK) are very different from the other samples because have both very low S/V ratios and D_{eff}. There is an outlier in this trend as well, the mixture with 10%MK having similar values of S/V ratio as the reference C_2S sample and mixture containing alkali, but a much lower D_{eff}. A particular aspect of this samples is the presence of alumina from the reacted metakaolin in the C-S-H, as well as in the pore solution of the microstructure. Ideally, if the diffusion would not be affected by chemistry of the surfaces and pore solution of the samples, all the points in the graph should pe positioned on a straight line. Still, one should not overlook the fact that out of the two figures, the one which considers the surface and amount of C-S-H provides some insight in the variation of the D_{eff}, as opposed to the one where only the total amount of bulk pore solution is considered.

The influence of pore network of the paste on the D_{eff} is clearly significant to some extent. For the same type of binder, by lowering the w/b ratio, the D_{eff} is as well decreased. This had been

reported in [144] where the pore connectivity parameter was determined for pastes of different composition. With lower w/b ratio, the pore connectivity parameter decreases and thus the path that chloride will follow through the matrix becomes geometrically more complex. Given the position of the alkali containing system on the plot in Figure 6-4, one could assume that the physical factor is the only one responsible for the change in D_{eff}. Nevertheless, it has been shown in [143] that the alkali content in the pore solution can directly influence the diffusion coefficient value, although the study only considered the apparent diffusion coefficient (from the bulk diffusion). The alkali content in the pore solution for hydrated C_2S prepared with NaOH solution was determined using mass balance and the corresponding D_{eff} values are plotted in Figure 6-6. For the determination of the pore solution volumes, the values given in Table 5-2 in the Appendix of Chapter 5 are considered together with the volume of curing limewater in which the samples were cured. The amount of alkali in the C_2S binder is practically 0 (as shown in Table 3-1 of Chapter 3) and the Na in C-S-H was extremely low, as described also in Chapter 3, so all the ions from the mixing water were considered to be exclusively in the pore solution. Indeed, with higher content of Na in the pore solution, the measured D_{eff} value increased. But this was valid only for systems without gypsum. Presence of gypsum decreased the D_{eff} value in both alkali free and alkali containing system, and surprisingly, the reduction was more considerable in the case of the alkali containing system. This effect is counter-intuitive and it cannot be explained without further investigation.
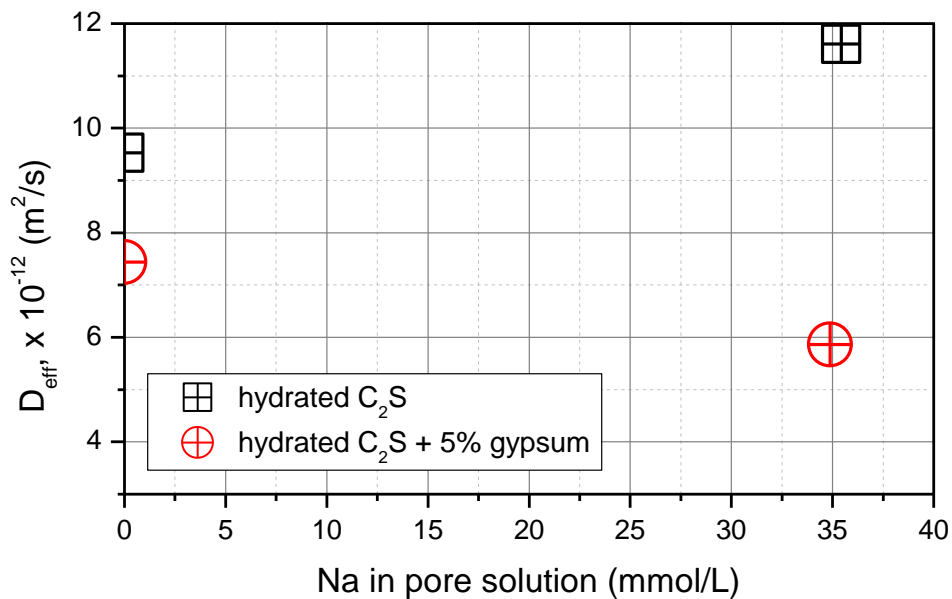
Figure 6-6. Relationship between the effective chloride diffusion coefficient, D_{eff}, and the sodium ions content in the pore solution

On the other hand, changes in the pore network and surface-to-volume ratio of C-S-H are not sufficient to cause the differences in the diffusion coefficient between the hydrated C_2S binder, the mixtures with silica and metakaolin and the white cement pastes. The densification of the matrix for systems containing silica and metakaolin is undeniable, but two of the systems had slightly lower critical entry pore diameter while having D_{eff} values four times lower. This has been reported before and in [144] it was mentioned the important role that bulk conductivity plays in the migration process. At lower values of bulk conductivity, the D_{eff} decreases. One could believe that addition of silica and metakaolin leads to lower values of the bulk conductivity, although a direct relationship has not been established. It is as well expected that the pH of the pore solution would decrease, with increased

content of silica and with hydration age [150]. Another consequence of presence of silica and metakaolin was the reduction of Ca/Si ratio of C-S-H (See Chapter 4 Figure 4-4). The white cement pastes have a lower Ca/Si ratio of C-S-H as well, as given in Table 6-3. The critical pore entry diameter for the white cement paste cured at 5° is slightly higher that the hydrated C_2S at w/b 0.30, but the D_{eff} is almost 50% lower. Given the high w/b ratio of the white cement pastes, this suggests that the D_{eff} hydrated C_2S with the same high w/b ratio (0.70) would have a D_{eff} at least one order of magnitude higher. This suggests there might be some fundamental differences when it comes the two types of C-S-H microstructures. The microstructures of the hydrated C_2S and the white cement paste are given in Figure 6-8 in the Appendix of this chapter, one could assume that the fast hydration of the reactive C_2S results in a high 'dispersion' of C-S-H in matrix and thus the pore connectivity parameter (β) would be much higher than for a hydrated OPC. Nevertheless, all the evidence in this study points out how much of a difference 10% silica can produce in the microstructure. The white cement pastes were also prepared using 10% silica, to consume part of the portlandite and maximize the content of C-S-H. We cannot appreciate how high the values of the D_{eff} would be if the samples were free of silica, but the comparison with the hydrated C_2S could be very different.

Table 6-3. Ca/Si ratio of C-S-H, measure by SEM/TEM for hydrated C_2S sample and white cement pastes

Sample	C_2S	C_2S + 10%S 10%MK	W.C.10%S – 5 °C	W.C.10%S – 55 °C
Ca/Si ratio	1.94 ± 0.04	1.28 ± 0.04 (SEM) 1.59 ± 0.04 (TEM)	1.51 ± 0.05	1.41 ± 0.05

As shown in Figure 6-3, the samples containing silica and/or metakaolin had the lowest D_{eff} values. These samples also gave the highest resistance when placed in the setup (see Table 6-1). This correlation is in agreement with an observation from Tong et al [151], where the conductivity of the NaCl saturated concrete and diffusivity were determined. The values were in good agreement, so they concluded that for a given binder system and type of concrete, measurements of initial electrical conductivity appear to provide a good basis both for estimation of chloride diffusivity and for routine control of concrete quality.

As suggested by the Figure 6-5-b), the surface-to-volume ratio of hydrates could directly influence the chloride diffusion. The migration path depends on the interconnected porosity and this is tightly connected with the C-S-H amount and possibly the gel pores. In Chapter 5 it was as well shown that the C-S-H is responsible for the significant amount of chloride binding, as compared to the free ions in the pore solution. To explore the possibility of C-S-H governing both migration and binding, the D_{eff} was plotted as function of the chloride content in C-S-H in Figure 6-7. The Cl in C-S-H was determined by subtracting from the total bound Cl, the amount of Cl in the pore solution (See Chapter 5 Figure 5-4b), then normalizing it to the amount of C-S-H estimated using XRD-Rietveld refinement. As observed, there is no clear relationship between the two results, various hydrated C_2S samples having similar Cl content in the C-S-H while the D_{eff} varies independently. All the hydrated mixtures with silica and metakaolin have low D_{eff} values, while in some systems, the chloride content in C-S-H was comparable to the plain hydrated C_2S or the white cement pastes. One can conclude that even for C-S-H systems less complex than SCMs containing systems, there is no straight-forward relationship between how much Cl can adsorb on C-S-H and how fast it can go through the connected porosity of the C-S-H. As suggested in [152], in a pore, the Cl ion will diffuse through the bulk solution,

since in the double layer, the positive ions are more concentrated and the diffusion through this space is negligible.
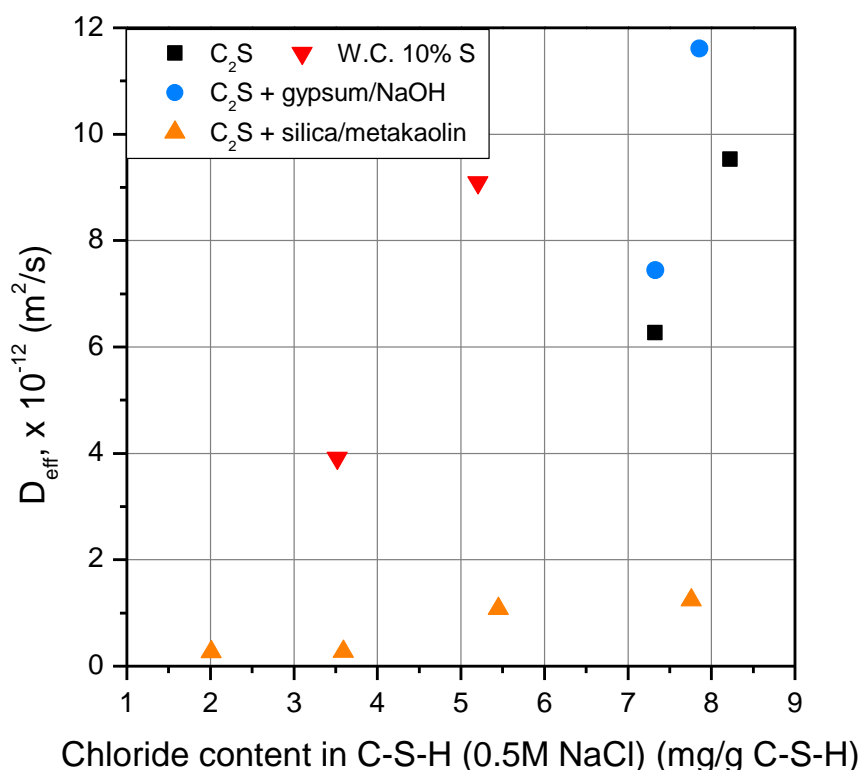
Figure 6-7. Effective chloride diffusion coefficient, D_{eff}, plotted together with the amount of chloride in C-S-H for various investigated systems

Generally, the transport process in hydrated cementitious materials has to be modelled accounting for the classical Fick's diffusion mechanism, as well as considering the electrical coupling between the various ions and chemical activity effects [153]. Reactive transport models and simulators were developed in which the microstructure is customizable [135]. The advantage of using the reactive C_2S is not having to focus on chemical binding and the physical binding does not affect the results, as only the steady-state regime is considered for the calculation of the effective diffusion coefficient. This cannot be achieved with hydrated Portland cements or composite cements, as their resulting microstructures always contain aluminate phases which lead to formation of Friedel or Kuzel's salts. Synthetic C-S-H is an excellent candidate to investigate particle properties, but a solid microstructure cannot be easily achieved, especially not with the same degree of complexity as in the hydrated cementitious systems. Although the mentioned models for reactive transport could have been simplified and used in this study, elaboration of a new model for transport in C-S-H was not an objective of this project. A different project in the ERICA programme, project no. 10 deals with understanding the transport phenomena from an atomic interactions point of view.

The transport process can only be understood when analyzed from a perspective which includes several factors. The physical and chemical influencing factors are not easy to decouple, as sometimes they can vary simultaneously. Nevertheless, the calcium silicate hydrates govern the transport through their surfaces, pores, and chemical structure. The effect of the gel pores on the transport was not investigated, due to limited availability of the ^{1}H NMR technique, but previous

studies have not reported significant differences in the gel pore structure of C-S-H of different types of hydrated cement pastes.

6.4. Conclusions

Effective chloride diffusion coefficients of various hydrated C_2S binder and white cement systems were determined using the mini-migration approach. Several parameters were shown to have an influence on the D_{eff} value: water-to-binder ratio, presence of alkali and gypsum, addition of silica and metakaolin. Overall, the plain hydrated C_2S is less resistant when it comes to chloride penetration than a hydrated white cement paste prepared with the same w/b ratio. The silica and metakaolin cause changes in C-S-H chemistry and microstructure that significantly increase the resistance to chloride penetration. These results are in good agreement with values from studies where variations in the pore connectivity parameter and conductivity of bulk samples and pore solution accounted for differences in D_{eff}.

Better characterization of the bulk samples is needed to fully understand the influence of type of binder and addition of silica and metakaolin. Additionally, very low water-to-binder ratio systems (0.25) with higher level of substitution of C_2S would be interesting to study, as the resulting microstructure could have a high degree of depercolation.

Acknowledgments

Appendix
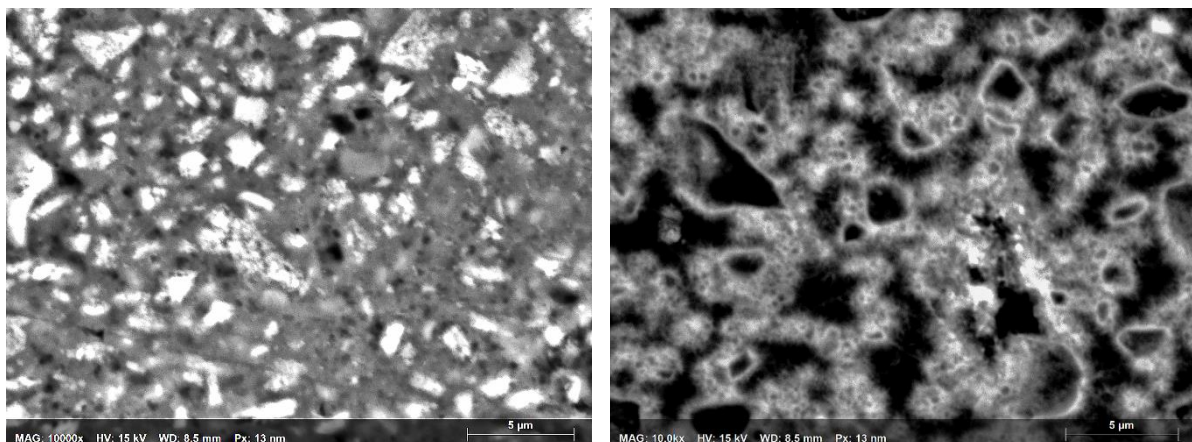
Figure 6-8. SEM micrographs of hydrated C_2S at w/b 0.35 (left) and hydrated W.C.10% S − 55 °C (right), hydration age 28 days. Despite the high porosity of the white cement paste, the D_{eff} of the two microstructures were comparable.

Chapter 7.   Conclusions and perspectives

The work presented in this thesis was developed in two directions to understand the evolution of C-S-H composition as function of several parameters and to characterize the transport properties of chloride through various C-S-H microstructures.

7.1. The C-S-H microstructure of the reactive C_2S binder

The reactive C_2S binder presented in this thesis is very different from the belite phase in Portland clinker. It was shown how, in a matter of a few days, all the reactive phases of the binder (the amorphous phase and the x-C_2S) are consumed to give a rich C-S-H microstructure. The hydration product was found to be homogenously dispersed and with interconnected, elongated particles. This allowed for the C-S-H composition and the microstructure features to followed in an easier manner, as opposed to the complex microstructure given by the hydrated OPC or SMCs containing cements. It was shown that with increasing the water-to-binder ratio, the C-S-H precipitated with lower Ca/Si ratios and the content of portlandite in the matrix increased. Introducing alkali ions in the pore solution lowered the final Ca/Si ratio of C-S-H and triggered the formation of portlandite even at w/b value 0.35, while by using 5% gypsum, the content of portlandite was lowered and the Ca/Si ratios remained high (close to 2.0). By hydrating the binder in suspension, the role of space and pH of pore solution was highlighted. With increasing pH, the content of portlandite increased, while the C-S-H formed at a Ca/Si ratio of 1.70, which is believed to be close to the thermodynamically stable form.

A more significant decrease in the Ca/Si ratio of C-S-H was observed for microstructures with added silica and metakaolin. The SEM-EDS method was used to show how the average Ca/Si ratio of the investigated volume is lower from the first day of hydration in mixtures containing silica, as compared to the plain hydrated C_2S. Given the interaction volume of the sample with the electron beam in the SEM, TEM was employed for a more accurate characterization of the atomic ratios. The expected Ca/Si ratios of the pastes with various contents of silica and metakaolin at 28 days were in the range $1.60 - 1.85$, while the Al/Si ratio of the samples containing metakaolin were in the range $0.07 - 0.10$. Although the degree of reaction of silica and metakaolin was not very high at 28 days, the reaction advances past this age. When compared to 9 months hydrated samples, characteristic silica signals in the FTIR spectra significantly decreased, the specific surface area of C-S-H decreased and the microstructure was slightly refined, especially in mixtures containing metakaolin. Morphology studies

carried out also by TEM showed there are several changes between the high Ca/Si ratio and the low Ca/Si ratio: the C-S-H fibers appeared to be thinner, less straight and more densely packed.

7.2. The transport properties

The chloride binding capacity of the various C_2S microstructures, as well as hydrated white cement pastes containing micro-silica and synthetic C-S-H powders was investigated by using thin slices or synthetic gel and equilibrating them for 6-10 months in solutions of different concentrations of NaCl. In this study, it was shown that the available C-S-H surface and Ca/Si ratio play the biggest role in the amount of adsorbed chloride. The C-S-H microstructures with higher specific surface area and higher Ca/Si ratio generally adsorbed higher amounts of Cl both per unit area and per unit weight of C-S-H. The mixtures prepared with the highest amount of silica and metakaolin, in which the Ca/Si ratio was the lowest, retained an extremely low amount of Cl on the C-S-H surface from the equilibrating solutions. At a given NaCl concentration, the white cement samples (which contained 10% micro-silica) retained lower amounts of Cl than the hydrated C_2S with high Ca/Si ratio C-S-H, but comparable amounts to the mixture containing 15% silica, in which the Ca/Si ratio of C-S-H was lower. The synthetic C-S-H powders retained at most NaCl concentrations more Cl than the hydrated C_2S pastes. In this experiment, no clear variation of the bound Cl with Ca/Si ratio of the synthetic C-S-H was observed. It was shown by desorption experiments that a large amount of chloride could be removed from the microstructure when the ground pastes were kept for 1 minute in distilled water, due to the weak interaction between the C-S-H surface and the chloride ions.

A mini-migration experiment was used to determine the effective chloride diffusion coefficients of various hydrated C_2S and white cement systems. The D_{eff} value was shown to be directly influenced by the following parameters:

- water-to-binder ratio – with higher values, the diffusion coefficient increased;
- presence alkali led to a slightly faster migration;
- by using 5% gypsum, the D_{eff} value was slightly decreased;
- addition of silica and metakaolin caused changes in C-S-H chemistry, pore solution and microstructure that significantly increase the resistance to chloride penetration.

The role of the pore connectivity parameter and conductivity of bulk samples and pore solution in the chloride migration was as well discussed for several systems. Overall, the plain hydrated C_2S binder is less resistant when it comes to chloride penetration than a hydrated white cement paste prepared with the same w/b ratio. To some extent, the impossibility of the C_2S system to chemically bind chloride can be responsible for this. A more significant role is played by the distribution of hydrates in the matrix, due to the fast reaction, the C-S-H is highly dispersed and interconnected, providing an environment easier for chloride to percolate.

It was proven that, although the C-S-H is responsible for the interconnected porosity of a paste, there is no straight-forward relationship between how much Cl can adsorb on C-S-H and how fast it can diffuse through the bulk solution of its gel pores.

7.3. Perspectives for future research

In this work, the evolution of the solid phase of the hydrated C_2S paste could be closely followed through various means. But the other important component of the paste remained unexplored. The study of the pore solution of a hydrated paste can provide vital information about the thermodynamic equilibrium between the solid and liquid phase at various hydration ages. The main limitation of the research plan in this work was that rather small amounts of the binder could be produced. Further optimization of the synthesis or exploring possibilities to process it on industrial scale could open the door to many interesting research directions. Characterization of the pore solution of pastes prepared with various w/b ratios could answer some questions regarding the C-S-H and CH equilibrium. This equilibrium could also be explored in a wider range of compositions with increasing content of alkali and gypsum. More concentrated solutions of NaOH could be used, as well as gypsum contents both lower and higher than 5%.

The consumption of silica and metakaolin in the absence of portlandite in the microstructure is another interesting outcome of the project. A direct quantification of the degree of reaction could be achieved by means of ^{29}Si MAS NMR, thus the kinetics of the reaction could be revealed. Improving the degree of reaction of the added SCMs could be attempted in two ways: by adding portlandite in the mix prior to hydration or by increasing the pH of the pore solution by using NaOH/KOH solutions. Although challenging, the analysis of the C-S-H at very early ages by TEM and a quantification of the Ca/Si ratio could show whether the C-S-H precipitates directly with a lower Ca/Si ratio or there is a strong decalcification happening over time.

Some possibilities remained still unexplored when it comes to chloride transport. Although it was shown that C-S-H can easily enable the passing of chloride ions, its direct contribution is yet to be fully understood. When analyzing the morphology of the C-S-H, as seen by TEM, one can imagine that chloride can access all the different classes of pores. An important question to answer would be which path is the one governing the transport? Is it only the gel pore path (see Figure 7-1), or are the small interhydrate pores contributing as well by accelerating or slowing down the transport? One way of isolating the influences coming from the different pore classes would be to subject unsaturated materials to transport tests. It is known there are certain relative humidity ranges at which pores above a certain diameter are emptied and, as a consequence, the transport would occur only though the filled pores. Nevertheless, care must be taken as even the slightest drying of C-S-H can produce changes in the microstructure and the obtain results could end up being altered. A different way of characterizing the movement of chloride ions in the different classes of pores would be through NMR. Dedicated magnets and special designs must be used to acquire a strong enough signal that can be translated in either self-diffusion coefficients of chloride or distribution of chloride in the gel and capillary pores.
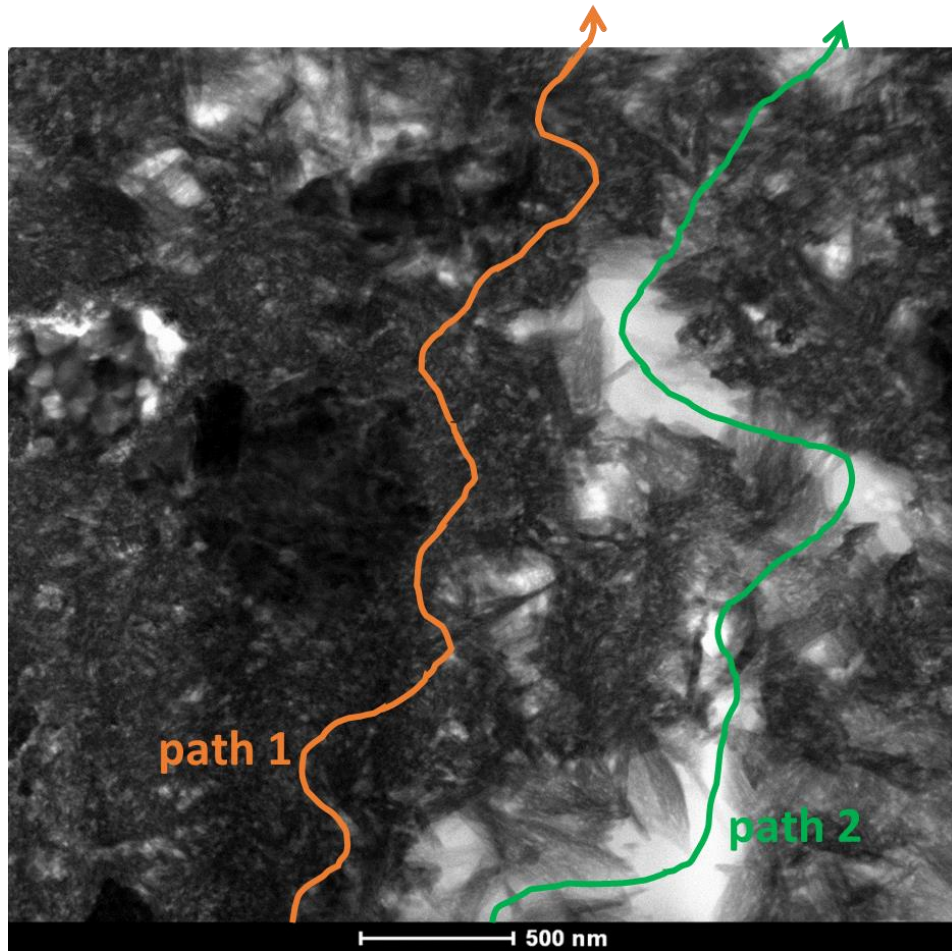
Figure 7-1. TEM image of hydrated C_2S microstructure (w/b 0.35, 28 days). The two paths describe the possible channels for chloride to follow during transport: path 1 – through C-S-H gel pores; path 2 – through small interhydrate pores.

Additionally, the two factors shown to have a great impact in reducing the effective diffusion coefficient, reducing the w/b ratio and addition of silica and metakaolin, could be further combined to produce very dense microstructures with high level of replacement, which could end up having a high degree of depercolation.

On a last note, although it was proven the reactive C_2S binder has a great potential for being used to understand C-S-H from fundamental aspects, upscaled studies on mortars or concretes prepared with this C_2S binder could as well be valuable for the future application of this type of binder.

Chapter 8. Supplementary information

A.1. Characterization of the α-C_2SH intermediate material

Table 8-1. Raw material composition determined by XRD-Rietveld refinement, using external standard method

α-C_2SH content	Other phases
88 %	$CaCO_3$ (calcite and aragonite) – 3.5% Scawtite – 3.0% Dellaite – 2 % Afwillite – 2% Portlandite – < 1%
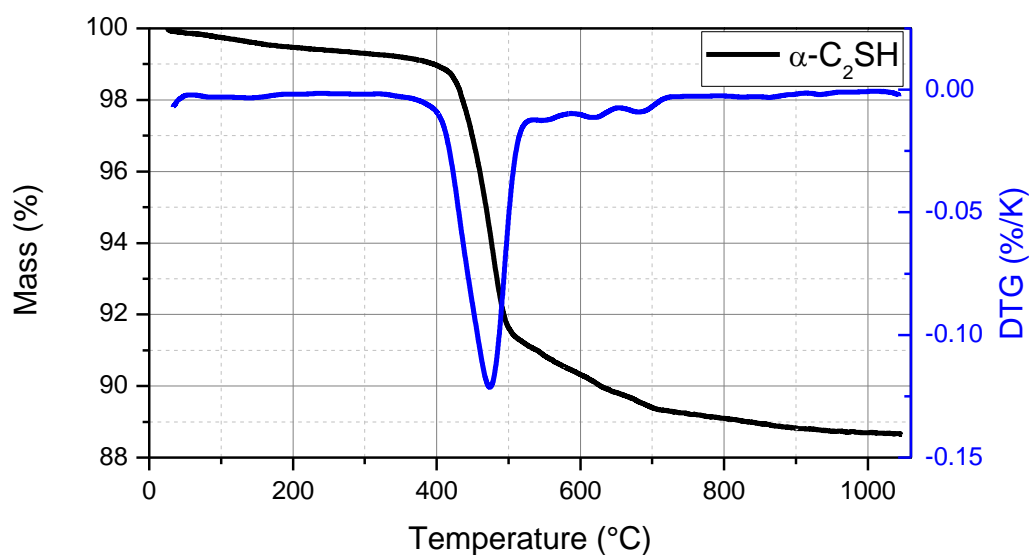
Figure 8-1. TG & DTG curves for the α-C_2SH raw material. The predominant mass loss occurs between 400 and 500 °C, due to conversion of α-C_2SH to C_2S, smaller mass losses occur as well beyond 500 °C due to the minor phases presented in Table 8-1.
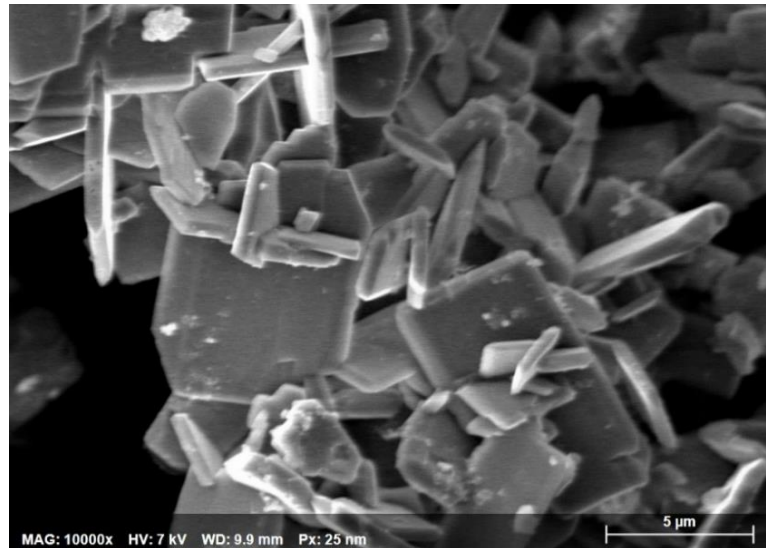
Figure 8-2. SEM micrograph of raw material; crystals are relatively compact, with plate-like aspect, with thickness < 1 µm, mostly agglomerated or intergrown

A.2. Optimization of synthesis of reactive C₂S binder

The two essential steps to obtain a highly reactive dicalcium silicate binder are an optimum grinding followed by calcination of the α-C$_2$SH. Using a laboratory oven, four calcination regimes were tested. The phase composition of the resulting binders is shown in Figure 8-3 and their calorimetry curves in Figure 8-4.
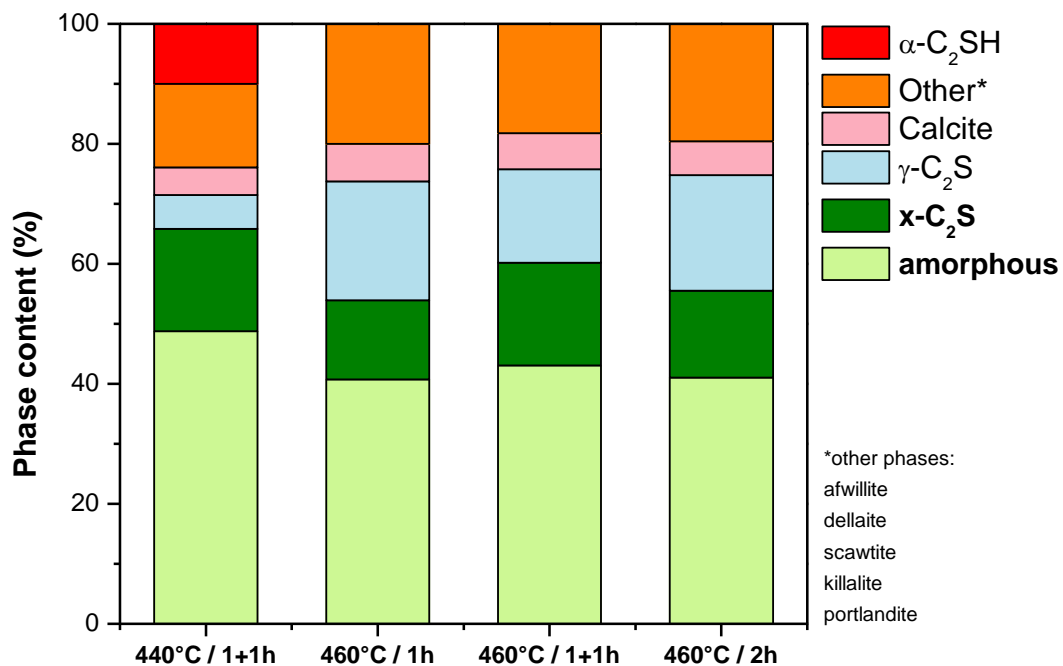
Figure 8-3. Binder phase composition as a function of calcination temperature and duration, determined by XRD-Rietveld refinement, using external standard. The 1+1h notation signifies that the total duration was 2 hours, but the door of the oven is open after 1 hour for 30 sec, to allow the partial vapor pressure inside the oven to decrease. This extra step leads to a slightly higher content of amorphous and x-C$_2$S, while the γ-C$_2$S phase is slightly decreased.
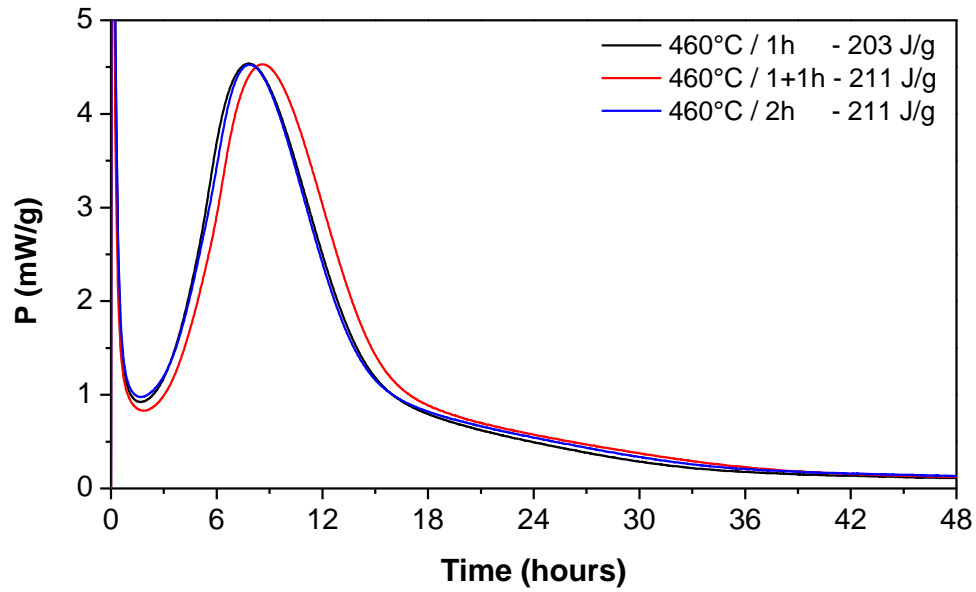
Figure 8-4. Calorimetry curves for three binders synthesized at same calcination temperature, but with different duration. Pastes were prepared at w/b=0.80 and the cumulated heat at 7 days is indicated in J/g. The hydration rates are very similar for the three binders.

Grinding of α-C$_2$SH prior to thermal treatment can as well affect the reactivity of the C$_2$S binder. The PSD of powders ground for 1 minute or 3 minutes are shown in Figure 8-5, the phase composition of the resulting binder is given in Figure 8-6, while the calorimetry curves are illustrated in Figure 8-7.
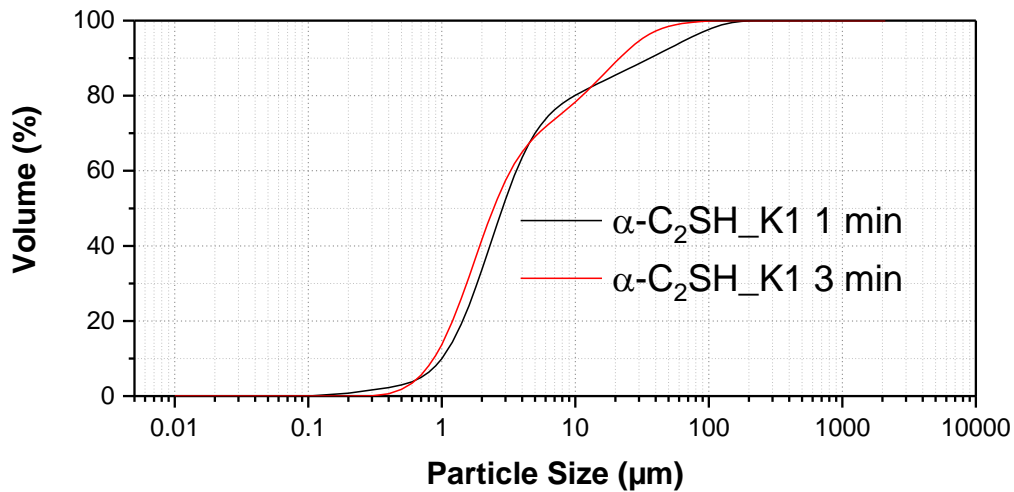
Figure 8-5. Particle size distribution of α-C$_2$SH raw material after griding for different duration using a disk mill. Increasing the grinding time does not change the d_{50} value, while the d_{90} value is slightly reduced.
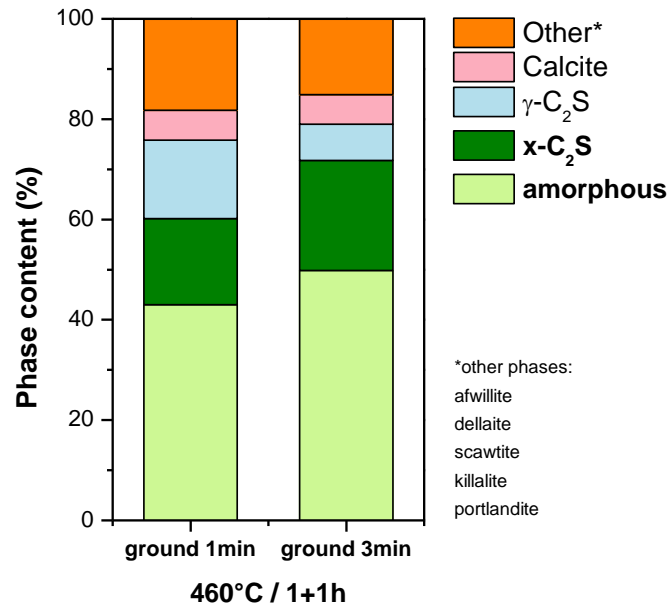
Figure 8-6. Binder phase composition as a function of griding duration of the α-C$_2$SH. Both materials have been calcinated at 460°C/1+1h. Grinding for longer time leads to a higher content of amorphous and x-C$_2$S, while the content of γ-C$_2$S is decreased.
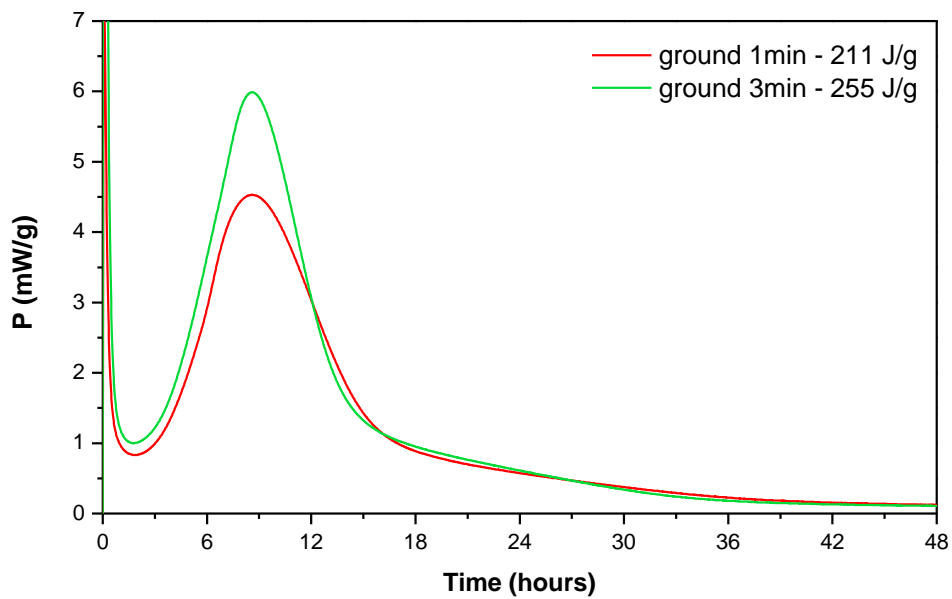
Figure 8-7. Calorimetry curves for the two binders produced from α-C$_2$SH ground for different amount of time. Pastes were prepared at w/b=0.80 and the cumulated heat at 7 days is indicated in J/g. When the raw material was ground for 3 minutes, the resulting binder had a higher initial hydration peak and higher cumulated heat at 7 days.
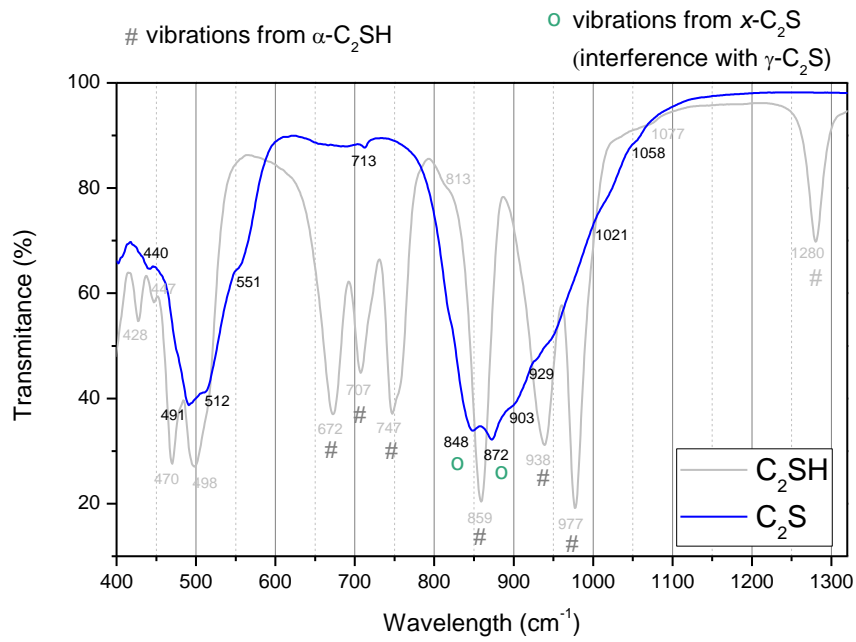
Figure 8-8. FTI-IR spectra of the α-C_2SH and C_2S binder. Characteristic absorption bands of the main phases were attributed according to [13]
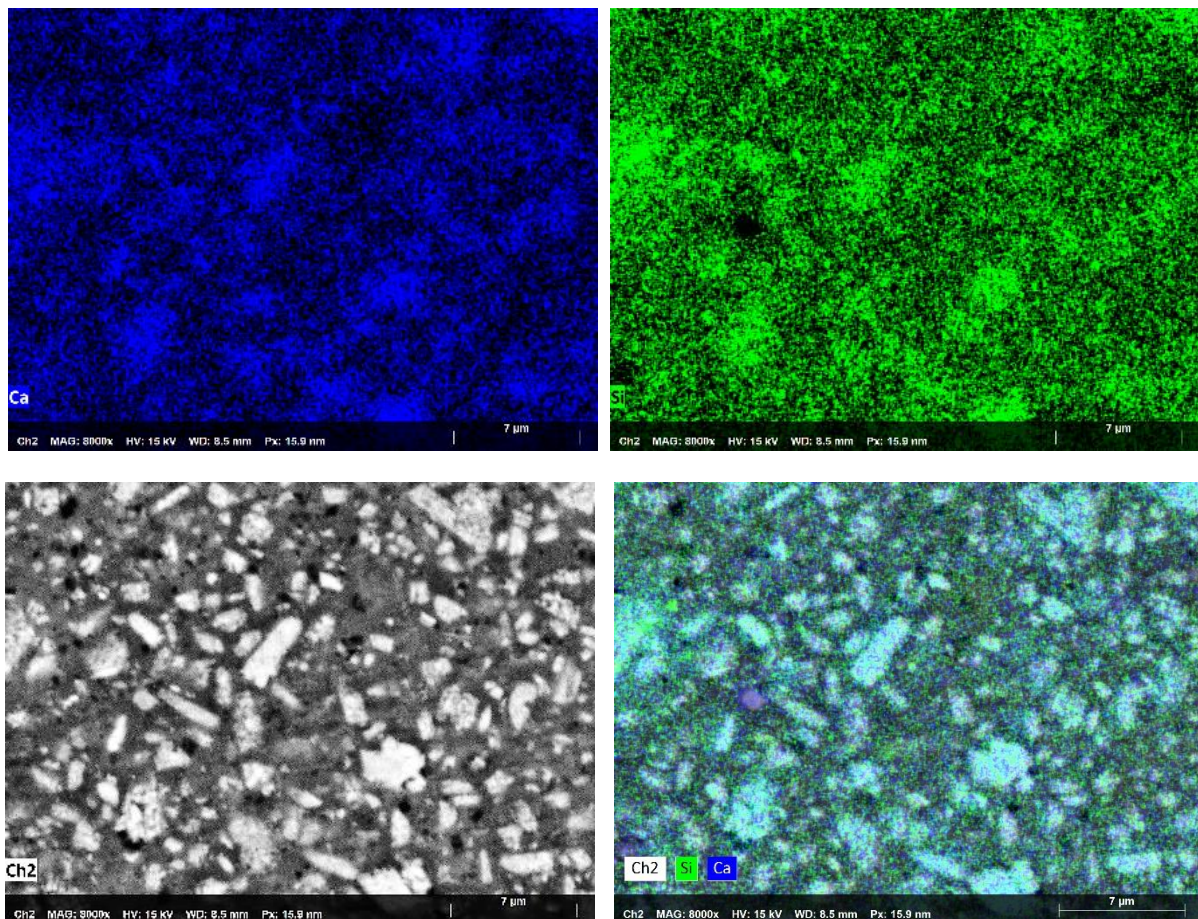
Figure 8-9. BSE mapping on a polished random area of the C_2S paste prepared with w/b ratio 0.35, hydrated for 28 days. Elemental distribution of Ca and Si is homogenous, only few particles rich in Ca or in Si from the inert phases can be identified

A.3. Correlation of unreacted silica/metakaolin with intensity of specific absorption bands in FT-IR

Limestone was used as an inert substrate to verify whether the intensity of the characteristic absorption band from micro-silica and metakaolin is dependent on the amount present in the mixture. FT-IR spectra of mixture containing micro silica and shown in Figure 8-10, while the results for metakaolin mixtures are presented in Figure 8-11.
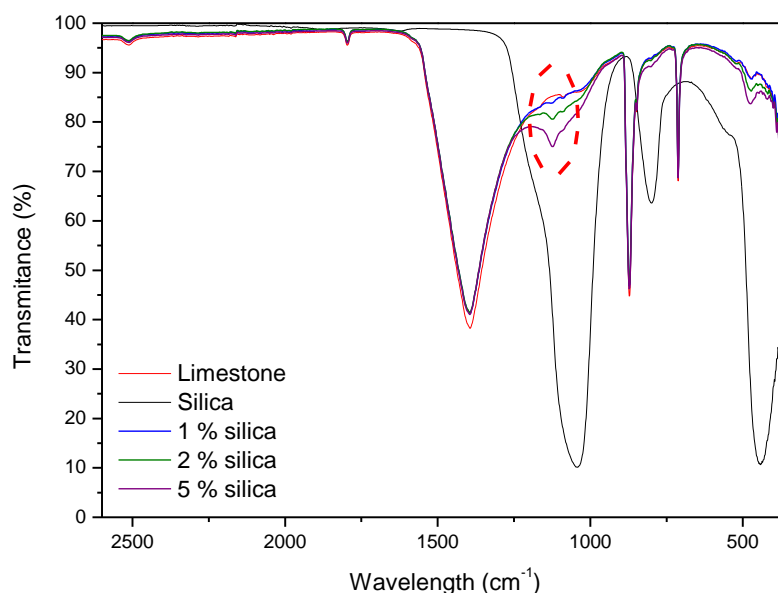
Figure 8-10. FT-IR spectra of limestone, micro-silica and mixtures of the two containing 1, 2 or 3 % micro-silica. The main absorption band characteristic to silica is circled in red. As observed, the intensity of the signal increases with increasing added material. Even 2% added micro-silica is sufficient to produce a peak on the FT-IR spectra of the mixture.
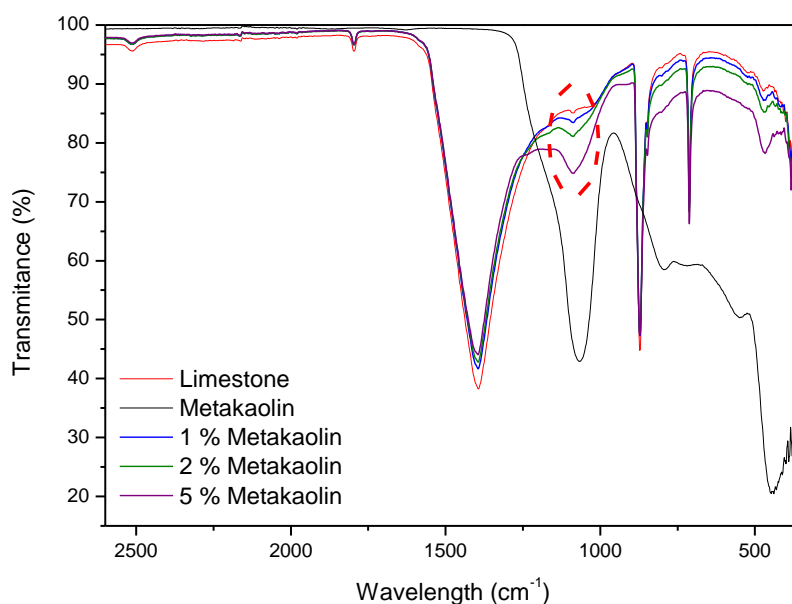
Figure 8-11. FT-IR spectra of limestone, metakaolin and mixtures of the two containing 1, 2 or 3 % metakaolin. The main absorption band characteristic to metakaolin is circled in red. As observed, the intensity of the signal increases with increasing added material. Even 2% added metakaolin is sufficient to produce a peak on the FT-IR spectra of the mixture

A.4. Microstructure of silica and metakaolin containing systems

a)
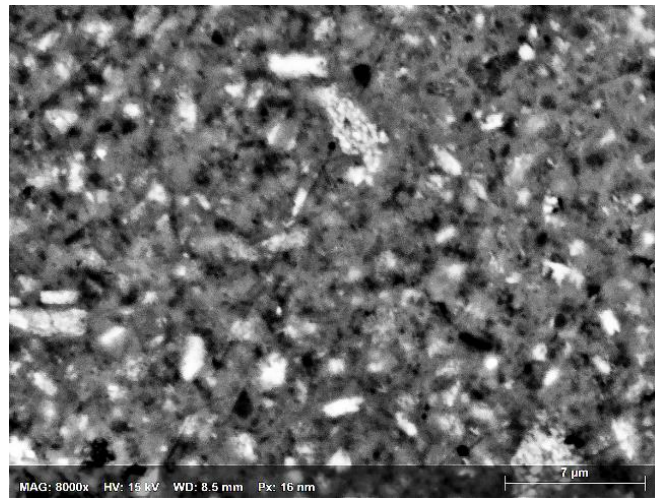
b)
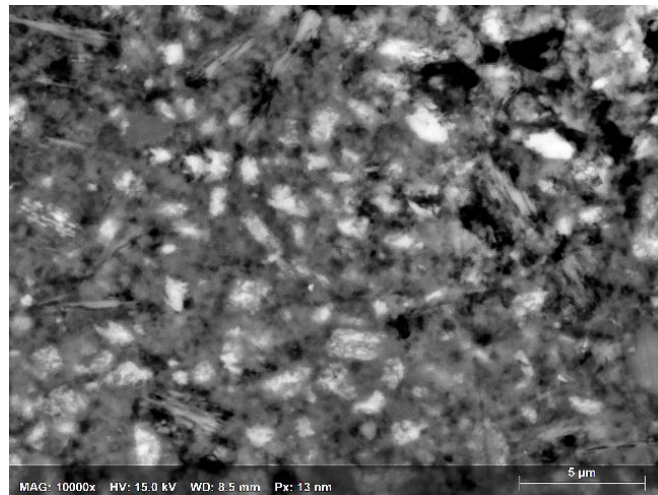
c)
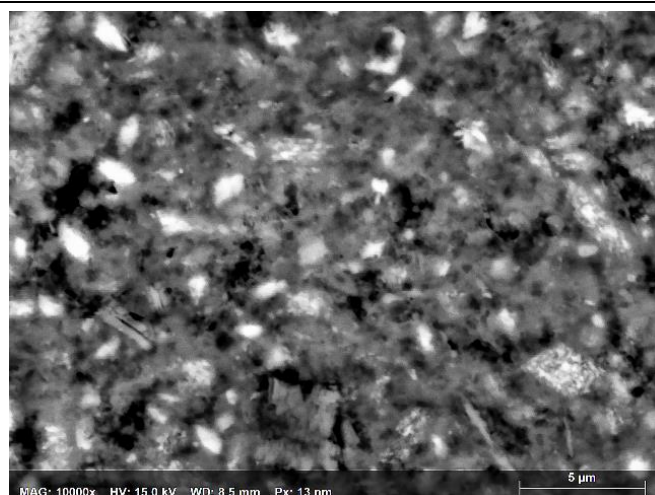
Figure 8-12. BSE images of polished sections of microstructures corresponding to C_2S systems containing (a) 15% silica, (b) 10% metakaolin, (c) 10% silica and 10% metakaolin. All samples have been hydrated at the same w/b ratio (0.35) for 28 days. The microstructures are quite similar, investigation at this scale on SEM is no able to show changes in the C-S-H structures. In samples containing metakaolin, elongated plates of few μm in length from unreacted material can be identified.

A.5. Additional insights from chloride binding isotherms

The results discussed in Chapter 5 were acquired after 10 months of equilibrating the slices in NaCl solutions of different concentrations. A series of preliminary titrations of the equilibration solutions was done as well after 3 months. The compared results for selected samples are shown in Figure 8-13.
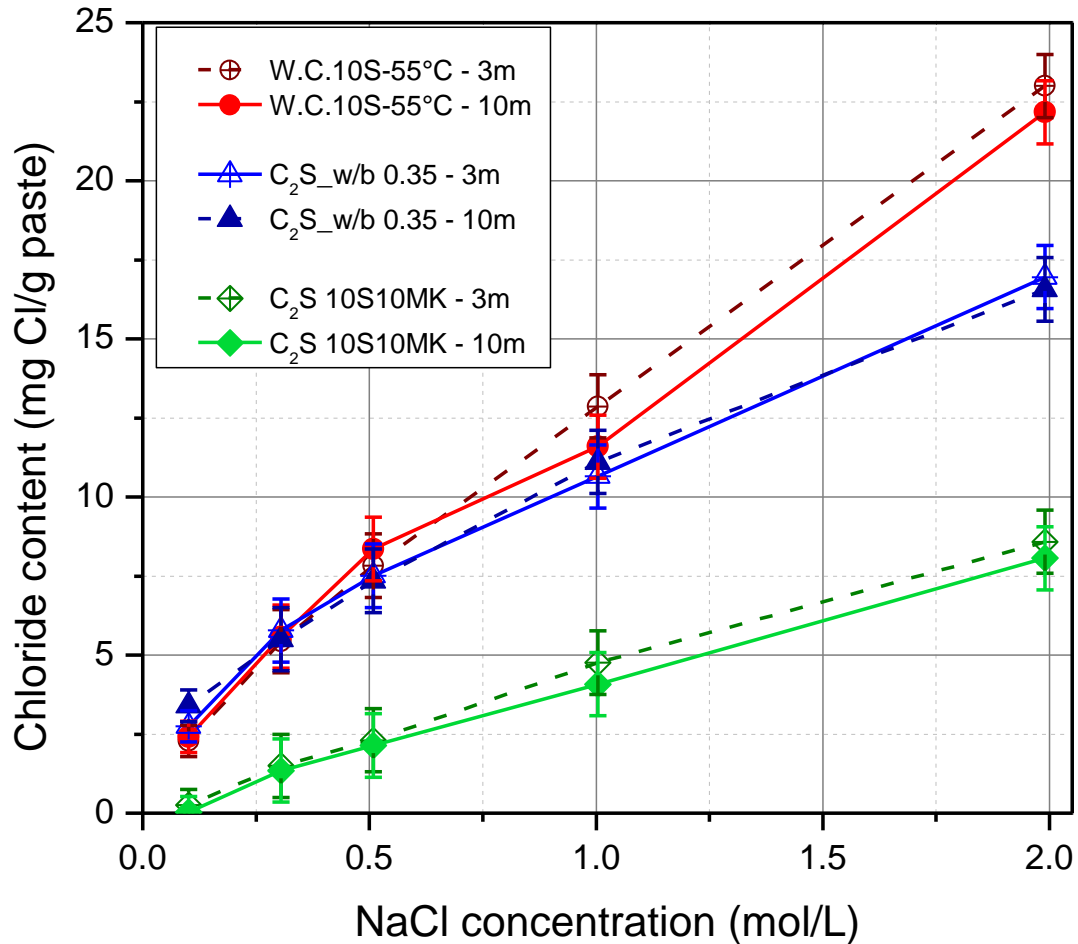
Figure 8-13. Binding isotherms for hydrated plain C_2S system, mixture of C_2S with 10%S10%MK and W.C.10%S-55°C at 3 and 10 months of equilibration in NaCl solutions. As observed, the differences between the amounts of chloride absorbed at the two time points are comparable. This is proof that equilibration of this sample size is quite fast and shorter equilibration times were sufficient for the maximum content on chloride to be adsorbed.

The investigation of desorption process was carried out on few samples, which were equilibrated in NaCl solutions as ground powders instead of slices. The bound chloride was as well determined before the samples were removed from the solution and the effect of the type of sample could be investigated, as observed from Figure 8-14.
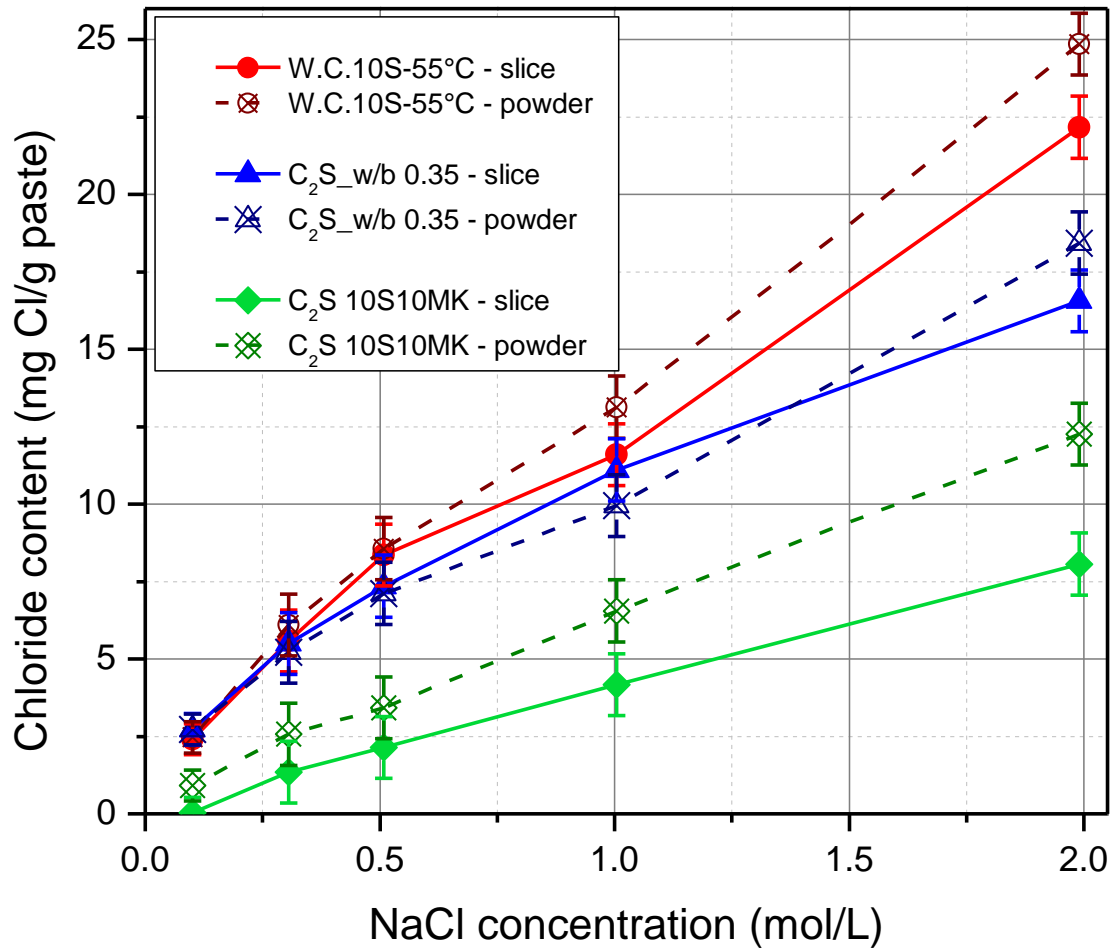
Figure 8-14. Binding isotherms for hydrated plain C_2S system, mixture of C_2S with 10%S10%MK and W.C.10%S-55°C at several months of equilibration in NaCl solutions both as slices and powder. For the plain binder sample, differences in bound chloride are not significant, while for the white cement sample there is slightly more chloride in powder samples but only at higher concentrations. For the C_2S sample containing both silica and metakaolin, there was more chloride absorbed in powder samples than in slices at almost all concentrations. It is important to mention that this sample had the lowest amount of chloride retained from all the samples. A slightly increased binding for powders samples as compared to slice samples can be caused by increased number of surfaces due to grinding of microstructure and possible improved degree of reaction of silica and metakaolin, which leads to more C-S-H being formed.

A.6. Additional insights from mini-migration experiment

After the mini-migration experiment was stopped, the wet samples were investigated by XRD to record possible changes in the microstructure due to exposure to chloride solution and external voltage. When the hydrated plain C_2S sample was measured directly after being removed from the setup, it was noticed that both sides of the slice (both the one in contact with downstream solution and upstream solution) were covered in calcite (See Figure 8-15).
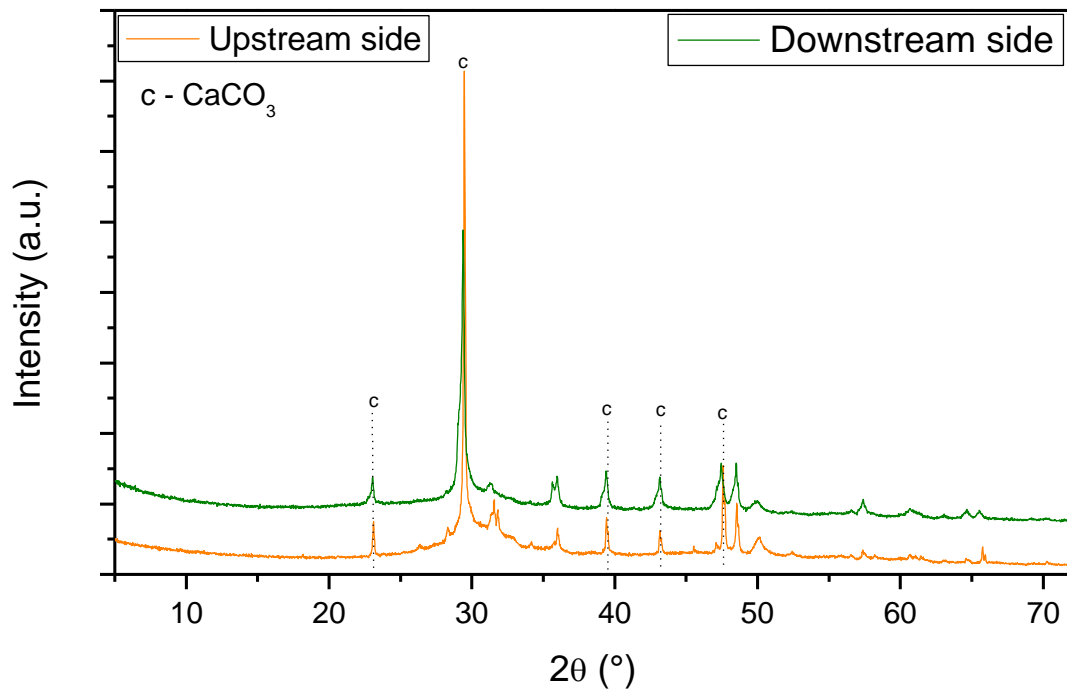
Figure 8-15. XRD patters of the two sides of the hydrated C_2S samples after the mini-migration test was completed. Both the side in contact with the downstream solution and the one in the upstream solution were covered with a layer of calcite.

The surface was then gently polished on sandpaper 2000 using a small amount of distilled water and the XRD spectra was recorded again. After removing the thin calcite layer, the exposed microstructure is very similar with the microstructure that has not been tested for chloride migration, as shown in Figure 8-16. There is only one difference when it comes to the two XRD patterns, for the sample subjected to mini-migration, the intensity of the γ-C_2S has decreased significantly.
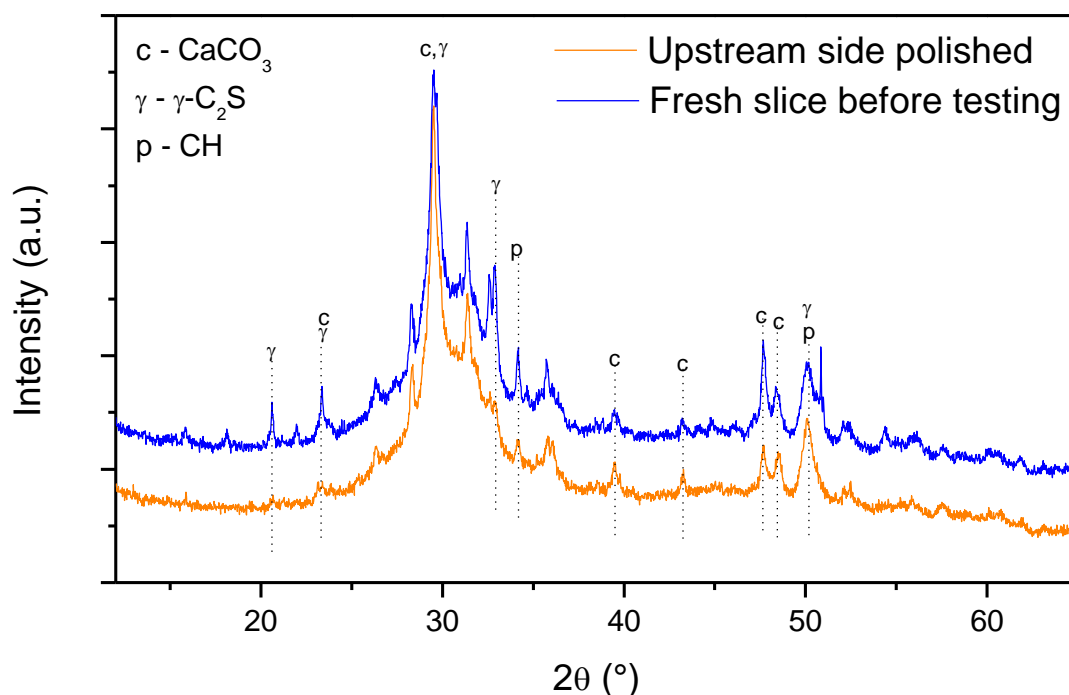
Figure 8-16. XRD pattern of the sample side in contact with the upstream solution after gently polishing on sandpaper 2000, as compared to a sample which was not measured for chloride migration. The main crystalline phases in the two samples are very similar, with the sample analyzed after mini-migration having a lower content of γ-C_2S phase.

The electrodes used for building the mini-migration cells were made of graphite, which is inert in the saturated lime solution containing NaCl. Nevertheless, due to applied voltage, some reactions are expected to happen at both anode and cathode:

- reactions at cathode:

$$2\ H_2O \rightarrow H_2\uparrow + 2\ OH^- \tag{1}$$

$$O_2 + 2\ H_2O \rightarrow 4\ OH^- \tag{2}$$

- reactions at anode:

$$2\ H_2O \rightarrow O_2\uparrow + 2\ H^+ \tag{3}$$

$$2Cl \rightarrow Cl_2\uparrow \tag{4}$$

As a consequence of the reaction (1), the pH of the upstream solution slightly increased for all samples (but not with more than 0.4 units), while in the downstream compartment, the pH usually decreased, due to reaction (3).

When some of the samples were measured, an increased degradation of the anode was noticed after several days. This was also accompanied by a severe drop in pH and in case the test was not stopped after the steady state regime had ended, in evaporation of chorine.

Elemental concentrations of the downstream solution at the end of the test for selected samples was determined by ICP-OES and is given in Table 8-2. The initial downstream solution is always saturated limewater. With few exceptions, we observed a decrease in the Ca concentration of the solution, due to precipitation of calcite. Silicon concentration was relatively low in all solutions, except for the case of the hydrated white cement sample containing micro-silica. Na concentration was insignificantly low compared to Cl concentration determined at the end of the test by titrating the solution, so the migration of Na together with Cl during the test is excluded. As observed from values in the Table 8-2, there is no direct relationship between the effective diffusion coefficient and the pH or the elemental concentrations of the downstream solution.

Table 8-2. Elemental concentrations of the downstream solution at the end of the test, determined by ICP-OES, together with the pH value, the final Cl concentration determined by titration and the associated D_{eff} value

Sample	C_2S	C_2S_NaOH	C_2S 10% MK	C_2S 15% S	C_2S 10%S 10%MK	W.C.10%S 55°C
Ca (mg/L)	545	663	399	321	575	723
Si (mg/L)	0.80	1.98	1.49	1.27	2.99	8.68
Na (mg/L)	1.98	6.03	2.40	3.33	2.02	2.36
Cl (mg/L)	708	1055	669	362	793	1716
pH value	11.91	3.90	3.37	11.91	8.84	2.00
Deff, x 10^{-12} m^2/s	9.53	11.61	1.08	2.83	0.29	9.09

References

[1]   NANOCEM, "Engineered Calcium-Silicate-Hydrates for Applications," 2017. https://www.erica-etn.eu/.

[2]   Reportlinker, "Global Cement Industry Report," 2020. [Online]. Available: reportlinker.com/p05817680/Global-Cement-Industry.

[3]   S. Sprung, "Cement," in *Ullmann's Encyclopedia of Industrial Chemistry*, Wiley-VCH Verlag GmbH & Co. KGaA, 2008.

[4]   R. H. Bogue, "Calculation of the Compounds in Portland Cement," *Ind. Eng. CHem. Anal. Ed.*, vol. 1, no. 4, pp. 192–197, 1929.

[5]   M. Collepardi, G. Baldini, and M. Pauri, "Trialcium aluminate hydration in the presence of lime, gypsum or sodium sulfate," *Cem. Concr. Res.*, vol. 8, pp. 571–580, 1978, doi: 10.1016/0008-8846(78)90040-6.

[6]   E. M. Gartner, J. F. Young, D. A. Damidot, and I. Jawed, "Hydration of portland cement," in *Structure and Performance of Cements*, 2nd Editio., J. Bested and P. Barnes, Eds. New York: Spon Press, 2002, pp. 57–113.

[7]   J. W. Bullard *et al.*, "Mechanisms of cement hydration," *Cem. Concr. Res.*, vol. 41, pp. 1208–1223, 2011, doi: 10.1016/B978-0-08-100693-1.00008-4.

[8]   V. Shah, K. Scrivener, B. Bhattacharjee, and S. Bishnoi, "Changes in microstructure characteristics of cement paste on carbonation," *Cem. Concr. Res.*, vol. 109, pp. 184–197, 2018, doi: 10.1016/j.cemconres.2018.04.016.

[9]   K. L. Scrivener, "Backscattered electron imaging of cementitious microstructures: Understanding and quantification," *Cem. Concr. Compos.*, vol. 26, no. 8, pp. 935–945, 2004, doi: 10.1016/j.cemconcomp.2004.02.029.

[10]   J. I. Escalante-García and J. H. Sharp, "Effect of Temperature on the Hydration of the Main Clinker phases in Portland Cements: Part I, Neat cements," *Cem. Concr. Res.*, vol. 28, no. 9, pp. 1245–1257, 1998.

[11]   B. Lothenbach, K. Scrivener, and R. D. Hooton, "Supplementary cementitious materials," *Cem. Concr. Res.*, vol. 41, no. 12, pp. 1244–1256, 2011, doi: 10.1016/j.cemconres.2010.12.001.

[12]   H. Ludwig and W. Zhang, "Research review of cement clinker chemistry," *Cem. Concr. Res.*, vol. 78, pp. 24–37, 2015, doi: 10.1016/j.cemconres.2015.05.018.

[13]   K. Garbev, G. Beuchle, U. Schweike, D. Merz, O. Dregert, and P. Stemmermann, "Preparation of a novel cementitious material from hydrothermally synthesized C-S-H phases," *J. Am. Ceram. Soc.*, vol. 97, no. 7, pp. 2298–2307, 2014, doi: 10.1111/jace.12920.

[14]   W. Kurdowski, S. Duszak, and B. Trybalska, "Belite produced by means of low-temperature synthesis," *Cem. Concr. Res.*, vol. 27, no. 1, pp. 51–62, 1997.

[15]   K. Garbev, "Struktur, Eigenschaften und quantitative Rietveldanalyse von hydrothermal kristallisierten Calciumsilikathydraten (C-S-H-Phasen)," Ruprecht- Karls-Universität Heidelberg, 2004.

[16]   H. Ishida, S. Yamazaki, K. Sasaki, Y. Okada, and T. Mitsuda, "α-Dicalcium Silicate Hydrate: Preparation, Decomposed Phase, and Its Hydration," *J. Am. Ceram. Soc.*, vol. 76, no. 7, pp. 1707–1712, 1993.

[17]   M. Miyazaki, S. Yamazaki, K. Sasaki, H. Ishida, and H. Toraya, "Crystallographic Data of a New Phase of Dicalcium Silicate," *J. Am. Ceram. Soc.*, vol. 81, no. 5, pp. 1339–1343, 1998, doi: 10.1111/j.1151-2916.1998.tb02487.x.

[18]   K. Garbev, B. Gasharova, and P. Stemmermann, "A modular concept of crystal structure applied to the thermal transformation of α-C2SH," *J. Am. Ceram. Soc.*, vol. 97, no. 7, pp. 2286–2297, 2014, doi: 10.1111/jace.12921.

[19]   M. Georgescu, J. Tipan, A. Badanoiu, D. Crisan, and I. Dragan, "Highly reactive dicalcium silicate synthesized by hydrothermal processing," *Cem. Concr. Compos.*, vol. 22, no. 5, pp. 315–319, 2000, doi: 10.1016/S0958-9465(00)00017-2.

[20]   J. Jernejcic, N. Vene, and A. Zajc, "Thermal decomposition of α-dicalcium silicate hydrate," *Thermochim. Acta*, vol. 20, pp. 237–247, 1977.

[21]   T. Yano, K. Urabe, H. Ikawa, T. Teraushi, N. Ishizawa, and S. Udagawa, "Structure of α-Dicalcium Silicate Hydrate," *Acta Crystallogr. Sect. C Struct. Chem.*, vol. C49, no. Part 9, pp. 1555–1559, 1993, doi: 10.1107/S0108270193004767.

[22]   T. Link, F. Bellmann, H. M. Ludwig, and M. Ben Haha, "Reactivity and phase composition of Ca2SiO4 binders made by annealing of alpha-dicalcium silicate hydrate," *Cem. Concr. Res.*, vol. 67, pp. 131–137, 2015, doi: 10.1016/j.cemconres.2014.08.009.

[23]   A. Guerrero, S. Goni, I. Campillo, and A. Moragues, "Belite Cement Clinker from Coal Fly Ash of High Ca Content.

Optimization of Synthesis Parameters," *Environ. Sci. Technol.*, vol. 38, no. 11, pp. 3209–3213, 2004.

[24]   A. Guerrero, S. Goñi, A. Moragues, and J. S. Dolado, "Microstructure and mechanical performance of belite cements from high calcium coal fly ash," *J. Am. Ceram. Soc.*, vol. 88, no. 7, pp. 1845–1853, 2005, doi: 10.1111/j.1551-2916.2005.00344.x.

[25]   P. Stemmermann, U. Schweike, K. Garbev, and G. Beuchle, "Celitement – a sustainable prospect for the cement industry," *Cem. Int.*, vol. 8, pp. 52–67, 2010.

[26]   K. Garbev, B. Gasharova, G. Beuchle, S. Kreisz, and P. Stemmermann, "First observation of α-Ca2[SiO3(OH)](OH)-Ca6[Si2O7][SiO4](OH)2 phase transformation upon thermal treatment in air," *J. Am. Ceram. Soc.*, vol. 91, no. 1, pp. 263–271, 2008, doi: 10.1111/j.1551-2916.2007.02115.x.

[27]   H. Toraya and S. Yamazaki, "Simulated annealing structure solution of a new phase of dicalcium silicate Ca2SiO4 and the mechanism of structural changes from α-dicalcium silicate hydrate to αL'-dicalcium silicate via the new phase," *Acta Crystallogr. Sect. B Struct. Sci.*, vol. 58, no. 4, pp. 613–621, 2002, doi: 10.1107/S0108768102005189.

[28]   S. Yamazaki and H. Toraya, "X-ray powder data for a new phase of dicalcium silicate, x-Ca2SiO4," *Powder Diffr.*, vol. 16, no. 2, pp. 110–114, 2001, doi: 10.1154/1.1351153.

[29]   T. Link, "Entwicklung und Untersuchung von alternativen Dicalciumsilicat-Bindern auf der Basis von α-C2SH," Bauhaus-Universität Weimar, 2017.

[30]   A. Bazzoni, "Study of early hydration mechanisms of cement by means of electron microscopy," École polytechnique fédérale de Lausanne, 2014.

[31]   H. M. Jennings, "A model for the microstructure of calcium silicate hydrate in cement paste," *Cem. Concr. Res.*, vol. 30, no. 6, pp. 101–116, 2000, doi: 10.1016/S0008-8846(00)00257-X.

[32]   I. G. Richardson, "The calcium silicate hydrates," *Cem. Concr. Res.*, vol. 38, no. 2, pp. 137–158, 2008, doi: 10.1016/j.cemconres.2007.11.005.

[33]   H. F. W. Taylor and J. W. Howison, "Relationships between calcium silicates and clay minerals," *Clay Miner. Bull.*, vol. 3, no. 16, pp. 98–111, 1956.

[34]   H. F. W. Taylor, "Proposed Structure for Calcium Silicate Hydrate Gel," *J. Am. Ceram. Soc.*, vol. 69, no. 6, pp. 464–467, 1986, doi: 10.1111/j.1151-2916.1986.tb07446.x.

[35]   I. G. Richardson, "Tobermorite/jennite- and tobermorite/calcium hydroxide-based models for the structure of C-S-H: Applicability to hardened pastes of tricalcium silicate, β-dicalcium silicate, Portland cement, and blends of Portland cement with blast-furnace slag, metakaol," *Cem. Concr. Res.*, vol. 34, no. 9, pp. 1733–1777, 2004, doi: 10.1016/j.cemconres.2004.05.034.

[36]   I. G. Richardson and G. W. Groves, "Models for the composition and structure of calcium silicate hydrate (CSH) gel in hardened tricalcium silicate pastes," *Cem. Concr. Res.*, vol. 22, no. 6, pp. 1001–1010, 1992, doi: 10.1016/0008-8846(92)90030-Y.

[37]   A. Kunhi Mohamed, S. C. Parker, P. Bowen, and S. Galmarini, "An atomistic building block description of C-S-H - Towards a realistic C-S-H model," *Cem. Concr. Res.*, vol. 107, no. March 2017, pp. 221–235, 2018, doi: 10.1007/s10514-018-9728-3.

[38]   A. Kunhi Mohamed, "Atomistic Simulations of The Structure of Calcium Silicate Hydrates: Interlayer Positions, Water Content And A General Structural Brick Model," vol. 8840, 2018, doi: 10.5075/EPFL-THESIS-8840.

[39]   I. G. Richardson, "Model structures for C-(A)-S-H(I)," *Acta Crystallogr. Sect. B Struct. Sci. Cryst. Eng. Mater.*, vol. 70, no. 6, pp. 903–923, 2014, doi: 10.1107/S2052520614021982.

[40]   E. L'Hôpital, B. Lothenbach, K. Scrivener, and D. A. Kulik, "Alkali uptake in calcium alumina silicate hydrate (C-A-S-H)," *Cem. Concr. Res.*, vol. 85, pp. 122–136, 2016, doi: 10.1016/j.cemconres.2016.03.009.

[41]   J. Haas and A. Nonat, "From C-S-H to C-A-S-H: Experimental study and thermodynamic modelling," *Cem. Concr. Res.*, vol. 68, pp. 124–138, 2015, doi: 10.1016/j.cemconres.2014.10.020.

[42]   R. F. Feldman and P. J. Sereda, "A new model for hydrated Portland cement and its practical implications," *Eng. J.*, vol. 53, no. 8/9, pp. 53–59, 1970.

[43]   T. C. Powers and T. L. Brownyard, *Studies of the physical properties of hardened portland cement paste*. Chicago: bulletin 22 Edition, Research Laboratories of the Portland Cement Association, 1948.

[44]   H. M. Jennings, "Refinements to colloid model of C-S-H in cement: CM-II," *Cem. Concr. Res.*, vol. 38, no. 3, pp. 275–289, 2008, doi: 10.1016/j.cemconres.2007.10.006.

[45]   D. D. Lasic *et al.*, "NMR spin grouping in hydrating cement at 200 MHz," *Cem. Concr. Res.*, vol. 18, no. 4, pp. 649–653, 1988, doi: 10.1016/0008-8846(88)90057-9.

[46]   A. C. A. Muller, K. L. Scrivener, A. M. Gajewicz, and P. J. McDonald, "Densification of C-S-H measured by 1H NMR relaxometry," *J. Phys. Chem. C*, vol. 117, no. 1, pp. 403–412, 2013, doi: 10.1021/jp3102964.

[47]   I. G. Richardson, "The nature of C-S-H in hardened cements," *Cem. Concr. Res.*, vol. 29, no. July, pp. 1131–1147, 1999, doi: 10.1016/S0008-8846(99)00168-4.

[48]   E. L'Hôpital, B. Lothenbach, D. A. Kulik, and K. Scrivener, "Influence of calcium to silica ratio on aluminium uptake in calcium silicate hydrate," *Cem. Concr. Res.*, vol. 85, pp. 111–121, 2016, doi: 10.1016/j.cemconres.2016.01.014.

[49]   A. Kumar *et al.*, "The Atomic-Level Structure of Cementitious Calcium Silicate Hydrate," *J. Phys. Chem. C*, vol. 121, no. 32, pp. 17188–17196, 2017, doi: 10.1021/acs.jpcc.7b02439.

[50]   J. Siramanont, B. J. Walder, L. Emsley, and P. Bowen, "Iron incorporation in synthetic precipitated calcium silicate hydrates," *Cem. Concr. Res.*, vol. 142, no. 106365, pp. 1–12, 2021, doi: 10.1016/j.cemconres.2021.106365.

[51]   X. Pardal, I. Pochard, and A. Nonat, "Experimental study of Si-Al substitution in calcium-silicate-hydrate (C-S-H)

prepared under equilibrium conditions," *Cem. Concr. Res.*, vol. 39, no. 8, pp. 637–643, 2009, doi: 10.1016/j.cemconres.2009.05.001.

[52] E. L'Hôpital, B. Lothenbach, K. Scrivener, and D. A. Kulik, "Alkali uptake in calcium alumina silicate hydrate (C-A-S-H)," *Cem. Concr. Res.*, vol. 85, pp. 122–136, 2016, doi: 10.1016/j.cemconres.2016.03.009.

[53] S.-Y. Hong and F. P. Glasser, "Alkali sorption by C-S-H and C-A-S-H gels Part II. Role of alumina," *Cem. Concr. Res.*, vol. 32, pp. 1101–1111, 2002, doi: 10.1016/S0008-8846(02)00753-6.

[54] W. Kunther, S. Ferreiro, and J. Skibsted, "Influence of the Ca/Si ratio on the compressive strength of cementitious calcium-silicate-hydrate binders," *J. Mater. Chem. A*, vol. 5, no. 33, pp. 17401–17412, 2017, doi: 10.1039/c7ta06104h.

[55] R. Alizadeh, J. J. Beaudoin, and L. Raki, "Mechanical properties of calcium silicate hydrates," *Mater. Struct.*, vol. 44, pp. 13–28, 2011, doi: 10.1617/s11527-010-9605-9.

[56] G. Plusquellec and A. Nonat, "Interactions between calcium silicate hydrate (C-S-H) and calcium chloride, bromide and nitrate," *Cem. Concr. Res.*, vol. 90, pp. 89–96, 2016, doi: 10.1016/j.cemconres.2016.08.002.

[57] I. G. Richardson, "Nature of the hydration products in hardened cement pastes," *Cem. Concr. Compos.*, vol. 22, no. 2, pp. 97–113, 2000, doi: 10.1016/S0958-9465(99)00036-0.

[58] I. G. Richardson and G. W. Groves, "Microstructure and microanalysis of hardened ordinary Portland cement pastes," *J. Mater. Sci.*, vol. 28, pp. 265–277, 1993.

[59] J. E. Rossen, B. Lothenbach, and K. L. Scrivener, "Composition of C-S-H in pastes with increasing levels of silica fume addition," *Cem. Concr. Res.*, vol. 75, pp. 14–22, 2015, doi: 10.1016/j.cemconres.2015.04.016.

[60] E. E. Lachowski, K. Mohan, H. F. W. Taylor, and A. E. Moore, "Analytical Electron Microscopy of Cement Pastes: II, Pastes of Portland Cements and Clinkers," *J. Am. Ceram. Soc.*, vol. 63, no. 7–8, pp. 447–452, 1980.

[61] R. Taylor, I. G. Richardson, and R. M. D. Brydson, "Nature of C-S-H in 20 year old neat ordinary Portland cement and 10% Portland cement-90% ground granulated blast furnace slag pastes," *Adv. Appl. Ceram.*, vol. 106, no. 6, pp. 294–301, 2007, doi: 10.1179/174367607X228106.

[62] D. L. Rayment and A. J. Majumdar, "The composition of the C-S-H phases in portland cement pastes," *Cem. Concr. Res.*, vol. 12, no. 6, pp. 753–764, 1982, doi: 10.1016/0008-8846(82)90039-4.

[63] D. L. Rayment and E. E. Lachowski, "The analysis of OPC pastes: A comparison between analytical electron microscopy and electron probe microanalysis," *Cem. Concr. Res.*, vol. 14, no. 1, pp. 43–48, 1984.

[64] M. Zajac, P. Durdzinski, Z. Giergiczny, and M. Ben Haha, "New insights into the role of space on the microstructure and the development of strength of multicomponent cements," *Cem. Concr. Compos.*, vol. 121, 2021, doi: 10.1016/j.cemconcomp.2021.104070.

[65] R. L. BERGER and J. D. McGREGOR, "Effect of Temperature and Water-Solid Ratio on Growth of Ca(OH)2 Crystals Formed During Hydration of Ca3SiO5," *J. Am. Ceram. Soc.*, vol. 56, no. 2, pp. 73–79, 1973, doi: 10.1111/j.1151-2916.1973.tb12361.x.

[66] E. Gallucci and K. Scrivener, "Crystallisation of calcium hydroxide in early age model and ordinary cementitious systems," *Cem. Concr. Res.*, vol. 37, no. 4, pp. 492–501, 2007, doi: 10.1016/j.cemconres.2007.01.001.

[67] A. Kumar, G. Sant, C. Patapy, C. Gianocca, and K. L. Scrivener, "The influence of sodium and potassium hydroxide on alite hydration: Experiments and simulations," *Cem. Concr. Res.*, vol. 42, no. 11, pp. 1513–1523, 2012, doi: 10.1016/j.cemconres.2012.07.003.

[68] B. Mota, T. Matschei, and K. Scrivener, "Impact of NaOH and Na2SO4 on the kinetics and microstructural development of white cement hydration," *Cem. Concr. Res.*, vol. 108, no. March, pp. 172–185, 2018, doi: 10.1016/j.cemconres.2018.03.017.

[69] D. E. Macphee, K. Luke, F. P. Glasser, and E. E. Lachowski, "Solubility and Aging of Calcium Silicate Hydrates in Alkaline Solutions at 25°C," *J. Am. Ceram. Soc.*, vol. 72, no. 4, pp. 646–654, 1989.

[70] E. M. J. Bérodier, A. C. A. Muller, and K. L. Scrivener, "Effect of sulfate on C-S-H at early age," *Cem. Concr. Res.*, vol. 138, no. September, 2020, doi: 10.1016/j.cemconres.2020.106248.

[71] H. Ishida, K. Sasaki, and T. Mitsuda, "Reactive b-Dicalcium Silicate: I, Hydration Behavior at Room Temperature," *J. Am. Ceram. Soc.*, vol. 75, no. 2, pp. 353–358, 1992.

[72] A. K. Chatterjee, "High belite cements-Present status and future technological options: Part I," *Cem. Concr. Res.*, vol. 26, no. 8, pp. 1213–1225, 1996.

[73] P. Stemmermann, K. Garbev, U. Schweike, and G. Beuchle, "Verfahren zur Herstellung von Belit-Bindemittel," DE 10 2005 037 771 B4, 2007.

[74] D. A. Kulik, "Gibbs energy minimization approach to modeling sorption equilibria at the mineral-water interface: Thermodynamic relations for multi-site-surface complexation," *Am. J. Sci.*, vol. 302, no. 3, pp. 227–279, 2002, doi: 10.2475/ajs.302.3.227.

[75] D. A. Kulik *et al.*, "GEM-Selektor geochemical modeling package : revised algorithm and GEMS3K numerical kernel for coupled simulation codes," *Comput. Geosci.*, vol. 17, pp. 1–24, 2013, doi: 10.1007/s10596-012-9310-6.

[76] W. Hummel, U. Berner, E. Curti, F. J. Pearson, and T. Thoenen, "Nagra/PSI Chemical Thermodynamic Data Base 01/01:," *Radiochim. Acta*, vol. 90, no. 9–11, pp. 805–813, 2002, doi: doi:10.1524/ract.2002.90.9-11_2002.805.

[77] T. Thoenen, W. Hummel, U. Berner, and E. Curti, "The PSI / Nagra Chemical Thermodynamic Database 12 / 07," Villigen PSI, Switzerland, 2014.

[78] B. Lothenbach *et al.*, "Cemdata18 : A chemical thermodynamic database for hydrated Portland cements and alkali-activated materials," *Cem. Concr. Res.*, vol. 115, pp. 472–506, 2019, doi: 10.1016/j.cemconres.2018.04.018.

[79]   K. De Weerdt, G. Plusquellec, A. Belda Revert, M. R. Geiker, and B. Lothenbach, "Effect of carbonation on the pore solution of mortar," *Cem. Concr. Res.*, vol. 118, no. March, pp. 38–56, 2019, doi: 10.1016/j.cemconres.2019.02.004.

[80]   B. Lothenbach, E. Bernard, and M. Urs, "Zeolite formation in the presence of cement hydrates and albite," *Phys. Chem. Earth*, vol. 99, pp. 77–94, 2017, doi: 10.1016/j.pce.2017.02.006.

[81]   J. Zhang and G. W. Scherer, "Comparison of methods for arresting hydration of cement," *Cem. Concr. Res.*, vol. 41, pp. 1024–1036, 2011, doi: 10.1016/j.cemconres.2011.06.003.

[82]   D. A. Kulik, "Improving the structural consistency of C-S-H solid solution thermodynamic models," *Cem. Concr. Res.*, vol. 41, no. 5, pp. 477–495, 2011, doi: 10.1016/j.cemconres.2011.01.012.

[83]   J. J. Chen, J. J. Thomas, H. F. W. Taylor, and H. M. Jennings, "Solubility and structure of calcium silicate hydrate," *Cem. Concr. Res.*, vol. 34, no. 9, pp. 1499–1519, 2004, doi: 10.1016/j.cemconres.2004.04.034.

[84]   M. Zajac, J. Skocek, B. Lothenbach, and B. H. Mohsen, "Late hydration kinetics: Indications from thermodynamic analysis of pore solution data," *Cem. Concr. Res.*, vol. 129, 2020, doi: 10.1016/j.cemconres.2020.105975.

[85]   J. Duchesne and E. J. Reardon, "Measurement and predicton of portlandite solubility in alkali solutions," *Cem. Concr. Res.*, vol. 25, no. 5, pp. 1043–1053, 1995.

[86]   G. W. Groves and S. A. Rodger, "The hydration of C3S and ordinary Portland cement with relatively large additions of microsilica," *Adv. Cem. Res.*, vol. 2, no. 8, pp. 135–140, 1989, doi: 10.1680/adcr.1989.2.8.135.

[87]   C. M. Dobson, D. G. C. Goberdhan, J. D. F. Ramsay, and S. A. Rodger, "29Si MAS NMR study of the hydration of tricalcium silicate in the presence of finely divided silica," *J. Mater. Sci.*, vol. 23, no. 11, pp. 4108–4114, 1988, doi: 10.1007/BF01106844.

[88]   B. Jo, C. Kim, G. Tae, and J. Park, "Characteristics of cement mortar with nano-SiO2 particles," *Constr. Build. Mater.*, vol. 21, no. 6, pp. 1351–1355, 2007, doi: 10.1016/j.conbuildmat.2005.12.020.

[89]   A. M. Said, M. S. Zeidan, M. T. Bassuoni, and Y. Tian, "Properties of concrete incorporating nano-silica," *Constr. Build. Mater.*, vol. 36, pp. 838–844, 2012, doi: 10.1016/j.conbuildmat.2012.06.044.

[90]   G. Land and D. Stephan, "The influence of nano-silica on the hydration of ordinary Portland cement," *J. Mater. Sci.*, vol. 47, no. 2, pp. 1011–1017, 2012, doi: 10.1007/s10853-011-5881-1.

[91]   L. P. Singh, S. K. Bhattacharyya, S. P. Shah, G. Mishra, S. Ahalawat, and U. Sharma, "Studies on early stage hydration of tricalcium silicate incorporating silica nanoparticles: Part I," *Constr. Build. Mater.*, vol. 74, pp. 278–286, 2015, doi: 10.1016/j.conbuildmat.2014.08.046.

[92]   B. B. Sabir, S. Wild, and J. Bai, "Metakaolin and calcined clays as pozzolans for concrete : a review," *Cem. Concr. Compos.*, vol. 23, pp. 441–454, 2001.

[93]   W. Kunther, Z. Dai, and J. Skibsted, "Research Thermodynamic modeling of hydrated white Portland cement – metakaolin – limestone blends utilizing hydration kinetics from 29Si MAS NMR spectroscopy," *Cem. Concr. Res.*, vol. 86, pp. 29–41, 2016, doi: 10.1016/j.cemconres.2016.04.012.

[94]   N. J. Coleman and C. L. Page, "Aspects of the pore solution chemistry of hydrated cement pastes containing metakaolin," *Cem. Concr. Res.*, vol. 27, no. 1, pp. 147–154, 1997.

[95]   M. Shekarchi, A. Bonakdar, M. Bakhshi, A. Mirdamadi, and B. Mobasher, "Transport properties in metakaolin blended concrete," *Constr. Build. Mater.*, vol. 24, no. 11, pp. 2217–2223, 2010, doi: 10.1016/j.conbuildmat.2010.04.035.

[96]   F. Avet, X. Li, and K. Scrivener, "Determination of the amount of reacted metakaolin in calcined clay blends," *Cem. Concr. Res.*, vol. 106, no. January, pp. 40–48, 2018, doi: 10.1016/j.cemconres.2018.01.009.

[97]   Y. Briki, F. Avet, M. Zajac, P. Bowen, M. Ben Haha, and K. Scrivener, "Understanding of the factors slowing down metakaolin reaction in limestone calcined clay cement (LC3) at late ages," *Cem. Concr. Res.*, vol. 146, no. May, p. 106477, 2021, doi: 10.1016/j.cemconres.2021.106477.

[98]   M. Antoni, J. Rossen, F. Martirena, and K. Scrivener, "Cement substitution by a combination of metakaolin and limestone," *Cem. Concr. Res.*, vol. 42, no. 12, pp. 1579–1589, 2012, doi: 10.1016/j.cemconres.2012.09.006.

[99]   C. A. Love, I. G. Richardson, and A. R. Brough, "Composition and structure of C – S – H in white Portland cement – 20 % metakaolin pastes hydrated at 25 ° C," *Cem. Concr. Res.*, vol. 37, pp. 109–117, 2007, doi: 10.1016/j.cemconres.2006.11.012.

[100]   Z. Dai, T. T. Tran, and J. Skibsted, "Aluminum Incorporation in the C – S – H Phase of White Portland Cement – Metakaolin Blends Studied by 27Al and 29Si MAS NMR Spectroscopy," *J. Am. Ceram. Soc.*, vol. 97, no. 8, pp. 2662–2671, 2014, doi: 10.1111/jace.13006.

[101]   K. Kupwade-Patil, S. D. Palkovic, A. Bumajdad, C. Soriano, and O. Büyüköztürk, "Use of silica fume and natural volcanic ash as a replacement to Portland cement: Micro and pore structural investigation using NMR, XRD, FTIR and X-ray microtomography," *Constr. Build. Mater.*, vol. 158, pp. 574–590, 2018, doi: 10.1016/j.conbuildmat.2017.09.165.

[102]   P. Yu, R. James Kirkpatrick, B. Poe, P. F. McMillan, and X. Cong, "Structure of Calcium Silicate Hydrate (C-S-H): Near-, Mid-, and Far-Infrared Spectroscopy," *J. Am. Ceram. Soc.*, vol. 83, no. 3, pp. 742–748, 1999.

[103]   M. Zajac, J. Skibsted, P. Durdzinski, F. Bullerjahn, J. Skocek, and M. Ben Haha, "Kinetics of enforced carbonation of cement paste," *Cem. Concr. Res.*, vol. 131, no. 106013, 2020, doi: 10.1016/j.cemconres.2020.106013.

[104]   R. Cai, Z. He, S. Tang, T. Wu, and E. Chen, "The early hydration of metakaolin blended cements by non-contact impedance measurement," *Cem. Concr. Compos.*, vol. 92, no. May, pp. 70–81, 2018, doi: 10.1016/j.cemconcomp.2018.06.001.

[105]   I. . F. Sáez del Bosque, S. Martínez-Ramírez, and M. T. Blanco-varela, "FTIR study of the effect of temperature and

nanosilica on the nanostructure of C – S – H gel formed by hydrating tricalcium silicate," *Constr. Build. Mater.*, vol. 52, pp. 314–323, 2014, doi: 10.1016/j.conbuildmat.2013.10.056.

[106] M. C. Garci Juenger and H. M. Jennings, "The use of nitrogen adsorption to assess the microstructure of cement paste," *Cem. Concr. Res.*, vol. 31, no. 6, pp. 883–892, 2001, doi: 10.1145/3010089.3016031.

[107] K. L. Scrivener, P. Juilland, and P. J. M. Monteiro, "Advances in understanding hydration of Portland cement," *Cem. Concr. Res. J.*, vol. 12, no. 3, pp. 106–112, 2016, doi: 10.1016/j.cemconres.2015.05.025.

[108] P. D. Tennis and H. M. Jennings, "A model for two types of calcium silicate hydrate in the microstructure of Portland cement pastes," *Cem. Concr. Res.*, vol. 30, pp. 855–863, 2000, doi: 10.1016/j.electacta.2017.07.126.

[109] A. C. A. Muller, K. L. Scrivener, J. Skibsted, A. M. Gajewicz, and P. J. McDonald, "Influence of silica fume on the microstructure of cement pastes: New insights from ^{1}H NMR relaxometry," *Cem. Concr. Res.*, vol. 74, pp. 116–125, 2015, doi: 10.1016/j.cemconres.2015.04.005.

[110] J. Skibsted and R. Snellings, "Reactivity of supplementary cementitious materials (SCMs) in cement blends," *Cem. Concr. Res.*, vol. 124, no. June, 2019, doi: 10.1016/j.cemconres.2019.105799.

[111] L. P. Singh, S. K. Bhattacharyya, S. P. Shah, G. Mishra, and U. Sharma, "Studies on early stage hydration of tricalcium silicate incorporating silica nanoparticles: Part II," *Constr. Build. Mater.*, vol. 102, pp. 943–949, 2016, doi: 10.1016/j.conbuildmat.2015.05.084.

[112] U. Angst, B. Elsener, C. K. Larsen, and Ø. Vennesland, "Critical chloride content in reinforced concrete - A review," *Cem. Concr. Res.*, vol. 39, no. 12, pp. 1122–1138, 2009, doi: 10.1016/j.cemconres.2009.08.006.

[113] F. P. Glasser, J. Marchand, and E. Samson, "Durability of concrete - Degradation phenomena involving detrimental chemical reactions," *Cem. Concr. Res.*, vol. 38, no. 2, pp. 226–246, 2008, doi: 10.1016/j.cemconres.2007.09.015.

[114] T. Luping and L.-O. Nilsson, "Chloride binding capacity and binding isotherms of OPC pastes and mortars," *Cem. Concr. Res.*, vol. 23, no. 2, pp. 247–253, 1993, doi: 10.1016/0008-8846(93)90089-R.

[115] A. Delagrave, J. Marchand, J. P. Ollivier, S. Julien, and K. Hazrati, "Chloride binding capacity of various hydrated cement paste systems," *Adv. Cem. Based Mater.*, vol. 6, no. 1, pp. 28–35, 1997, doi: 10.1016/S1065-7355(97)90003-1.

[116] C. Arya, "Factors influencing chloride-binding in concrete," *Cem. Concr. Res.*, vol. 20, pp. 291–300, 1990.

[117] K. A. Anders, B. P. Bergsma, and C. M. Hansson, "Chloride concentration in the pore solution of Portland cement paste and Portland cement concrete," *Cem. Concr. Res.*, vol. 63, pp. 35–37, 2014, doi: 10.1016/j.cemconres.2014.04.008.

[118] V. S. Ramachandran, "Possible states of chloride in the hydration of tricalcium silicate in the presence of calcium chloride," *Mater. Struct.*, vol. 4, no. 19, pp. 3–12, 1971.

[119] J. Tritthart, "Chloride binding in cement," *Cem. Concr. Res.*, vol. 19, pp. 586–594, 1989.

[120] H. Hirao, K. Yamada, H. Takahashi, and H. Zibara, "Chloride Binding of Cement Estimated by Binding Isotherms of Hydrates," *J. Adv. Concr. Technol.*, vol. 3, no. 1, pp. 77–84, 2005.

[121] S. Sui *et al.*, "Quantification methods for chloride binding in Portland cement and limestone systems," *Cem. Concr. Res.*, vol. 125, no. August, 2019, doi: 10.1016/j.cemconres.2019.105864.

[122] H. Zibara, "Binding of external chlorides by cement pastes," University of Toronto, 2001.

[123] K. De Weerdt, A. Colombo, L. Coppola, H. Justnes, and M. R. Geiker, "Impact of the associated cation on chloride binding of Portland cement paste," *Cem. Concr. Res.*, vol. 68, pp. 196–202, 2015, doi: 10.1016/j.cemconres.2014.01.027.

[124] K. De Weerdt, D. Orsáková, and M. R. Geiker, "The impact of sulphate and magnesium on chloride binding in Portland cement paste," *Cem. Concr. Res.*, vol. 65, pp. 30–40, 2014, doi: 10.1016/j.cemconres.2014.07.007.

[125] A. Machner, M. Zajac, M. Ben Haha, K. O. Kjellsen, M. R. Geiker, and K. De Weerdt, "Chloride-binding capacity of hydrotalcite in cement pastes containing dolomite and metakaolin," *Cem. Concr. Res.*, vol. 107, no. March, pp. 163–181, 2018, doi: 10.1016/j.cemconres.2018.02.002.

[126] J. J. Beaudoin, V. S. Ramachandran, and R. F. Feldman, "Interaction of chloride and C-S-H," *Cem. Concr. Res.*, vol. 20, pp. 875–883, 1990.

[127] Z. Shi *et al.*, "Role of calcium on chloride binding in hydrated Portland cement–metakaolin–limestone blends," *Cem. Concr. Res.*, vol. 95, pp. 205–216, 2017, doi: 10.1016/j.cemconres.2017.02.003.

[128] M. Gbozee, K. Zheng, F. He, and X. Zeng, "The influence of aluminum from metakaolin on chemical binding of chloride ions in hydrated cement pastes," *Appl. Clay Sci.*, vol. 158, pp. 186–194, 2018, doi: 10.1016/j.clay.2018.03.038.

[129] Q. Yuan, C. Shi, G. De Schutter, K. Audenaert, and D. Deng, "Chloride binding of cement-based materials subjected to external chloride environment - A review," *Constr. Build. Mater.*, vol. 23, no. 1, pp. 1–13, 2009, doi: 10.1016/j.conbuildmat.2008.02.004.

[130] P. Lambert, C. L. Page, and N. R. Short, "Pore solution chemistry of the hydrated system tricalcium silicate/sodium chloride/water," *Cem. Concr. Res.*, vol. 15, no. 4, pp. 675–680, 1985, [Online]. Available: https://www.jstage.jst.go.jp/article/jgeography1889/94/1/94_1_45/_pdf.

[131] M. Harris, G. Simpson, K. Scrivener, and P. Bowen, "A method for the reliable and reproducible precipitation of phase pure high Ca/Si ratio (>1.5) synthetic calcium silicate hydrates (C-S-H)," *Cem. Concr. Res.*, vol. 151, no. October 2021, p. 106623, 2022, doi: 10.1016/j.cemconres.2021.106623.

[132] Q. Yuan and M. Santhanam, "Test Methods for Chloride Transport in Concrete," in *Performance of Cement-Based Materials in Aggressive Aqueous Environments*, Springer, 2013, pp. 319–343.

[133]   K. Stanish and M. Thomas, "The use of bulk diffusion tests to establish time-dependent concrete chloride diffusion coefficients," *Cem. Concr. Res.*, vol. 33, no. 1, pp. 55–62, 2003, doi: 10.1016/S0008-8846(02)00925-0.

[134]   M. D. A. Thomas and P. B. Bamforth, "Modelling chloride diffusion in concrete effect of fly ash and slag," *Cem. Concr. Res.*, vol. 29, no. 4, pp. 487–495, 1999, doi: 10.1016/S0008-8846(98)00192-6.

[135]   F. Georget, J. H. Prévost, and B. Huet, "Reactive transport modelling of cement paste leaching in brines," *Cem. Concr. Res.*, vol. 111, no. May 2017, pp. 183–196, 2018, doi: 10.1016/j.cemconres.2018.05.015.

[136]   R. A. Patel *et al.*, "Diffusivity of saturated ordinary Portland cement-based materials: A critical review of experimental and analytical modelling approaches," *Cem. Concr. Res.*, vol. 90, pp. 52–72, 2016, doi: 10.1016/j.cemconres.2016.09.015.

[137]   P. Spiesz and H. J. H. Brouwers, "The apparent and effective chloride migration coefficients obtained in migration tests," *Cem. Concr. Res.*, vol. 48, pp. 116–127, 2013, doi: 10.1016/j.cemconres.2013.02.005.

[138]   K. D. Stanish, R. D. Hooton, and M. D. A. Thomas, "Testing the Chloride Penetration Resistance of Concrete : A Literature Review," Toronto, Ontario, Canada, 1997. doi: 10.1016/j.jfoodeng.2008.09.025.

[139]   C. Andrade, "Calculation of chloride diffusion coefficients in concrete from ionic migration measurements," *Cem. Concr. Res.*, vol. 23, no. 3, pp. 724–742, 1993, doi: 10.1016/0008-8846(93)90023-3.

[140]   "NT Build 492, Concrete, mortar and cement-based repair materials: Chloride migration coefficient from non-steady-state migration experiments, Nordtest Method," 1999.

[141]   P. Spiesz and H. J. H. Brouwers, "Influence of the applied voltage on the Rapid Chloride Migration (RCM) test," *Cem. Concr. Res.*, vol. 42, no. 8, pp. 1072–1082, 2012, doi: 10.1016/j.cemconres.2012.04.007.

[142]   Y. Sakai, "Relationship between pore structure and chloride diffusion in cementitious materials," *Constr. Build. Mater.*, vol. 229, 2019, doi: 10.1016/j.conbuildmat.2019.116868.

[143]   S. Sui, F. Georget, H. Maraghechi, W. Sun, and K. Scrivener, "Towards a generic approach to durability: Factors affecting chloride transport in binary and ternary cementitious materials," *Cem. Concr. Res.*, vol. 124, no. June, 2019, doi: 10.1016/j.cemconres.2019.105783.

[144]   W. Wilson, F. Georget, and K. Scrivener, "Unravelling chloride transport/microstructure relationships for blended-cement pastes with the mini-migration method," *Cem. Concr. Res.*, vol. 140, no. July 2020, 2021, doi: 10.1016/j.cemconres.2020.106264.

[145]   J. Zhang and G. W. Scherer, "Permeability of shale by the beam-bending method," *Int. J. Rock Mech. Min. Sci.*, vol. 53, pp. 179–191, 2012, doi: 10.1016/j.ijrmms.2012.05.011.

[146]   W. J. Weiss, R. P. Spragg, O. B. Isgor, M. T. Ley, and T. Van Dam, "Toward Performance Specifications for Concrete: Linking Resistivity, RCPT and Diffusion Predictions Using the Formation Factor for Use in Specification," in *High Tech Concrete: Where Technology and Engineering Meet*, 2017, vol. 1, pp. 2057–2065, doi: 10.1007/978-3-319-59471-2.

[147]   D. Jansen, C. Stabler, F. Goetz-Neunhoeffer, S. Dittrich, and J. Neubauer, "Does Ordinary Portland Cement contain amorphous phase ? A quantitative study using an external standard method," *Powder Diffr.*, vol. 26, no. 1, pp. 31–38, 2011, doi: 10.1154/1.3549186.

[148]   R. A. Millikan, *Elements of Electricity: A Practical Discussion of the Fundamental Laws and Phenomena*. Chicago, 1917.

[149]   M. D. Hürlimann, L. L. Latour, and C. H. Sotak, "Diffusion measurement in sandstone core: NMR determination of surface-to-volume ratio and surface relaxivity," *Magn. Reson. Imaging*, vol. 12, no. 2, pp. 325–327, 1994, doi: 10.1016/0730-725X(94)91548-2.

[150]   B. Lothenbach, D. Rentsch, and E. Wieland, "Hydration of a silica fume blended low-alkali shotcrete cement," *Phys. Chem. Earth*, vol. 70–71, pp. 3–16, 2014, doi: 10.1016/j.pce.2013.09.007.

[151]   L. Tong and O. E. Gjørv, "Chloride diffusivity based on migration testing," *Cem. Concr. Res.*, vol. 31, no. 7, pp. 973–982, 2001, doi: 10.1016/S0008-8846(01)00525-7.

[152]   S. Chatterji and M. Kawamura, "Electrical double layer, ion transport and reactions in hardened cement paste," *Cem. Concr. Res.*, vol. 22, no. 5, pp. 774–782, 1992.

[153]   E. Samson and J. Marchand, "Modeling the transport of ions in unsaturated cement-based materials," *Comput. Struct.*, vol. 85, no. 23–24, pp. 1740–1756, 2007, doi: 10.1016/j.compstruc.2007.04.008.

Curriculum Vitae

PERSONAL INFORMATION   **Adrian-Alexandru Pîrvan**

Schillerstr. 4-8, 69115 Heidelberg, Germany

Email: a.alexpirvan@gmail.com

Mobile: +49 1522 6920532

LinkedIn

WORK EXPERIENCE

Jan 2018–Jun 2021	Early stage researcher HeidelbergCement Technology Center, Leimen (Germany)
Jan 2016–Dec 2017	Chemical engineer Laboratory of Construction Materials - Technical University of Civil Engineering Bucharest (Romania)
Mar 2017–May 2017	Chemical adviser BASF, Bucharest (Romania)
15 Jul 2013–15 Sep 2013	Internship Student TenarisSilcotub, Zalău (Romania)

EDUCATION AND TRAINING

1 Jan 2018–Jan 2022	Doctoral Degree – Materials Science and Engineering École polytechnique fédérale de Lausanne, Lausanne (Switzerland)	EQF level 8
1 Oct 2015–30 Jun 2017	Master's Degree - Advanced Composite Materials with Specific Destinations Department of Science and Engineering of Oxide Materials and Nanomaterials, Faculty of Applied Chemistry and Materials Science, POLITEHNICA University of Bucharest Ghe. POLIZU Street, no 1-7, Bucharest (Romania)	EQF level 7

| 1 Oct 2011–15 Jul 2015 | Engineer Degree | EQF level 6 |

Department of Science and Engineering of Oxide Materials and Nanomaterials, Faculty of Applied Chemistry and Materials Science, POLITEHNICA University of Bucharest Ghe. POLIZU Street, no 1-7, Bucharest (Romania)

| CONFERENCE PRESENTATIONS | 2021 - ERICA CASH II Final Conference, Heidelberg, Germany |
| | 2019 - 39th Cement and Concrete Science Conference, University of Bath, UK |

| POSTER CONTRIBUTIONS | 2021 – 3rd International Conference on the Chemistry of Construction Materials (ICCCM), virtual via Zoom |
| | 2019 – CCMX Summer School "Characterization of Materials, EPFL, Switzerland |

| PUBLICATIONS | Pirvan, Adrian-Alexandru; Ben Haha, Mohsen; Boehm-Courjault, Emmanuelle; Scrivener, Karen, *Calcium-silicate-hydrates from reactive dicalcium silicate binder*, Conference Paper - 39th Cement and Concrete Science Conference, University of Bath, UK, 2019. |

| Mother tongue | Romanian |

Other languages

	Listening	Reading	Spoken interaction	Spoken production	Writing
English	C1	C1	C1	C1	C1
Certificate in Advanced English (CAE), International ESOL Examinations, awarded by University of Cambridge					
German	B1	B1	B1	B1	B1
The European Language Certificates (telc) Deutsch B1					
French	B1	B1	A2	A2	A2

Levels: A1 and A2: Basic user - B1 and B2: Independent user - C1 and C2: Proficient user

Other skills and qualifications	Good competences in characterization techniques of microstructure of hydrated cement, critical analysis and evaluation of experimental findings, good abilities for time management and resources management for experimental research planning.
	Good presentation skills and scientific writing skills through science communication opportunities.
	Excellent communication skills gained through coordinating the communication department in the Young Chemists Section of the Romanian Chemical Society.